Doctoral thesis for a doctoral degree

at the Graduate School of Life Sciences

Julius-Maximilians-Universität Würzburg

Section Biomedicine

Establishment of a 3D *in vitro* skin culture system for the obligatory human parasite *Onchocerca volvulus*

***

Etablierung eines 3D-*in-vitro*-Hautkultursystems für den obligat humanen Parasiten *Onchocerca volvulus*

submitted by

Christoph Malkmus

Würzburg 2022

Submitted on: 14.12.2022

Members of the Thesis Committee

Chairperson:	Prof. Dr. Uwe Gbureck
Primary Supervisor:	Prof Dr. Jan Hansmann
Supervisor (Second):	Prof. Dr. Christian Janzen
Supervisor (Third):	Dr. Sara Lustigman

Abstract

Onchocerciasis, the world's second-leading infectious cause of blindness in humans – prevalent in Sub-Saharan Africa – is caused by *Onchocerca volvulus (O. volvulus)*, an obligatory human parasitic filarial worm. Commonly known as river blindness, onchocerciasis is being targeted for elimination through ivermectin-based mass drug administration programs. However, ivermectin does not kill adult parasites, which can live and reproduce for more than 15 years within the human host. These impediments heighten the need for a deeper understanding of parasite biology and parasite-human host interactions, coupled with research into the development of new tools – macrofilaricidal drugs, diagnostics, and vaccines. Humans are the only definitive host for *O. volvulus.* Hence, no small-animal models exist for propagating the full life cycle of *O. volvulus*, so the adult parasites must be obtained surgically from subcutaneous nodules. A two-dimensional (2D) culture system allows that *O. volvulus* larvae develop from the vector-derived infective stage larvae (L3) *in vitro* to the early pre-adult L5 stages. As problematic, the *in vitro* development of *O. volvulus* to adult worms has so far proved infeasible. We hypothesized that an increased biological complexity of a three-dimensional (3D) culture system will support the development of *O. volvulus* larvae *in vitro*. Thus, we aimed to translate crucial factors of the *in vivo* environment of the developing worms into a culture system based on human skin. The proposed tissue model should contain 1. skin-specific extracellular matrix, 2. skin-specific cells, and 3. enable a direct contact of larvae and tissue components. For the achievement, a novel adipose tissue model was developed and integrated to a multilayered skin tissue comprised of epidermis, dermis and subcutis. Challenges of the direct culture within a 3D tissue model hindered the application of the three-layered skin tissue. However, the indirect co-culture of larvae and skin models supported the growth of fourth stage (L4) larvae *in vitro*. The direct culture of L4 and adipose tissue strongly improved the larvae survival. Furthermore, the results revealed important cues that might represent the initial encapsulation of the developing worm within nodular tissue. These results demonstrate that tissue engineered 3D tissues represent an appropriate *in vitro* environment for the maintenance and examination of *O. volvulus* larvae.

Zusammenfassung

Onchozerkose, die weltweit zweithäufigste infektionsbedingte Ursache für Erblindung von Menschen, wird durch *Onchocerca volvulus (O. volvulus)* verursacht, ein parasitärer Fadenwurm. Die allgemein als Flussblindheit bekannte Onchozerkose wird mit dem Medikament Ivermectin bekämpft, das jedoch nicht die adulten Parasiten tötet, die im Menschen mehr als 15 Jahre lang leben und sich vermehren. Ein tieferes Verständnis der Biologie des Parasiten und dessen Interaktionen im menschlichen Wirt ist für die Erforschung und Entwicklung neuer Instrumente – makrofilarizide Medikamente, Diagnostika und Impfstoffe – erforderlich. Da der Mensch der einzige Endwirt für *O. volvulus* ist, gibt es keine Tiermodelle für dessen Vermehrung. Zu Forschungszwecken werden adulte Würmer daher chirurgisch aus subkutanen Knoten erkrankter Individuen gewonnen. Ein zweidimensionales (2D) Kultursystem ermöglicht die Entwicklung von aus dem Vektor isolierten infektiösen *O. volvulus*-Larven (L3) bis zu einem frühen präadulten Stadium. Als problematisch erwies sich bisher die i*n vitro* Entwicklung von *O. volvulus* bis zum adulten Wurm. Unsere Hypothese ist, dass eine erhöhte biologische Komplexität des Kultursystems die Entwicklung von *O. volvulus*-Larven *in vitro* unterstützt. Daher wurden entscheidende Faktoren der *in vivo*-Umgebung entwickelnder Larven – die menschliche Haut – auf ein dreidimensionales (3D) Kultursystem übertragen. Dieses Kultursystem sollte 1. Haut-spezifische extrazelluläre Matrix enthalten, 2. hautspezifische Zellen und 3. einen direkten Kontakt zwischen Larven und Gewebekomponenten ermöglichen. Dafür wurde ein neuartiges Fettgewebemodell entwickelt, das in ein mehrschichtiges Hautgewebe integriert wurde – bestehend aus Epidermis, Dermis und subkutanem Fettgewebe. Die Anwendung des dreischichtigen Hautgewebes als direktes Kultursystem wurde durch technische Herausforderungen verhindert. Jedoch unterstützte die indirekte Ko-Kultur von Hautmodellen das Wachstum der Larven (L4) *in vitro*. Die direkte Kultur mit dem Fettgewebemodell verbesserte die Viabilität der Larven signifikant. Darüber hinaus konnten Anzeichen für eine beginnende Verkapselung der Larven durch humane Zellen und Matrix gezeigt werden kann. Die Ergebnisse demonstrieren, dass humane Gewebemodelle eine angemessene *in vitro*-Umgebung für die Kultur und die Erforschung von *O. volvulus* darstellen.

Table of content

List of Figures

List of Tables

List of Abbreviations

The abbreviations are listed alphabetically.

2D - two-dimensional

3D - three-dimensional

αSMA - α-Smooth muscle actin

ADFP - adipose differentiation-related protein or Perilipin-2

ADM - adipogenic differentiation medium

APOC - African Programme for Onchocerciasis Control

ATGL - adipose triglyceride lipase

BMI - body mass index

C/EBPs - CCAAT/enhancer-binding proteins

Col - Collagen

CK - Cytokeratin

DALY - disability-adjusted life years

DAPI - 4′,6-Diamidin-2-phenylindol

E1 - 2D keratinocyte medium

E10 - 3D keratinocyte medium

ECM - extracellular matrix

EM - hMSC expansion media

EOT - elimination of transmission

FAT - fatty acid transport protein-1

FTSM - full-thickness skin model

FM - fibroblast medium

GBD - Global Burden of Disease

GLUT4 - glucose transporter-4

h – hour(s)

hADSC - adipose-derived stromal cells

hBMSC - bone marrow-derived stromal cells

hDF - human dermal fibroblasts

HE - hematoxylin and eosin

hEK - human epidermal keratinocytes

HLA-DR - human leukocyte antigen-DR

hMSC - human mesenchymal stromal cells

HSL - hormone-sensitive lipase

HUVEC - human umbilical vein endothelial cells

IATA - International Air Transport Association

IBMX - 3-isobutyl-1-methylxanthine

IF - Immunofluorescence

IL-1β - interleukin-1 beta

KGF - keratinocyte growth factor

L3 - larval stage 3

L4 - larval stage 4

L5 - pre-adult larvae

LPL - lipoprotein lipase

MDA - mass drug administration

mf - microfilariae

MGL - monoacylglycerol-lipase

MHC - major histocompatibility complex

min - minute(s)

NC - Negative Control

NEFA - non-esterified fatty acids

NIH - National Institutes of Health

NTD - neglected tropical diseases

NYBC - New York Blood Center

OECD - Organization for International Cooperation and Development

OEPA - Onchocerciasis Elimination Program for the Americas

OSD - onchocercal skin disease

PBMC - peripheral blood mononuclear cells

PPARμ - peroxisome proliferator activated receptor μ

REACH - Registration, Evaluation, Authorization and Restriction of Chemicals

RHE - reconstructed human epithelium

SEM - scanning electron microscopy

SOP - standard operating procedure

TG - triglycerides

VLDL - very low-density lipoproteins

WAT - white adipose tissue

WHO - World Health Organization

YLDs - years lived with disability

YLLs - years of life lost

1. Introduction

The Global Burden of Disease study (GBD) published by the Institute for Health Metrics and Evaluation at the University of Washington delivers a worldwide observation of health issues confronting people and societies across the globe. It provides an important overview of data collected since 1990 on 369 diseases and 87 risk factors for human health in 204 countries and territories. Derived from these data, the GBD estimates morbidity, mortality, incidence and prevalence of these diseases and injuries. Moreover, the consequences for people are summarized and expressed in years of life lost (YLLs), years lived with disability (YLDs) and disability-adjusted life years (DALYs) [1]. The top ranked causes for DALYs from 1990 to 2019 demonstrate the progression of diseases in societies of all ages and sex. Notably, non-communicable diseases that are also classified as diseases of civilization are increasing in the DALYs during the observation time. In 1990, ischaemic heart disease and stroke were ranked as the 4th and 5th leading cause of DALYs, whereas in 2019 these diseases climbed to the 2nd and 3rd place. Especially the DALYs caused by diabetes were strongly increased by 148 %, climbing from place 20 to 8 of the ranking [1]. This massive increase in the prevalence of diseases of civilization can be explained by various factors, such as high levels of inactivity, the western diet pattern, alcohol, and tobacco consumption. These unhealthy habits lead to a rising number of people suffering from chronic and degenerative diseases. In 2016, 50 % of the American population suffered from at least one chronic health issue with a projected increase of 1 % per year [2]. A major driver for this development is overweight and obesity. In 2016, 13 % of the world population was classified as obese that is indicated by a body mass index (BMI) above or equal to 30 kg/m^2. In the same time 39.6 % of the adult population (20 years and older) in the US were obese [3], whereas the prevalence for obesity in Germany was 18.1 % in 2015 [4]. As a modifiable risk factor, overweight is a main cause for the burden of diabetes, which explains the climb of the disease over the years [5].

In contrast, the DALYs caused by infectious diseases worldwide were decreased. In 1990, Tuberculosis and Malaria were ranked as number 7 and 10 for top causes of DALYs, whereas in 2019 these diseases dropped to place 12 and 14. Notably, measles ranked as number 9 were drastically reduced, thus ranked as number 71 in 2019 [1]. These data provide a powerful overview on the progression of diseases and social

health developments. The current GBD states a constant level of global health, which can be explained by the progress in medicine on one side and the growing and aging world population on the other side. Whereas the western countries suffer from the rise of civilization diseases, countries of the global south face diseases that mainly occur in tropical regions, primarily in developing countries.

1.1 Neglected Tropical diseases

Neglected tropical diseases (NTDs) define a broad group of maladies that predominantly affect people and societies in tropical and subtropical environments. Inadequate sanitation, constant contact to vectors and live-stock and a limited availability of health services in countries of the developing world are factors for the persistence of NTDs [6]. In contrast, NTDs were eliminated in most of the developed countries, thus these diseases mainly compromise countries and societies in poverty, coining the term "neglected" [7]. Generally, insufficient or no treatment results in illness, suffering, impairment and social stigma [8,9]. Aside from the medical and social consequences, a loss of economic productivity of affected individuals has been described [10]. Taken together, this progression of NTDs causes a cycle of disease and poverty for whole communities and countries [7]. The World Health Organization (WHO) defined 20 major NTDs: Bilharzia, Blinding trachoma, Buruli ulcer, Chagas disease, Dengue, Echinococcosis, Elephantiasis, Foodborne trematodiases, Guinea worm disease, Intestinal worms, Leprosy, Mycetoma, Onchocerciasis, Rabies, Scabies, Sleeping Sickness, Taeniasis and cysticercosis, Visceral leishmaniasis and Yaws. The only non-infectious NTD is snakebite envenoming, which was added to the list in 2018, due to its prevalence and impact [11]. These 20 diseases threaten approximately 2 billion people worldwide and are responsible for roughly 200,000 deaths annually [7]. An analysis of the GBD 2013 with focus on NTDs estimated a loss of 8.21 million YLLs, thereby causing 25.1 million DALYs and 16.9 million YLDs [12].

For the control of NTDs the WHO postulates five key measures: preventive chemotherapy, innovative disease management, vector ecology and management, veterinary health service and the improvement of water supply and hygiene [7,11]. In the past, pharmaceutical companies donated drugs for the treatment of NTDs.

However, an inefficient distribution of these drugs due to non-reliable health care reduces the efficacy of the mass drug administration (MDA) programs [7]. Moreover, poor effectivity of applied drugs and prolonged treatment courses cause the non-adherence of patients [13]. So far, the development of preventive or therapeutic vaccines against the majority of NTDs was unsuccessful and the interest of pharmaceutical companies is low because these diseases mainly occur in poor countries [14,15]. Nevertheless, non-profit product development partnerships are endeavored to introduce vaccines against distinct diseases, such as onchocerciasis [15,16]. The company BionTech – known for the mRNA-based COVID-19 vaccine Comirnaty® – announced the development of a vaccine against malaria [17]. Recently, BionTech started the construction of an mRNA vaccine production plant in Rwanda [18]. The new vaccine technology gives hope for a prompt development of more NTD vaccines.

Besides the recent COVID-19 pandemic, the current world affairs are diverting the public attention from the problems of the global south. The pandemic threatens global health and concentrated measures and efforts to fight the spread of SARS-CoV-2 in most countries and globally. Unfortunately, this hampered the progress of NTD control [19]. Moreover, the climate change represents another global threat that will negatively influence the elimination of NTDs by contributing to the distribution of vectors and thus to a rise of NTD transmission [20]. To make matters worse, the war in Ukraine will cause a shortage of supplies to many African countries that might cause a famine. Summarizing, these current global challenges highlight the need of reinforced efforts in the post-pandemic time to achieve the sustainable development goals on NTDs set by the WHO [7,11,21].

These goals define a time point by which a disease is projected to be eliminated. In case of river blindness – one of the 20 NTDs and after trachoma the second leading cause of blindness resulting from an infection worldwide – the goal for elimination is currently set to 2025 [22].

1.2 Onchocerciasis

Onchocerciasis, or commonly known as River blindness is caused by the obligatory human parasitic filarial worm *Onchocerca volvulus (O. volvulus)*. Primarily in Sub-Saharan Africa, more than 204 million people are at risk to an infection with *O. volvulus*, about 21 million are infected, of which 1.2 million suffer from impaired vision [23]. Figure 1A highlights the countries around the globe that are endemic for *O. volvulus*. Notably, 99 % of all infections can be found in 31 African countries [24]. Infected black flies of the genus *Simulium* are responsible for the transmission of the parasite. As the disease name indicates, these insects breed along rivers predominantly in regions of Sub-Saharan Africa. People living in these areas are exposed to repeated bites of infected flies that eventually cause the manifestation of the *O. volvulus* infection. The life cycle of *O. volvulus* is demonstrated in Figure 1B.

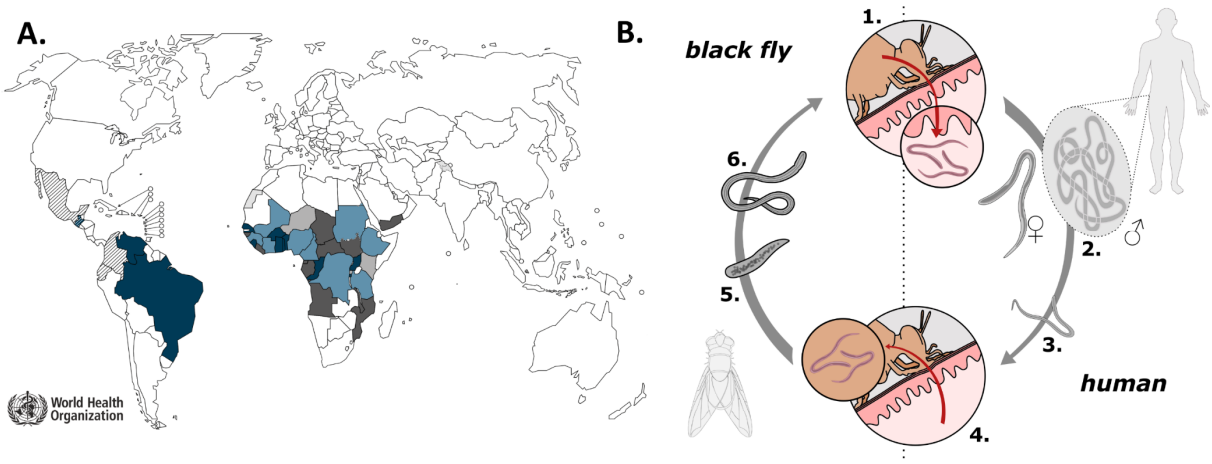

Figure 1: Endemic regions and life cycle of *O. volvulus*. A. Map of countries endemic for onchocerciasis. Source: https://www.afro.who.int/pt/node/580 (09.09.2021) **B.** Life cycle of *O. volvulus*. 1. Transmission of microfilariae during the blood meal of the black fly to the human host. 2. Adult parasites in subcutaneous nodule. Male worms migrate to nodule-resident females for fertilization. 3. Generation of thousands of microfilariae that migrate. 4. Ingestion of larvae by black fly during blood meal. 5. Microfilariae develop to black fly specific stages and 6. migrate as infectious larvae to the head.

The black fly ingests larvae of stage 1, called microfilariae (mf), during the blood meal on infected individuals. The mf molt twice within the vectors body to the larval stage 3 (L3). These infective larvae migrate towards the insect's head, specifically ending in the proboscis. From there, L3 enter the human body by their deposition in the wounded skin during the bite. The larvae migrate to the underlying skin and subcutaneous tissues, where they develop and molt to the first human specific larval

stage 4 (L4). Finally, after about 8 weeks, the worms reach the final human-specific stage [25]. After this last molt, worms are developing the sex organs and are therefore classified as pre-adult (L5) [26]. The adult parasites are embedded within highly vascularized collagenous nodules located in subcutaneous tissues, known as onchocercomas [27]. Whereas the female worm resides within the onchocercoma, the males migrate for their fertilization [28]. Female parasites can release up to 3000 mf each day, that can survive in the human body for up to 18 months [29]. Finally, these mf are ingested again by feeding black flies, the starting point of the parasitic life cycle. Embedded in the nodule, *O. volvulus* can live within the human host for more than 15 years and reach a size of 70 cm [29,30]. The nodules are mostly distributed on the lower extremities, the legs and pelvis [31]. From here, mf are mainly located in the human skin and are able to cover big distances in the human host by eventually reaching the human eye. For the migration, mf and male adults secrete proteases that degrades the matrix proteins of the host connective tissue, such as collagens, fibronectin and laminin [32,33]. A role of the lymphatic system was postulated to be of importance for the migration of mf in the human body [34], but to date could not have been proved [30].

The pathophysiology of onchocerciasis and various disease patterns

Still, the pathophysiology of river blindness is not yet fully understood. However, strong inflammatory responses of the human host to a massive and chronic load of degenerating mf take place within the eye [35]. Also, the endosymbiotic bacterium *Wolbachia* of *O. volvulus* worms could be the trigger for an immunogenic response. This theory is supported by the higher *Wolbachia* content of severe strains and its ability to cause more severe eye damages, whereas mild strains cause mild ocular pathogenesis [36]. Furthermore, autoimmune reactions could represent a crucial pathogenic factor for the manifestation of blindness [37]. Although, pathologic reactions can occur in all parts of the eye, the disease patterns are subdivided for their location [38]. The atrophy of the retinal pigment epithelium and subretinal fibrosis is characterized as posterior eye disease [39]. When the anterior chamber or the cornea is affected, it is classified as anterior eye disease. In this case, the immunogenic response to dead mf induces corneal opacification beginning as

punctuate keratitis, which affects the corneal epithelium. Due to the ongoing mf loads in the cornea, the opacification increases from the peripheral stroma towards the central area, which can finally lead to sclerosing keratitis, resulting in irreversible blindness [38].

Besides the most prominent and eponymous symptom, the loss of sight, an infection with *O. volvulus* also results in other disease patterns. The onchocercal skin disease (OSD) is evoked by the high numbers of mf in the human skin. The also called onchodermatitis has been neglected as symptom but was recently reported as socioeconomic burden for African communities [24]. OSD causes itching, depigmentation, atrophy and the so called hanging groin [24]. The malady of these symptoms, especially severe itching provokes infected people to suffer from insomnia, debilitation and has therefor a social influence, creating social stigma, affecting family formation and the mothers ability of breast-feeding [9,40]. Moreover, economical and agricultural productivity is reduced in endemic areas of *O. volvulus* [10,41]. Referring to the GBD Study 2017, out of nearly 21 million infected people, patients can be subdivided into 5.1 million asymptotic cases, 14.7 million cases of OSD and 1.2 million of blindness. The total burden is estimated with 1.34 million years lived with disability for onchocerciasis, of which 1.25 million YLD account for OSD and 96,100 YLD for river blindness [42]. These numbers do not take the onchocerciasis-associated epilepsy into account. In recent years, the occurrence of epileptic disorders correlating with *O. volvulus* infections were further studied, rising the term of river epilepsy [43,44]. The so-called Nodding syndrome is one of the neuronal disorders, that was shown to be triggered by an autoimmune dysfunction resulting from an infection with *O. volvulus* [45].

Strategies for the control of onchocerciasis

For a community-directed treatment of onchocerciasis, the WHO launched the Onchocerciasis Elimination Program for the Americas (OEPA) in 1992 and the African Programme for Onchocerciasis Control (APOC) in 1995. These programs were initially based on the MDA of ivermectin, a chemotherapeutic agent, which could be shown to have a microfilaricidal activity. Merck & Co. committed to these projects by the production of ivermectin (Mectizan®) and agreed to distribute the

drug for free [24]. In 2011, 2 billion ivermectin tablets were donated to 117,000 communities in Yemen, 5 countries in South America and 27 African countries [35]. The OEPA program could successfully demonstrate the feasibility of controlling cases of onchocerciasis. From 2013 to 2016, all affected South-American countries announced the elimination of transmission (EOT), except for two small foci in the border region of Brazil and Venezuela [46,47]. The EOT defines a reduction of the incidence of new cases to zero [48]. The microfilaricidal activity of ivermectin enables the control of *O. volvulus* transmission by reducing the mf load, and thus the transmission to the black fly vector. Moreover, it reduces symptoms and morbidity, mainly caused by the mf. An embryostatic effect on adult female worms as well as an inhibition of fecundity was also reported [44,48–50]. A study revealed that until 2015 the MDA of ivermectin has prevented 19 million DALYs [51].

Despite these advantages of this therapeutic strategy and the success in the Americas, the success of ivermectin in Africa is limited. Since the launch of APOC in 1995 until 2013 the incidence of onchocerciasis has only been reduced by 31 % [52]. In 2017, the WHO estimated 204 million people in Africa requiring MDA, whereas 142 million people got actually treated, resulting in a coverage of only 69.6 % [23]. Currently, the goals for EOT in 80 % of affected African countries was declared by the APOC for 2025 [22]. Predictions from mathematical models and leading experts are rather negative about the effectiveness of ivermectin alone, which will not be sufficient to eliminate onchocerciasis in Africa [53]. The lack of macrofilaricidal activity prompts the need of ivermectin treatment courses exceeding the parasites lifespan (more than 15 years). The earlier mentioned deficiency of treatment coverage and adherence in endemic African countries highlights infrastructural and healthcare system problems [13,54]. An additional big obstacle for ivermectin administration in 11 Central African countries is the co-endemicity of *Loa loa* – another filarial parasite – as the treatment causes the risk of severe adverse events [55,56]. In relation to the microfilarial load of *L. loa,* the risk of side effects is increased. The reactions range from itching, headache and edema to serious neurological dysfunctions [57]. Furthermore, resistance of *O. volvulus* against ivermectin has been reported, thus potentially reducing the applicability of the drug [58].

An alternative treatment strategy of *O. volvulus* infections targets the intercellular endosymbiont. The majority of filarial worm species that infect the human host have a symbiosis with *Wolbachia* bacteria [59]. The supply of essential metabolites from the bacterial symbionts is proven to be crucial for the reproduction, pathogenicity and survival of the filarial parasite [60,61]. The effects of targeting the symbiotic bacteria by antibiotic drugs were analyzed. A prominent candidate is represented by doxycycline that could demonstrate an effective depletion of *Wolbachia* within adult *O. volvulus* worms in clinical trials. Thereby, a macrofilaricidal effect was observed, accompanied by an inhibition of reproduction and transmission [62–64]. However, long-term treatment with doxycycline is required, thus hindering its broad administration, due to adverse events and contra-indications [65].

Progress on the development of *O. volvulus* research

To accelerate the progress of alternative intervention strategies the APOC called for the development and testing of novel technologies in 2014 [66]. To achieve this progress, a fundamental knowledge on the parasite biology is required, especially on the interaction between the parasite and the human host. The research of *O. volvulus* has always been challenging, as the filarial parasite is obligated to humans as definitive host. For this reason, no small animal model can be applied to propagate and thereby produce adult and matured worms for the evaluation of novel treatment strategies. So far, the nodulectomy – the excision of nodules containing worms from infected individuals – represents the only way to obtain the adult parasite [29]. Consequently, the strongly limited availability reduces the progress of research applications and drug discovery studies. To circumvent this problem, surrogate filarial parasites, such as cattle *Onchocerca ochengi*, *Brugia* spp and *Litomosoides sigmodontis*, which can be maintained in animals *in vivo* and/or *in vitro* are serving as a model system to analyze the effect of novel drugs [25,29]. However, the use of surrogate parasites and animal models cannot resemble the specific interaction between *O. volvulus* and the human host, specifically within the onchocercoma, representing a parasite-specific environment.

As an alternative to surrogate models, *in vitro* cultures have been applied to filarial parasites. Basic two-dimensional (2D) culture approaches principally allow the

usage of human cells and represent an easy maintainable culture system. The applicability and sufficiency for the maintenance of filarial larvae was demonstrated for *Mansonella perstans* L3, that showed 33 % viability of the initial number of larvae after 77 days [67]; 60 – 90 % of *Loa* L3 survived over 15 to 17.8 days in culture [68,69]; and 69 % of *Brugia malayi* L3 were viable after 30 days [70]. For the *in vitro* maintenance of *O. volvulus* larvae, a culture system based on a feeder layer of human umbilical vein endothelial cells (HUVEC) has been developed by researchers of the New York Blood Center (NYBC) [29]. The HUVEC-conditioned culture medium supports the growth and development of L4 larvae towards the pre-adult L5 stage. However, the survival of larvae is strongly decreasing during the *in vitro* culture to 20 % of their initial number after 7 weeks. Figure 2 demonstrates the co-culture setup and the survival rate of larvae *in vitro*. Typically for pre-adult stages, the worms obtained from the co-culture system show no matured gonads, thus they are not fecund. Moreover, worms of comparable age from nodulectomy are significantly bigger by the factor 10 – 50 [27].

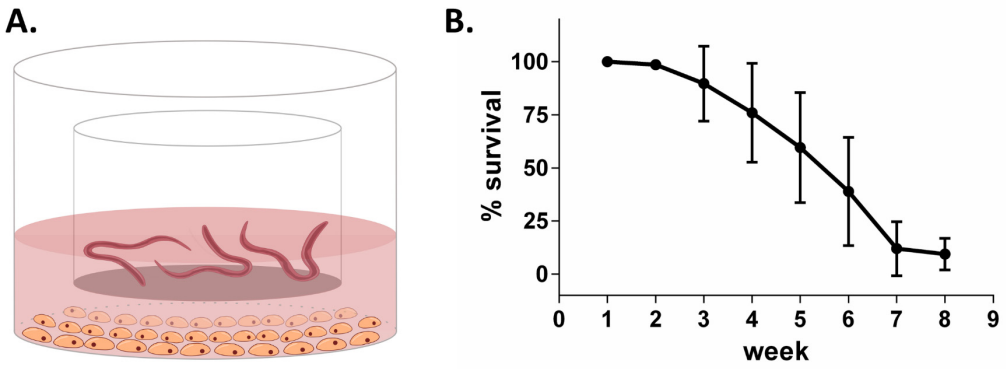

Figure 2: 2D *in vitro* culture of *O. volvulus* L4 larvae. A. The conditioned medium by the co-cultured 2D HUVEC monolayer supports the development of the larvae that are placed above in a culture insert. **B.** Survival of *O. volvulus* larvae in the 2D culture system. The graph was published by Malkmus *et al.*, 2020 [71].

It is hypothesized, that a simple 2D culture of a single human cell type is sufficient to maintain and develop the larvae to pre-adult L5s, but the lack of biological complexity hampers higher survival rates and eventually the maturation to adult parasites [71]. An increased complexity is represented by biological factors, such as organ specific cell types, extracellular matrix (ECM), and physiological properties, e.g. blood flow and mechanical stimuli. So far, these interacting parameters all

together can only be delivered by a living organism. As the obligation to the human host avoids the usage of small animal models, *in vivo* studies using approaches that are more sophisticated were performed. Therefore, diffusion chambers containing *O. volvulus* L3 larvae were implanted to primates – evolutionary closer to humans. Only 15 % of living larvae could be obtained after 63 days that were molted to stage L4 [26]. An even more ambitious approach was using humanized mice to model the human host [72]. Unfortunately, only a poor larvae retrieval of 1.4 % of the initial inoculum could be achieved. Even though, providing a complex *in vivo* environment, the advanced animal models do not represent the appropriate human host environment for *O. volvulus* larvae and thus are not an adequate solution for the endeavor of producing adult parasites for therapeutic research attempts.

This highlights the complicatedness of a culture approach that combines the biological stimuli needed for the development and survival of larvae together with the feasibility and practicability. To close this gap, we hypothesized that three-dimensional (3D) human tissue models provide a culture platform that allows practical workflows. More importantly, it allows the *in vitro* presentation of the parasite-specific environment in the human host – subcutaneous tissues – the niche of *O. volvulus*.

1.3 The human skin – Niche of *O. volvulus*

The subcutaneous tissue is the innermost layer of the human skin. With a size of two m^2, the skin represents the largest organ of the human body, accounting for 15 % of the body weight. It covers the complete outer surface and thus is responsible for the protection of the body against outer harmful impacts, caused by sunlight/irradiation, chemical agents and pathogens. Moreover, the skin regulates the water household, body temperature and is involved in immunologic reactions, hormone synthesis and sensory perception [73]. Figure 3 illustrates the principal anatomy of human skin, which is formed by three major layers: from outside epidermis, dermis and the subcutis.

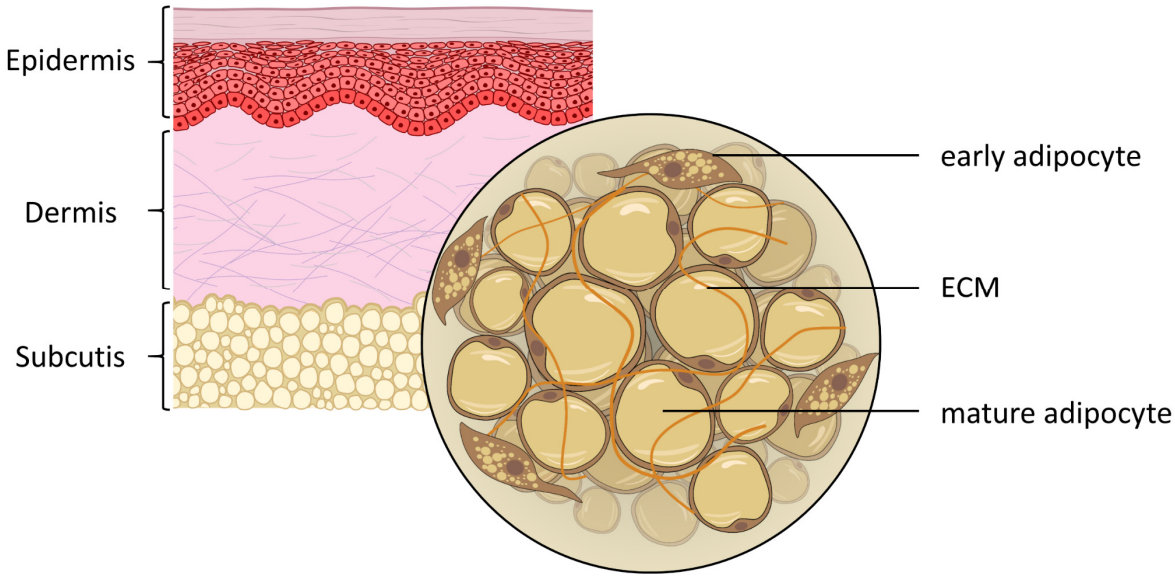

Figure 3: Principle anatomic structure of the human skin. The skin is composed of three major layers: epidermis, dermis and subcutis. Adipocytes represent the most prominent cell type of subcutaneous adipose tissue. As a highly dynamic organ, cells are in different stages of differentiation. Early differentiating adipocytes contain numerous lipid vacuoles that fuse to become eventually a single lipid vacuole, a major morphological feature of mature adipocytes. Cells are embedded in ECM.

Subcutaneous tissue mainly consists of adipose tissue which is composed of cells of the stromal-vascular fraction – adipocytes, endothelial cells, pericytes, immune cells and pre-adipocytes [74]. Nowadays it is commonly known that besides its function as storage organ for energy, adipose tissue is involved in diverse physiological processes, e.g. thermoregulation, immunology and endocrine signaling and the regulation of appetite [74]. As the physiological relevance of adipose tissue is increasingly understood, the biology of the different adipose tissue depots, their functions and involvement in various physiological mechanisms should be considered for the *in vitro* modelling.

In general, adipose tissues are morphologically subdivided into a brown and white subgroup that also differ in their location. Brown adipose tissue is characterized by a high degree of vascularization and densely packed mitochondria, which contributes to the brownish color. Brown adipocytes are also characterized as multilocular, thereby containing multiple lipid droplets of different size [74]. It accounts for only 1 – 2 % of total fat mass in humans and is only located in cervical, paraspinal and axillary regions of the body [75]. The function of brown adipose tissue is the non-shivering thermogenesis, the production of heat by oxidative phosphorylation of circulating free fatty acids. Thereby, it maintains the core body

temperature and it clarifies the blood plasma from triglycerides [76]. In contrast, white adipose tissue (WAT) is further classified by its location. Visceral fat is located intra-abdominally and surrounding the inner organs [76], predominantly found in obese individuals. The high metabolic activity causes a constant release of free fatty acids, contributing to symptoms of cardiovascular diseases and diabetes, such as systemic inflammation, hyperinsulinemia, and atherosclerosis [77].

The most abundant WAT is represented by the subcutaneous adipose tissue, which makes roughly 80 % of the total fat in healthy individuals [78]. Histologically, adipocytes of this fat depot show different stages of maturation. Figure 3 shows schematically the composition of differentiating multilocular cells with multiple lipid droplets and matured adipocytes, unilocular cells containing a single vacuole for the storage of lipid. The cells are embedded into ECM which consists of collagens (I, II, III, IV), fibronectin and laminin [79]. An extensive network of vasculature is responsible for the transport of nutrients. Only 30 – 50 % of cells are adipocytes, however they make about 90 % of the tissue volume [76,80]. As already mentioned, the remaining cells are of the stromal vascular fraction, namely endothelial cells, pericytes, immune cells and importantly adipocyte precursors [81]. Adipocytes differentiate from adipose tissue resident stem cells of mesenchymal origin [74]. The so called adipogenesis is regulated by key transcription factors, such as peroxisome proliferator activated receptor γ (PPARγ) and CCAAT/enhancer-binding proteins (C/EBPs) [82]. The most critical pro-adipogenic transcription factor is PPARγ, a member of the hormone nuclear receptor family. It could be shown *in vitro*, that activating and inhibiting factors of adipogenesis mainly modulate PPARγ expression or activity [83]. During the adipogenic differentiation, the developing adipocyte accumulates lipids in small vacuoles that fuse during the ongoing maturation. In WAT, the lipid vacuole has a share of 90 % of the cytoplasm, causing the flattening of the nuclei at the cell periphery. The size of mature adipocytes ranges from 20 – 300 µm in diameter [80]. A major function of subcutaneous adipose tissue is the homeostasis of energy. Therefore, energy is stored as triglycerides in adipocytes. Two mechanisms enable the storage of excess energy. The expansion of adipose tissue by cell proliferation and thus an increasing number of adipocytes is called hyperplasia. In contrast, the increase in size of adipocytes by the accumulation of triglycerides is hypertrophy [76]. If the level of supplied energy exceeds the capacity of hyperplasia and hypertrophy, triglycerides are stored as ectopic fat in

visceral adipose tissue depots. While exercise and fasting require an elevated level of energy, lipids are released as non-esterified fatty acids to cover the demand [84]. This constant flux of triglycerides results in the ability of the adipose tissue to expand and decrease in size in dependency to the level of energy required for the activity of the human individual. Multiple organs rely on the supply of energy, such as brain, pancreas, liver and muscles. In this regard, the adipose tissue fulfills the function of an "energy balance hub" [76,85]. On a molecular level, the synthesis and accumulation of triglycerides is described by *de novo* lipogenesis as shown in Figure 4.

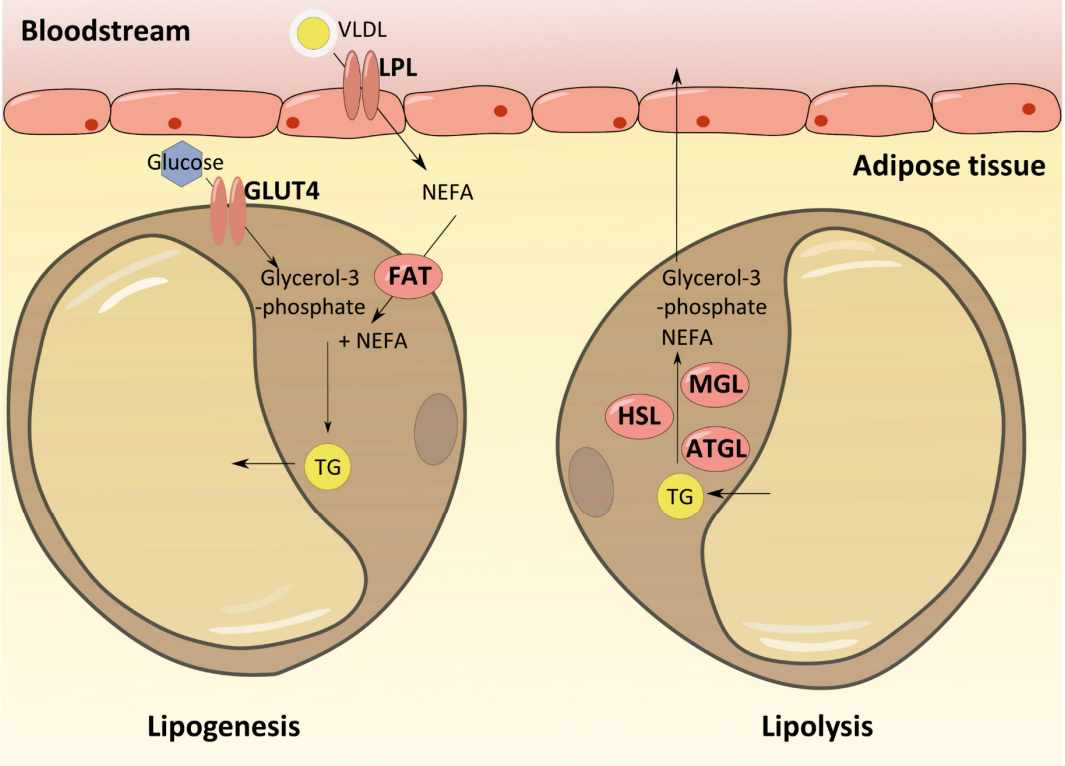

Figure 4: Energy storage and mobilization of adipocytes. Lipogenesis (left) requires Glucose and free non-esterified fatty acids (NEFA) from the bloodstream, finally stored as triglycerides (TG) within the lipid vacuole. In **Lipolysis (right)** TG are sequentially processed by lipases to NEFA and glycerol-3-phosphate. For energy supply, these products are transported via the bloodstream to peripheral organs.

The required fatty acids for lipogenesis either are synthesized within the adipocyte or derive from circulating triglycerides of the blood stream. The latter are transported as very low density lipoproteins (VLDL) [86]. Insulin-stimulated lipoprotein lipase (LPL) located on the luminal surface of vascular endothelial cells of the WAT hydrolyze triglycerides to non-esterified fatty acids (NEFA) [87]. The NEFAs are transported into adipocytes by the fatty acid transport protein-1 (FAT)

[88,89]. Besides LPL activation, insulin enhances the uptake of glucose via the glucose transporter-4 (GLUT4) located on the adipocyte membrane. By the esterification of a glycerol-3-phosphate originated from glucose and three fatty acyl chains triglycerides are synthesized and stored in the lipid vacuole [83]. Contrarily, lipolysis describes the energy mobilization of the adipocytes by converting the stored triglycerides back into glycerol and three fatty acids. Therefore, three lipases are functioning sequentially. The adipose triglyceride lipase (ATGL) cleaves the molecule, resulting in diacylglycerol, which is further hydrolyzed by the hormone-sensitive lipase (HSL) to monoacylglycerol. Eventually, the monoacylglycerol-lipase (MGL) finalizes the lipolysis. The lipolytic products are transported via the blood stream, energy is obtained by e.g. oxidation of fatty acids in muscle cells and the glycerol serves as substrate for e.g. gluconeogenesis in hepatocytes [90].

For this important function of WAT – the storage and supply of energy- lipogenesis and lipolysis are crucial processes. These functions are controlled by the nutritional status, exercise and endocrine signaling [86]. The uptake of carbohydrates results in rising levels of blood glucose and insulin that is secreted by pancreatic β-cells. Insulin represents an important regulator of *de novo* lipogenesis through the activation of lipogenic enzymes, such as LPL and GLUT4 and therefore increasing the supply of the substrates, glycerol and free fatty acids. A second important regulator of lipogenesis is leptin, an adipokine secreted by adipocytes [91] acting as hormone in the control of food intake, the expenditure of energy and thus has an impact on body weight by acting in the medial basal hypothalamus [92]. It could be shown that neuronal signaling via sympathetic neurons innervating white adipocytes cause a leptin-induced lipolysis [93]. This interaction with neuronal signaling highlights a second important function of adipose tissue as an active secretory organ. Since the discovery of leptin and adiponectin [91,94], numerous adipocyte secreted polypeptides called adipokines with regulatory function have been discovered and described. These factors show autocrine, paracrine and endocrine function, thus communicating with the hypothalamus (leptin), pancreas, liver, muscle, kidney, etc. and underlining again its function as "energy balance hub" [74,76]. Hence, the awareness for WAT as a regulatory organ involved in systemic metabolic homeostasis has risen [93]. It could be shown, that a healthy WAT in mice attenuates the lipotoxic effect on peripheral organs mediated by

adipokine signaling [95]. A dysfunctional adipose tissue causes an impaired adipokine secretion, which can eventually lead to insulin resistance associated with obesity and type 2 diabetes, diseases of civilization [79,96].

Mechanically, the subcutaneous adipose tissue provides protection by functioning as a cushion. In addition, it is responsible for thermal insulation and for the defense of pathogens arising from the skin [84]. Due to the exposed position of the body surface, the upper skin layers epidermis and dermis have an important barrier function. Figure 5 illustrates the anatomical organization of the human skin with a focus on the epidermis and dermis.

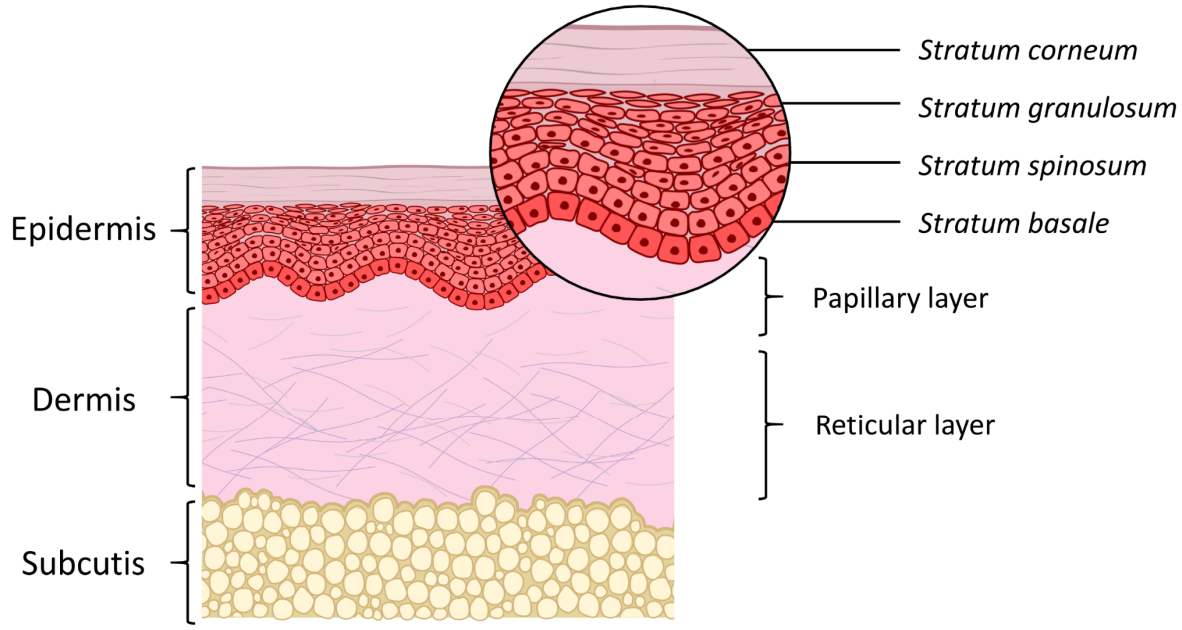

Figure 5: Anatomic structure of the epidermis and dermis of human skin. The epidermis is subdivided into *stratum basale*, *stratum spinosum*, *stratum granulosum* and the outermost *stratum corneum*. Underneath, the fibrous dermis mainly consists of collagen. The dermis is subdivided into the upper papillary layer, followed by the reticular layer. The main proportion of the subcutis is the highly vascularized adipose tissue.

As the outermost skin tissue, the epidermis covers the human body. The majority of cells are human epidermal keratinocytes (hEK), which are organized in distinct layers that represent the differentiation status of the cells and form a stratified squamous epithelium. In the *stratum basale*, highly proliferative precursor cells form a monolayer that is based on the basement membrane. These cells undergo a permanent mitosis and newly divided cells migrate upwards towards the *stratum spinosum*. The hEKs flatten as they move further to the *stratum granulosum*. The cells

undergo a nuclear degradation, while keratohyalin granules accumulate in the cytoplasm. The cornified *stratum corneum* consists of dead, nuclei-free corneocytes – the terminally differentiated keratinocytes. Besides the barrier that is generated by tight junctions between keratinocytes of the living layers [97,98], the *stratum corneum* is responsible for the major barrier function of the epidermis and gives mechanical protection. This barrier is generated by extracellular lipid accumulations and crosslinked proteins between the corneocytes according to "bricks and mortar", generating a sealing of the skin [99,100]. The epidermis is a continuously renewing tissue, as the basal cells undergo mitosis, hEKs differentiate, and corneocytes are shed. Besides hEKs, Melanocytes protect against UV-irradiation by the exocytosis of melanin towards keratinocytes and as tissue-resident macrophages, Langerhans cells detect and process pathogens. Additionally, these cells are highly migrative and form a network within the epidermis [101].

Whereas the epidermis forms a vital barrier function towards the outer environment, the underlying dermis sustains the major mechanical strength of the skin [100]. Both tissue compartments are separated by the basal lamina, a structure of ECM. This basement membrane is responsible for physical stabilization of the keratinocytes by giving an adhesion interface and anchoring the cells. This anchor consists of intracellular keratin filaments bound via hemidesmosomes to the basal lamina [102]. The protein components for the ECM structure are secreted by both, hEKs and human dermal fibroblasts (hDF), the major cell type of the dermis. Whereas collagen IV and VII is synthesized by both cell types, laminins are originated from hEKs [103]. As shown in Figure 5 the interface of both tissues is structured by dermal papillae and connected to the rete ridges. In this papillary region of the dermis, a dense network of vasculature and the increased surface given by the papillary structure enable an optimal exchange of nutrients and oxygen towards the epidermis. The dermal vasculature also supports the immunological response to pathogens by the transport of inflammatory cells as well as thermoregulation [104]. The papillary layer is responsible for nourishing the epidermis and is a loose connective tissue. In contrast, the reticular dermis contains thick bundles of collagen fibers that are arranged and orientated along the surface of the skin. This arrangement generates the tensile strength and elasticity of the dermis [100]. The dermis-resident hDF are responsible for the synthesis and secretion of the ECM components, such as

collagens, fibronectin and elastin [73]. Different structures, such as hair follicles, sweat glands, nerves, blood and lymph vessels are mainly located in the reticular layer [104].

Together all three layers of the human skin represent a complex organ, of which every tissue layer is specialized for its function, ranging from a vital barrier function generated by the epidermis, a mechanically stable protection given by the dermis and the adipose tissue regulating systemic energy homeostasis. Because of its relevance for research and medicine, the understanding of the human skin and other tissues is of great interest. The evolving field of Tissue Engineering enables the application of human tissue equivalents for various research domains.

1.4 Tissue Engineering of human *in vitro* tissue models

Tissue Engineering is an interdisciplinary research environment combining cell biology, material science, electrical and mechanical engineering for bio-reactor development and 3D bio-printing [105]. The aim of Tissue Engineering is the generation of functional tissues that represent a sufficient model system for research applications and ultimately as a future source for tissue repair and replacement in regenerative medicine. Recently, the automation of tissue engineering and downstream applications are of great interest for clinical research and industry [106–108].

General Tissue Engineering approaches and applications

Figure 6 demonstrates the basic principle of Tissue Engineering. Primary cells isolated from a human donor (1) are expanded in 2D culture (2), followed by seeding on 3D scaffold materials (3). The 3D environment generates more tissue-specific stimuli for cell differentiation and the formation of a tissue-like morphology. The resulting matured *in vitro* tissue model is thought for clinical implantation (4) or research use (5) [109].

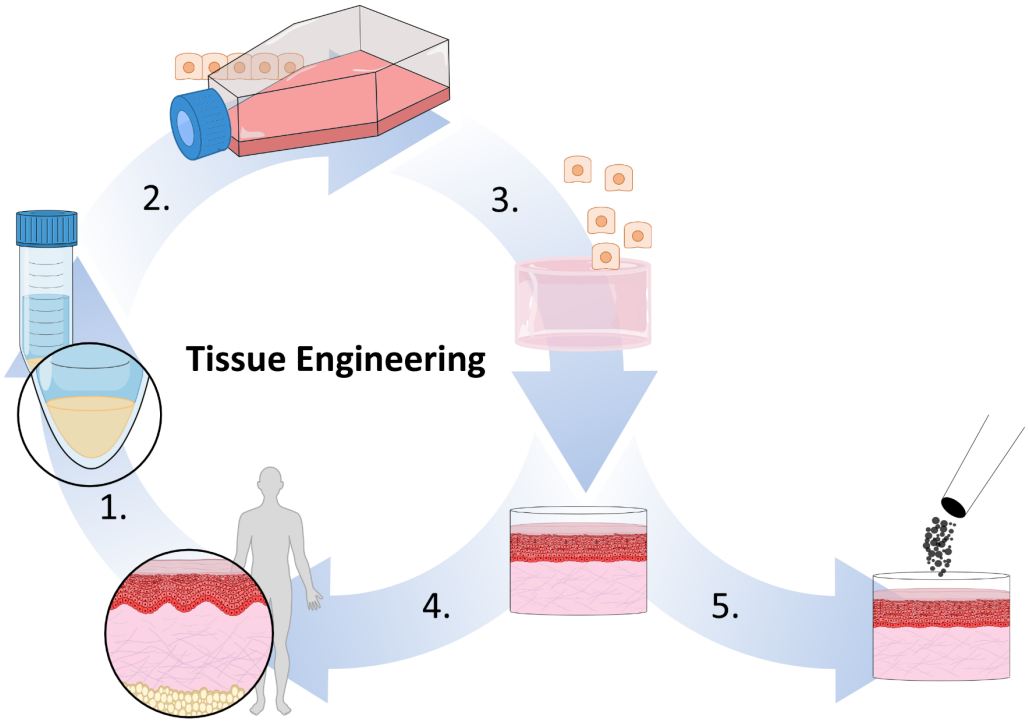

Figure 6: General principle of Tissue Engineering. Primary cells from a human donor are isolated (1), expanded (2) and seeded onto 3D scaffold material (3). By the cultivation, the tissue matures and is eventually implanted to the donor (4) or applied for research (5).

A variety of human tissues has been translated to 3D *in vitro* models for various applications [105]. In the field of drug testing in clinical research, *in vitro* tissues are of interest for multiple reasons. Animal models have been the gold standard for the analysis of safety and efficacy of drug candidates and chemical compounds [110]. Despite its advantage for research over many decades [111], recent attempts aim to replace animal testing by advanced *in vitro* approaches, as the differences in anatomy and physiology reduce the transferability of results to the human. This discrepancy is demonstrated in clinical trials by the number of drug candidates failing in humans that were pre-tested in animals [112]. Moreover, many human diseases, such as onchocerciasis and also pertussis, are caused by obligatory human pathogens, thus no animal models are able to serve as a study platform [113]. Also, these days ethical concerns and animal-welfare are in public discourse and gain importance. In 1959, Russel and Burch defined the basic principle 3R – Refine, Reduce, Replace animal testing [114]. A ban of animal testing was legally implemented for cosmetics and household products in the EU in 2013. Together, these factors are responsible for the growing market of Tissue Engineering.

Human tissue models represent an increasingly applied tool for disease modelling and the research of host-pathogen interactions [115,116]. 3D culture systems are specifically applied to study helminth interactions with the human host [117]. However, the relevance as a barrier organ against outer harms and thus a crucial role for human health makes the skin an important tissue of special interest, not only in the field of host-pathogen-interactions.

Tissue Engineering of human skin equivalents

Nowadays, engineered skin equivalents of different complexity fulfill a crucial role for industrial usage as well as for a potential application in clinical wound dressing. Compared to other tissues of the human body, the development of engineered skin has been pushed by commercial interests of the pharmaceutical and cosmetic industry [118]. Historically, animals served as model system to analyze the effect of new drugs or topically applied substances. Therefore, the prominent Draize rabbit skin irritation test was developed in the 1940s [119]. Alternatives for animal testing have been developed, mainly representing *ex vivo* tissues of animal and human origin [120,121]. However, legislations such as the "Registration, Evaluation, Authorization and Restriction of Chemicals" (REACH) of the European Union regulate animal use and ultimately the 7th amendment to the European cosmetic directive permit animal testing for the cosmetic industry. Thus, the development of alternative testing was accelerated by the industry. The SkinEthic™ model represents the human epidermis, generated with human epidermal keratinocytes on a permeable membrane, a reconstructed human epithelium (RHE). This skin substitute was developed and applied for skin irritation testing by L'Oreal, a cosmetics company [122]. An important application of RHE is the testing of skin corrosion and irritation caused by topically applied substances. Therefore, the Organization for International Cooperation and Development (OECD) developed test guidelines that define criteria for test procedures and tissue models. These legal implementations of alternative testing again pushed the development of *in vitro* skin. The Open Source RHE model was published and enabled the access of the broad research community to the manufacturing protocol [123]. The applications of RHE range from basic skin biology, such as pigmentation [124] and wound healing [125]; diseased skin, e.g.

psoriasis [126] and melanoma formation [127]; and the study of pathogen interactions like percutaneous parasite invasion [128]. The efforts made by the industry led to a fast progress in the application of *in vitro* skin that also results in the development of advanced skin models and analytical methodologies, such as gene toxicity analysis [118].

RHE could demonstrate its applicability as a versatile research tool. However, its relatively low complexity limits the degree of physiological resemblance. Extensive crosstalk between keratinocytes and fibroblasts via paracrine signaling regulates tissue homeostasis. It could be shown that hEKs induce the release of the keratinocyte growth factor (KGF) by hDFs through the secretion of interleukin-1 beta (IL-1β), thereby enhancing keratinocyte migration and proliferation in wound healing [129]. Also, the cross-talk between dermis and epidermis results in a metabolic activity profile closer to native skin than the RHE [130]. The full-thickness skin model (FTSM) recapitulates this epidermal-dermal interaction with an integrated dermal compartment. To model the ECM rich dermal tissue and enable a 3D *in vivo*-like architecture, the scaffold material for the generation of the connective tissue is a crucial aspect. Materials of natural and synthetic origin in the form of hydrogel or polymer fibers have been applied to give the structural basis for the culture of human cells [131]. Collagen type I and III represent the most prominent ECM proteins in native dermis. Hydrogels of collagen have been applied for the production of FTSM [132]. Unfortunately, hydrogels of especially natural polymers such as collagen show weak mechanical stability. The high-water content of collagen type I hydrogels and the remodeling by hDF result in physical contraction of the matrix [133]. This mechanical instability reduces the standardization of FTSMs and their long-term culture, thus limiting its applicability for many research problems. Strategies for the improvement of the physical properties have been developed. Two major modifications of collagen hydrogels are made – chemical cross-linking and the reduction of water. The former uses chemical cross-linkers that bind collagen fibers, which eventually reduces the contraction induced by fibroblasts [134]. However, many cross-linking agents, such as glutaraldehyde show severe cytotoxic effects [135]. Thus, the model generation protocol requires the elution of remaining cross-linker prior to cell seeding. This provokes the problem to generate collagen hydrogels with a homogeneous cell distribution [136]. The latter modification – the

reduction of water content – is facilitated by plastic compression of the matrix [137,138]. Collagen hydrogels represent the most common scaffold material to model the human dermis and full-thickness skin. Recently, the plastically compressed FTSM could be infected with *Trypanosoma brucei*, the causative agent of the African sleeping sickness, by natural transmission through the tsetse fly [139]. This very specific application using an animal vector to bite artificial skin proves the resemblance of the FTSM with native human skin. Nevertheless, epidermis and dermis are insufficient to cover the whole life cycle of this parasite.

As described earlier, the adipose tissue gains more importance as the understanding of its involvement in fundamental biological processes is continuously increased. The complex interplay of this tissue is important for the understanding of many diseases of civilization as well as NTDs. The human adipose tissue represents a crucial niche tissue and reservoir for many parasites, such as *Plasmodium falciparum*, the causative agent of Malaria, *Trypanosoma cruzi*, causing Chagas disease and *T. brucei* [140]. The latter specifically adapts to the tissue environment by the differentiation to a specialized adipose tissue form enabling the parasite to change its metabolism for using fatty acids as carbon source [139]. Besides these unicellular parasite, also filarial worms inhabit the subcutaneous adipose tissue, such as *Loa loa*, *Mansonella streptocerca* and *O. volvulus* [71,141]. Importantly, all these mentioned parasites except for *P. falciparum* cause NTDs. Not only in the context of parasitology, the modelling of a subcutaneous tissue is of interest for various research domains. The distribution of an administered drug is dependent on the mobility throughout the different tissues of the human body as well as the chemical properties. Within a tissue, various factors influence the drug distribution, e.g. blood perfusion, pH gradients, membrane permeability, plasma protein binding and the accumulation in the adipose tissue [142]. The storage of drugs in the lipophilic adipose tissue has not been addressed thoroughly, either of compounds administered systemically or topically. Thus, *in vitro* skin composed of epidermis, dermis and adipose tissue represents an optimal research platform to analyze the accumulation of drugs [143] and importantly the host-parasite interactions.

Similar to all to all tissues of interest, the most *in vitro* studies addressing the adipose tissue have been performed in 2D with cultures of the commonly used murine 3T3-L1 cell line [144]. However, to enable the development of a reconstructed adipose

tissue, eventually with the potential to serve as an implant, primary human cells are commonly used in adipose tissue engineering. Different strategies have evolved, of which the majority is based on seeding pre-adipocytes or matured adipocytes on a 3D scaffold material, followed by adipogenic differentiation respectively their maintenance [145,146]. Materials of biological and synthetic origin that were considered are hyaluronic acid, collagen, alginate or polyethylene glycol in different structures and constitutions, such as hydrogel, sponge, foam or microspheres [147]. Depending on the cell type used for the tissue formation, different advantages and disadvantages have been discovered. Mature adipocytes can be obtained from liposuction, a relatively low-invasive method for the cell donor. However, matured adipocytes are fragile and susceptible to mechanical damage, that can occur during the aspiration [148]. Due to the terminal adipogenic differentiation, the aspirated adipocytes only show a limited proliferation *in vitro* [147]. However, it could be shown that matured adipocytes were integrated into a multilayered skin model [143]. In contrast, different stem cells have been applied to achieve the adipose tissue formation. Human mesenchymal stromal cells (hMSCs) represent an abundant type of multipotent stem cells that can be isolated from different tissues. The most prominent and well described sources are bone marrow and the adipose tissue [149]. Moreover, an increasing number of tissues containing hMSCs have been identified, hence cells were isolated from dental tissue, salivary glands, skin, umbilical cord and limb buds [150]. This very heterogenous cell type cannot be classified by a distinct combination of markers, thus a set of minimal criteria is applied for the categorization of hMSCs [151]. These criteria include the plastic adherence in standard *in vitro* cell culture; multipotent differentiation capacity towards adipogenic, osteogenic and chondrogenic lineage; and a set of cellular expression markers – positive for cluster of differentiation (CD) 73, CD90 and CD105, negative for CD14, CD34, CD45 and human leukocyte antigen-DR (HLA-DR). Due to the relatively easy procedure to obtain adipose-derived stromal cells (hADSC), this tissue source gains more importance for clinical applications compared to bone marrow-derived stromal cells (hBMSC) with an invasive and painful procedure [145,150]. Typically, hMSCs have a high capacity for *in vitro* expansion and offer the possibility of cryopreservation. Due to the relatively low demands, hMSCs commonly represent a cell source of choice for *in vitro* adipose tissue applications [146]. It is often reported that *in vitro* differentiated adipocytes derived from hMSCs remain in

a pre-mature state, shown by multilocular lipid vacuoles and gene expression patterns [152]. However, hMSCs show additional properties that are advantageous for clinical applications of reconstructed adipose tissue. A conventional treatment for soft tissue defects and the resulting volume deficit is represented by the transplantation of autologous adipose tissue. Unfortunately, after transplantation the autologous draft volume is decreased up to 60 %, due to a reduced viability of adipocytes caused by the preceding liposuction and an insufficient supply, thereby inducing hypoxia and ischemia [153,154]. For tissue reconstruction, especially the low-invasive isolation of hADSCs and the low immunogenicity mark hMSCs for autologous but also allogeneic implantation, representing a key feature for clinical application. hBMSCs do not express the major histocompatibility complex (MHC) class II that allow the immune escape as an allospecific T cell response is not induced. Similar immunosuppressive properties were shown for ADSCs, which were *in vitro* pre-differentiated ADSCs and implanted to healthy allogenic recipients [155]. A small scale clinical trial revealed that the implanted adipocytes were not rejected by the patient's immune system and thus were classified as clinically safe [156].

The broad applicability of engineered human *in vitro* tissues could be demonstrated. Due to its involvement in many physiological processes, the adipose tissue represents a very important tissue for Tissue Engineering approaches and regenerative medicine. The scope of application ranges from testing of therapeutics, basic research but as it is correlated with the pathophysiology of diseases of civilization, such as obesity and diabetes, it will be important for disease modelling. With the focus of this work on parasitology, the adipose tissue is a niche tissue to developmental stages of various parasites and pathogens, as earlier described. This aspect was addressed in this project.

1.5 Aim of the study

All tissue engineering approaches represent highly interdisciplinary methodologies. For this doctoral research project, tissue engineering is combined with the field of molecular parasitology. Therefore, a cooperation with Dr. Sara Lustigman of the NYBC was established. The parasitology unit of the NYBC is an expert lab for the research of filarial parasites and especially the agent of river blindness. The chair of Tissue Engineering and Regenerative Medicine of the University Hospital Würzburg together with the Fraunhofer ISC Translational Center is experienced in the modelling of human tissues, especially the human skin. Together, this interdisciplinary background was aimed to enable the development of a culture system based on human skin that enables the *in vitro* maintenance and development of *O. volvulus* larvae.

As earlier described, the APOC called for novel therapeutic strategies and testing to enable the control of onchocerciasis [66]. So far, the progress is hindered by the obligation of *O. volvulus* to the human host. Thus, typically applied animal models are insufficient for the propagation of the worms. The 2D culture system enabled the *in vitro* development until the pre-adult L5 stage [29]. These worms could be utilized for drug testing. Nevertheless, for the development of a macrofilaricidal drug, the research requires adult parasites for testing the efficacy. Moreover, the ability to generate adult worms would allow to gain a deeper insight of host-parasite-interaction, which in return could elevate the drug development. The low complexity of the 2D culture system is hypothesized to not match the demands of the developing larvae on signaling and the supply of crucial soluble factors. Hence, an increased biological complexity in a niche-specific manner is hypothesized to deliver the appropriate stimuli that are required for an *in vitro* development of *O. volvulus* larvae. Figure 7A illustrates the *in vivo* situation of the parasite within the skin tissues. The adult parasite is embedded within a highly vascularized subcutaneous nodule. Three major factors were hypothesized to be crucial for the translation from the *in vivo* environment to an *in vitro* culture system to improve the limited survival and development of *O. volvulus*. Importantly, these factors shown in Figure 7B are enabled by Tissue Engineering and were not realizable in the 2D culture system. First, the skin dermal tissue consists of hDF-secreted **ECM (Factor 1)** that is mainly composed of collagens. Hence, a collagen scaffold is to be applied to mimic the

composition of the skin matrix and generate a 3D environment. Second, the skin tissue layers are characterized by **organotypic cell types (Factor 2)**. These skin-specific cells of primary human origin will be included into the culture system – namely hEKs as part of the epidermis, hDFs as the major cell type of the dermis and adipocytes that represent the most prominent cell type in the subcutaneous tissue. Ultimately, a **direct contact (Factor 3)** of tissue components, such as cells and ECM with the larvae is to be generated within the culture system.

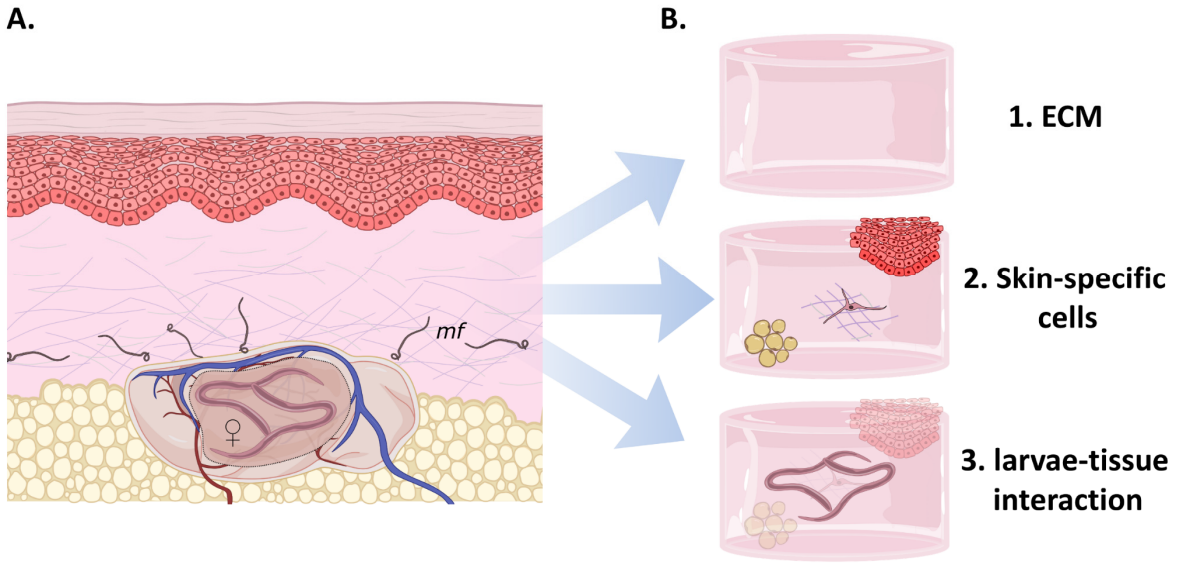

Figure 7: *In vivo* situation of *O. volvulus* and translation to an *in vitro* culture system. A. Schematic illustration of adult *O. volvulus* worms embedded in subcutaneous nodule. The adult female worms produce high numbers of mf that migrate in the surrounding dermal tissue. **B.** Crucial aspects for the translation of the parasite *in vivo* niche to a *in vitro* culture system, namely a 3D ECM scaffold, skin-specific cell types and the direct interaction of *O. volvulus* larvae.

For the achievement of all three factors within a multilayered skin model resembling the human host tissue, the already established and well described FTSM serves as platform for the development of the culture system, thereby representing epidermis and dermis. To model the subcutis, a novel adipose tissue based on adipogenically differentiated hMSCs is to be developed and integrated to the FTSM.

We hypothesize that the crucial factors 1-3 in a 3D multilayered skin model supply the appropriate stimuli to support the larval survival, growth and development, which was shown to be limited in a low complex 2D culture.

2. Material and Methods

2.1 Materials

The following section lists all chemicals, reagents, solutions for cell culture and histology, devices and software that have been applied for this study.

2.1.1 Chemicals and Reagents

Table 1: Applied Chemicals and Reagents and culture media components.

Chemical/Solution	Manufacturer	Product No.
2-Propanol	Carl Roth, Karlsruhe (GER)	6752.2
3-isobutyl-1-methylxanthine (IBMX)	AppliChem, Darmstadt (GER)	A0695
4',6-Diamidin-2-phenylindol (DAPI)	Sigma (USA)	D9542-10MG
Accutase	Thermo Fisher Scientific (USA)	A1110501
Antibiotic-Antimycotic	Thermo Fisher Scientific (USA)	15240062
Antibody dilution buffer	DCS Innovative Diagnostic-System (GER)	AL120R500
Calcium chloride dihydrate	Sigma (USA)	C7902
Descosept	Dr. Schumacher, Malsfeld-Beiseförth (GER)	00-311-050
Dexamethasone	Sigma (USA)	D4902
D-Glucose	Sigma (USA)	G8769
Dimethyl sulfoxide (DMSO)	Sigma (USA)	D2438
Dispase II powder	Thermo Fisher Scientific (USA)	17105041
DMEM high glucose culture medium	Thermo Fisher Scientific (USA)	61965026
DMEM/F12 culture medium	Thermo Fisher Scientific (USA)	31331028
DMEM/F12 culture medium	Thermo Fisher Scientific (USA)	10565018
Donkey serum	Biozol, Eching (GER)	
EGM-2 culture medium	Thermo Fisher Scientific (USA)	Lonza CC-3156
Entellan	Merck, Darmstadt (GER)	107960
Epilife culture medium	Thermo Fisher Scientific (USA)	MEPI-500CA
Ethylenediaminetetraacetic acid disodium salt dihydrate (EDTA)	Sigma (USA)	E5134

Chemical/Solution	Manufacturer	Product No.
Eosin 1 % aqueous	Morphisto, Frankfurt (GER)	10177
Ethanol 99.8 %	Carl Roth, Karlsruhe (GER)	K928.4
Fetal calf serum (FCS)	Biochrom (GER)	S0415
Fetal calf serum (FCS)	Bio&Sell, Feucht (GER)	FBS.EUA.0500
Fetal bovine serum (FBS)	Sigma (USA)	F0926
FGF2 (hbFGF)	R&D Systems, Minneapolis (USA)	233-FB
Fibrolife culture medium	Lifeline cell technology (USA)	LL-0001
Fluoromount-G™ DAPI	Invitrogen, Carlsbad (USA)	SBA-0100-20
Gel neutralization liquid (GNL)	inhouse production	
Hematoxylin solution acidic	Morphisto, Frankfurt (GER)	10231
Human Keratinocyte Growth Supplement (HKGS)	Thermo Fisher Scientific (USA)	S0015
IMDM culture medium	Thermo Fisher Scientific (USA)	31980030
Indomethacin	Sigma (USA)	I8280
Insulin solution human	Sigma (USA)	I9278
Insulin transferrin selenium	Thermo Fisher Scientific (USA)	51500–056
Keratinocyte growth factor (KGF)	Sigma (USA)	K1757
KO-Serum	Thermo Fisher Scientific (USA)	10828-028
L-Ascorbic acid 2-phosphate	Sigma (USA)	A8960
Lipid mixture-1	Sigma (USA)	L0288
MEM-alpha culture medium	Thermo Fisher Scientific (USA)	12571063
NCTC-109 culture medium	Thermo Fisher Scientific (USA)	21340039
Nile Red	Sigma (USA)	19123
Non-Essential Amino Acids	Thermo Fisher Scientific (USA)	11140–050
Oil Red O	Sigma (USA)	O1391
Paraffin	Sigma (USA)	6642.8
Penicillin/Streptomycin	Sigma (USA)	P4333
Phosphate Buffered Saline with $MgCl_2$ and $CaCl_2$ (PBS^+)	Sigma (USA)	D8862
Phosphate Buffered Saline without $MgCl_2$ and $CaCl_2$ (PBS^-)	Sigma (USA)	D8537
Roti-Histofix 4 %	Carl Roth, Karlsruhe (GER)	P087

Chemical/Solution	Manufacturer	Product No.
Saponin 0.2 %		
Serum replacement	Thermo Fisher Scientific (USA)	10828010
Sodium pyruvate	Thermo Fisher Scientific (USA)	11360070
Trypan blue	Sigma (USA)	T8154
Trypsin/EDTA	Thermo Fisher Scientific (USA)	R001100
TWEEN® 20	Sigma (USA)	P1379-1L
Vasculife VEGF-Mv Medium Complete Kit	Lifeline cell technology (USA)	LL-0005
Xylene	Carl Roth, Karlsruhe (GER)	9713

2.1.2 Solutions prepared for cell culture and histological methods

Table 2: Applied solutions for Cell Culture.

Solution	Composition	
0.05 % Trypsin/EDTA	10 %	0.5 % Trypsin-EDTA solution in PBS^-/EDTA-solution
Ascorbat-2-phosphate-solution	73 mg/ml	L-Ascorbic acid 2-phosphate in E1 medium, sterile filtered
$CaCl_2$-solution	44 mg/ml	Calcium chloride dihydrate in ultrapure water, sterile filtered
Dexamethason (stock solution)	10 mM	Dexamethason in 99.9 % Ethanol working solution - 1:10 in 99.9 % Ethanol
Dispase-solution	4 mg/ml	Dispase in PBS^-, sterile filtered
IBMX solution	500 mM	IBMX in DMSO
Indomethacin solution	100 mM	Indomethacin in DMSO
Insulin (stock solution)	10 mg/ml	ready to use working solution - 1:10
KGF-solution	10 µg/ml	KGF in Epilife
MTT-solution	1 mg/ml	MTT in PBS^-

Solution	Composition	
PBS^-/EDTA-solution	0.2 mg/ml	EDTA in PBS^-

Table 3: Applied solutions for Histology.

Solution	Composition	
Blocking solution	5%	donkey serum in antibody dilution buffer
Citrate buffer 1x	10%	Citrate buffer 10x in purified water
Citrate buffer 10x	42 mg/ml 17.6 mg/ml	Citric acid monohydrate sodium hydrogen carbonate in purified water
PBS^- solution 0.5 M	9.55 mg/ml	PBS powder without $MgCl_2$ and $CaCl_2$ in purified water
PBS^- /EDTA-solution	500 ml 0.54 mM	PBS- EDTA
Oil Red O stock solution	0.5 g 100 ml	Oil Red O 2-Propanol
Oil Red O working solution	60% 40%	Oil Red O stock solution in purified water After 24 h filtration
Wash buffer	10% 0.5 %	PBS solution 0.5 M Tween 20 in purified water

2.1.3 Laboratory devices and disposable materials

Table 4: Laboratory devices and disposable materials used for this study.

Device		Manufacturer
Accu-Jet Pro		Brand, Wertheim (GER)
Autoclave		Systec GmbH, Karlsruhe (GER)
Biopsy Pads		VWR International SAS, Radnor (USA)
Cell culture flasks	T175	Greiner BioOne, Frickenhausen (GER)
	T150	TPP Techno Plastic Products AG, Trasadingen (CHE)

Device		Manufacturer
	T75	TPP Techno Plastic Products AG, Trasadingen (CHE)
Cell culture inserts		
Millicell	PIHP01250	Merck Millipore, Darmstadt (GER)
Snapwell Cell culture inserts	3407	Corning Life Sciences, New York (USA)
Corning Transwells	CLS3472	Sigma (USA)
Cell culture plates 6-well 12-well 24-well 48-well 96-well		TPP Techno Plastic Products AG, Trasadingen (CHE)
Cell strainer 100 µm		Greiner BioOne, Frickenhausen (GER)
Centrifuge, Heraeus Multifuge X1R		Thermo Fischer Scientific, Waltham (USA)
Centrifuge tubes 15 ml 50 ml		Greiner BioOne, Frickenhausen (GER)
Cold storage room, 4 °C		Viessmann, Allendorf (GER)
Combitips plus 2,5 ml 5 ml 10 ml		Eppendorf, Hamburg (GER)
Cooling plate, HistoCore Arcadia C		Leica, Wetzlar (GER)
Cover slips		Menzel-Gläser, Braunschweig (GER)
Cryogenic vial (2 ml)		Thermo Fisher Scientific, Dreieich (GER)
Disposable pipettes 5 ml 10 ml 25 ml 50 ml		Sarstedt, Nürmbrecht (GER)
Drying oven 37 °C 60 °C		Memmert, Schwabach (GER)
Duran® laboratory bottles 50 ml 100 ml		Schott, Mitterteich (GER)

Device	Manufacturer
250 ml 1000 ml	
Embedding cassettes	VWR International SAS, Radnor (USA)
EVOS® XL Imaging System	Thermo Fisher Scientific, Dreieich (GER)
Filter paper	Hartenstein, Würzburg (GER)
Fluorescence Microscope BZ-9000	Keyence, Neu-Isenburg (GER)
Forceps	Karl Hecht Assistenz, Sondheim vor der Rhön (GER)
Freeze container (Mr. Frosty)	VWR, Darmstadt (GER)
Gloves Latex Nitril	Hartmann, Heidenheim an der Brenz (GER)
Hioki impedance analyzer	LCR HiTESTER 3522-50, Hioki E.E. Corporation, Nagano (JPN)
Ice machine AF-80	Scotsman, Mailand (ITA)
Incubator, Heraeus BBD 6220	Thermo Fisher Scientific, Dreieich (USA)
Infinite M200	Tecan, Crailsheim (GER)
Keyence microscope Biorevo BZ-9000	Keyence, Osaka (JPN)
Labelling device for cassettes, VCP 6001	Vogel, Senftenberg (GER)
Labelling device for slides, VSP 6001	Vogel, Senftenberg (GER)
Liquid nitrogen tank (-180 °C)	German-cryo, Jüchen (GER)
Microscope slides Superfrost™ Polysine™	Thermo Fisher Scientific, Dreieich (GER)
Microscope, Leica DMi1	Leica, Wetzlar (GER)
Micro scale	Kern, Balingen-Frommern
Microtome, HistoCore AutoCut	Leica, Wetzlar (GER)
Microtome blades A35, R35, S35	Pfm medical, Köln (GER)
Multistep pipette	Eppendorf, Hamburg (GER)
Neubauer chamber	Thermo Fisher Scientific, Dreieich (GER)
Orbital shaker, KM2	Edmund Bühler GmbH, Hechingen (GER)
PAP pen	Dako, Hamburg (GER)

Device	Manufacturer
Parafilm®	Carl Roth, Karlsruhe (GER)
Paraffin Embedding Centre	Leica, Wetzlar (GER)
Pasteur pipettes	Brand, Wertheim (GER)
Petri dish	Greiner BioOne, Frickenhausen (GER)
Pipette research plus 0.5 – 10 µl 20 – 200 µl 100 – 1000 µl	Eppendorf, Hamburg (GER)
Pipette tips 0.5 – 20 µl 2 – 200 µl 50 – 1000 µl	Eppendorf, Hamburg (GER)
Reaction tubes 1.5 ml 2 ml	Sarstedt, Nürmbrecht (GER)
Scalpel	Bayha, Tuttlingen (GER)
Scalpel blades	Bayha, Tuttlingen (GER)
Sterile bench, Safe 2020	Thermo Fisher Scientific, Dreieich (GER)
Sterile filter 0,2 µm	Sartorius, Göttingen (GER)
Serological pipettes 5 ml 10 ml 25 ml 50 ml	Greiner BioOne, Frickenhausen (GER)
Tecan plate reader Infinite 200	Tecan Group, Crailsheim (GER)
Ultrapure water system	MerckMillipore, Darmstadt (GER)
Vortex, Genie 2	Scientific Industries, New York (USA)
Water bath	Memmert, Schwabach (GER)

2.1.4 Software

Table 5: Software applied for analysis and Literature Reference management.

Software	Developer
BZ-II Analyzer 2.1	Keyence, Osaka (JPN)
BZ-II Viewer 2.1	Keyence, Osaka (JPN)
GraphPad PRISM 6.07	GraphPad Software (USA)
Inkscape 1.1	Open Source Scalable Vector Graphics Editor
Image J 1.52a	National Institute of Health (USA)
Mendeley 1.19.8	Mendeley Ltd.
LabVIEW	National Instruments, Austin (USA)
Tecan i-control	Tecan Group, Crailsheim (GER)

2.2 Ethical statement

Primary hEK and hDF used for the generation of skin tissue models were isolated from juvenile foreskin. The biopsies were taken from donors aged between 1 and 5 years under informed consent. hMSCs were isolated from bone marrow of the femur head of osteoarthritis patients undergoing surgical femur head replacement. All cells were obtained according to ethical approval granted by the institutional ethics committee of the Julius-Maximilians-University Würzburg (vote 280/18 and 182/10).

Deidentified leukopak units collected by the NYBC Component Laboratory were used for the isolation of peripheral blood mononuclear cells (PBMCs) for the molting of *O. volvulus* L3 larvae. A written informed consent was collected from all donors. All protocols were conducted according to National Institutes of Health (NIH) guidelines for the care and use of human subjects.

The *O. volvulus* L3 larvae used for this study were isolated following protocols approved by the Le Comité National d'Ethique de la Recherche pour la Santé Humaine, Yaoundé, Cameroon (Protocol 677). Consenting infected donors were exposed to black flies (*Simulium damnosum*) to allow blood meal. After the 6-month duration of their participation in the study the donors were offered ivermectin treatment. After maintenance for 7 days the infected black flies were dissected. The

harvested L3 larvae were washed extensively and cryopreserved before being shipped to the NYBC and further distribution to Würzburg.

2.3 Shipping

For the cooperation between UKW and NYBC in this project and to ensure a continuous work flow in the laboratory, human cells and collagen, as well as media components were sent from Würzburg to New York. *O. volvulus* larvae and PBMCs were sent from the NYBC to Würzburg. The shipments were conducted via air freight according to the International Air Transport Association (IATA) regulations on dry ice, at 4 °C or room temperature.

2.4 Culture media:

The culture of living organisms requires special media to deliver appropriate nutrition and factors for e.g. maintenance, expansion or differentiation. For the *in vitro* culture of *O. volvulus* larvae, stage specific media were applied. L4-H medium lacks the endothelial cell medium EGM-2, which is supplemented for the co-culture of HUVEC feeder layers, and was applied as base medium for skin model co-culture.

Table 6: Culture media for *O. volvulus* larvae and primary human cells.

Culture Medium	Base Medium		Supplementation		Note	
L3 wash medium	50 %	NCTC-109	2x	Antibiotic-Antimycotic		*O. volvulus* culture
	50 %	IMDM				
L4 medium	20 %	NCTC-109	20 %	FBS (Sigma)		
	20 %	MEM-alpha	1x	Antibiotic-Antimycotic	1x larvae supplements	
	20 %	DMEM/F12	1 %	D-Glucose		
	40 %	EGM-2	1 mM	Sodium pyruvate		
			1x	Insulin transferrin selenium		
			0.1 %	Lipid Mixture-1		
			1x	Non-Essential Amino Acids		

Culture Medium	Base Medium		Supplementation		Note	
L4-H medium	30 % 30 % 40 %	NCTC-109 MEM-alpha DMEM/F12	20 % 2x	FBS (Sigma) larvae supplements		
FM Fibroblast medium		DMEM HG	10 % 1x	FCS (Biochrom/Bio&Sell) Penicillin/Streptomycin		Primary human cell culture
E1		Epilife	1x 1x	HKGS Penicillin/Streptomycin		
E10		Epilife	1x 1x 1.44 mM 10 ng/ml 252 µM 10 %	HKGS Penicillin/Streptomycin $CaCl_2$ KGF ascorbic acid Fibrolife		
EM Expansion medium		DMEM/F12	10 % 1x 5 ng/ml	FCS (Bio&Sell) Penicillin/Streptomycin hbFGF		
ADM Adipocyte diff. medium		DMEM HG	10 % 1 µM 1 µg/ml 100 µM 500 µM 1 % 0.1 %	FCS (Bio&Sell) Dexamethasone Insulin Indomethacin IBMX D-Glucose Lipid Mixture-1	ADM+ supplements	

For enhanced lipid accumulation 1 % D-Glucose and 0.1 % Lipid mix were added to the adipocyte differentiation medium (ADM), referred to as ADM+ [71].

2.4.1 Co-culture media supporting human cells and *O. volvulus* larvae:

For the co-culture of more complex human tissue models and *O. volvulus* larvae simultaneously, the culture media has to support the larval fitness, as well as different primary cell types. Therefore, three experimental media combinations of E10 as base medium were gradually supplemented with larvae specific supplements and increased concentrations of FBS usually added to the L4 medium, which is used in the 2D culture system.

Table 7: Composition of experimental co-culture media for *O. volvulus* larvae and human skin models.

Culture Medium		Base Medium		Supplementation		Note
E10	Skin medium	Epilife		E10 supplementation		Co-culture skin model reduction of FBS to 10 %
3D-1			E10	10 %	FBS	
3D-2			E10	10 %	FBS	
				1x	larvae suppl.	
3D-3		50 %	E10	10 %	FBS	
		50 %	L4-H	1x	larvae suppl.	
L4	2D control	L4 medium		1x larvae suppl., 20 % FBS		normal FBS conc. 20 %
L4-H	2D control	L4-H medium		2x larvae suppl., 20 % FBS		

2.5 Culture of primary human cells

Cell culture was performed in Biosafety cabinets class II in a Biosafety S2 laboratory. This work environment is a prerequisite for the handling of primary patient material and cells. Cell cultures were incubated at 37 °C, 95 % humidity and 5 % CO2 under normoxic conditions. Typically, the culture medium was replaced routinely three times per week, on Mondays, Wednesdays and Fridays. Primary human cells were typically centrifuged at 300 g for 5 minutes (min). Cell culture was performed according to standard operating procedures (SOP).

2.5.1 Isolation of cells from human skin:

Juvenile foreskin biopsies were used for the isolation of human skin cells. To exclude microbial contaminations, the biopsy transport medium was incubated overnight as a sterile control. The skin tissue was washed three times with PBS^+, followed by the excision of fat and the conjunctive tissue from the dermis and epidermis. After rinsing with PBS^+, strips of 2-3 mm in width were transferred into a petri dish containing 10 ml of dispase solution and incubated at 4 °C for 16-18 h (hours).

For the isolation of hEK, the epidermal strips were separated from the dermis and cut into small squares that were transferred to a centrifuge tube. After incubation in trypsin/EDTA for 5 min at 37 °C, the enzymatic digestion was stopped by the addition

of 1 ml FCS. The extraction of cells from the digested tissue was supported by applying mechanical forces. Therefore, the suspension was pipetted up and down thoroughly for 5 min, followed by filtration through a 100 µm cell strainer. The resulting cell suspension was centrifuged at 300 g for 5 min. After resuspension of keratinocytes in E1 medium, the cells were cultured for expansion in T175 cell culture flasks with a seeding density of 1-2 x 10^4 cells/cm2 in 18 ml of E1 medium.

For the isolation of hDF, the remaining dermal strips were incubated in collagenase. After 1 h of enzymatic digestion at 37 °C, the solution was centrifuged for the removal of the enzyme mix. After resuspension, the cells were seeded in fibroblast medium (FM) for expansion in T150 flasks.

2.5.2 Culture of human dermal fibroblasts

Culture:

Fibroblasts were cultured within T150 flasks with 20 ml of FM. For passaging of hDF, cells were detached by washing with 10 ml of PBS^-, followed by using 7 ml of 0.05 % trypsin/EDTA solution. After 5 min at 37 °C, the digestion was stopped by adding 1 ml FCS or 5 ml FCS-containing FM to the culture flask. After collecting the cells and rinsing the flask with PBS^-, the cells were centrifuged at 300 g for 5 min, followed by resuspension in an appropriate volume (1-3 ml of FM). The number of detached cells was determined by using a Neubauer chamber and the following equation (1), $\sum 4\ squares$ represents the number of viable cells within the grids of the chamber. Typically, the cells were diluted by factor 10 in trypan blue dye and PBS^-.

$$\frac{\sum 4\ squares}{4}\ x\ chamber\ factor\ (10^4)\ x\ dilution\ factor\ = number\ of\ cells\ /\ ml \qquad (1)$$

hDF were reseeded with 4 x 10^3 cells/cm^2 into T150 flasks. The media is replaced routinely.

Cryopreservation and thawing:

hDF were cryopreserved by adjusting the number of cells to 1 x 10^6 in a volume of 900 µl FM. The cell suspension was then transferred to a cryotubes, followed by the addition of 100 µl DMSO. After gently inverting, the tubes were then stored within a

Mr Frosty at -80 °C for 24 h. The cells were then transferred into liquid nitrogen. hDF were thawed by rapidly warming up the cryotube in the water bath at 37 °C, followed by transfer of the cells to 7 ml prewarmed FM in a centrifuge tube. To remove the remaining DMSO, the cells were centrifuged at 300 g for 5 min and subsequently resuspended in 2 ml FM. The fibroblasts were transferred to a pre-incubated T150 flask with 18 ml FM.

2.5.3 Culture of human epidermal keratinocytes

Culture:

After the isolation, keratinocytes were cultured in T175 flasks in 20 ml E1 until 70-90 % confluency, followed by passaging of the cells. Therefore, hEKs were detached by using Accutase for 10 min at 37 °C. The T175 flasks were rinsed with PBS^- and the cells were centrifuged at 300 g for 5 min. After resuspension in an appropriate volume of E1 (3-5 ml) the cells were counted using a Neubauer chamber. hEKs were reseeded in T175 flasks with a density of $4 \times 10^3/cm^2$.

Cryopreservation and thawing:

Similar to hDFs, keratinocytes were cryopreserved with 10 % DMSO in 1 ml total volume. Typically, 3×10^6 hEK were cryopreserved per cryotube. The cells were transferred into liquid nitrogen for storage. For thawing, prewarmed E1 medium from a centrifuge tube was dispensed onto the frozen cells, followed by three steps of pipetting. The resulting solution was transferred back to the E1 containing tube. This step was repeated until the cryotube was completely thawed. The resulting 8 ml of cell solution was distributed into four pre-incubated T175 flasks, each containing 18 ml E1. Typically, hEKs were thawed on Thursdays, followed by an early media exchange the following day for the DMSO removal. The cells were cultured to 70-90 % of confluency, which was usually reached on Tuesday (5 days).

2.5.4 Isolation of mesenchymal stem cells:

For the establishment of an in-house bio bank, hMSCs were isolated from bone marrow of the femur head of osteoarthritis patients undergoing surgical femur head replacement. All isolated cells were analyzed for the minimal criteria applied for the categorization of hMSCs [151]. These criteria include the plastic adherence in standard *in vitro* cell culture; multipotent differentiation capacity towards adipogenic, osteogenic and chondrogenic lineage; and a set of cellular expression markers – positive for CD73, CD90 and CD105, negative for CD14, CD34, CD45 and HLA-DR.

2.5.5 Culture of human mesenchymal stromal cells

Culture:

Mesenchymal stromal cells from the human bone marrow were cultured with 20 ml expansion medium (EM) in T150 flasks. The cells were cultured with routinely media exchanges until 100 % confluency. Similar to hDF, hMSCs were detached by 7 ml trypsin. After 5 min, the digestion was stopped by the addition of 1 ml FCS or 5 ml of FCS-containing EM. The cells were collected and the flasks rinsed with PBS^-, followed by centrifugation. After cell number determination, hMSCs were reseeded in T150 flasks with a density of $2.5 \times 10^3/cm^2$. For 2D differentiation experiments, hMSCs were seeded into 12-well plates with a density ranging from 1×10^4 – 1×10^5 cells/cm^2 in EM. To initiate the differentiation of hMSCs to adipocytes the medium was changed to ADM on the following day.

Cryopreservation and thawing:

For the cryopreservation typically 1×10^6 hMSCs in EM were mixed with 10 % DMSO and 10 % serum replacement in a total volume of 1 ml. After 24 h at -80 °C the cryotubes were transferred to liquid nitrogen for long-term storage. The cells were rapidly thawed by gently shaking the tubes in the water bath at 37 °C, followed by direct seeding into three T150 flasks. For the removal of DMSO the media can be replaced after cell detachment after roughly 4 h or latest the next day.

2.5.6 Culture of human umbilical vein endothelial cells

HUVECs were cultured for the 2D co-culture with *O. volvulus* L4 larvae. The cells were cultured with 10 ml of Vasculife in a T75 flask until a confluency of 70-90 %. Typically, the cells are detached on Monday using trypsin. 3 x 10^5 cells were seeded into a new T75 flask for the next passage. For the 2D co-culture, 24-well plates were seeded with 1 x 10^4 HUVECs/well. The following day, L4 larvae were transferred from the former co-culture plate on the wells containing freshly seeded HUVECs. The medium was therefore changed to L4 medium. This replacement of HUVEC feeder layers was done every week of larvae co-culture.

2.6 Generation of human 3D tissue models

2.6.1 Full-thickness skin model

After isolation from juvenile foreskin, hDFs and hEKs were expanded followed by cryopreservation. hDFs of passages 3 to 5 were used for the generation of the dermal component of the FTSM. hDFs were detached as described before. The number of cells was determined by a Neubauer counting chamber. One day in advance, pCol (collagen type I, isolated from rat tails) was filled in a syringe, thereby reducing the final amount of air bubbles. The following table 8 shows an example calculation for the mixing ratio of pCol and hDFs in gel neutralization liquid (GNL).

Table 8: Example calculation for collagen-hDF-GNL mix.

Number of FTSM	Hydrogel Volume	Collagen / GNL (2:1)	Number of hDF	hDF/FTSM
12x (15)	10.5 ml	7 ml / 3.5 ml	6.75 x 10^5	4.5 x 10^4
6x (9)	6 ml	4 ml / 2 ml	4.05 x 10^5	4.5 x 10^4

According to the number of models, the desired number of hDF was centrifuged and resuspended in the referring volume of GNL. pCol and GNL were finally mixed in a ratio of 2:1. The alkaline pH of the GNL neutralizes the pCol that was resolved in acidic acid, followed by polymerization of the collagen. The mixing was performed by using two syringes, containing the collagen and the hDF-GNL. The syringes were

connected by a three-way cock and mixed into each other for six times. The resulting neutralized collagen-hDF mix was rapidly transferred to a Multistep pipette for the dispensation of 700 µl per prepared culture insert. The culture inserts were perforated using the needles (0.5 mm) of a Derma Pen to facilitate a better diffusion of the culture medium. The dermal models were incubated for 30 min to let the collagen polymerize. The dermal models were then cultured within 6-well plates with 5 ml of FM for 1 week with routinely media exchanges.

As an optional step, the plastic compression of the dermis generates a highly concentrated collagen construct, resulting in a more mechanically stable dermal model during the culture. As previously described [137,139], the collagen was compressed within the insert using a compression reactor. This tailor-made reactor uses a linear motor or defined weights to produce a plastic compression by stamps pressing equally on the surface of a polymerized hDF containing collagen hydrogel.

After 1 week of culture, the epidermal model was generated on top of the dermis. After detachment of hEKs (p3) 5 x 10^5 hEKs in 250 µl of E10 medium were then seeded on top of the dermal component. After an incubation of 2 h, the cells have attached to the surface of the collagen and 4 ml E10 medium were added to the well. After 24 h, the models were then set to the Air-liquid-interface by removing the supernatant and thereby exposing the epidermal surface to air. The now developing FTSM were cultured for up to 21 days, depending on the experimental application.

2.6.2 3D adipose tissue models

Subcutaneous adipose tissue constructs were developed for the integration into the FTSM with the aim of a three-layered skin model. Stand-alone models of the adipose tissue could also serve for larvae co-cultures. For the generation of adipose tissue models, hMSCs were expanded in 2D, followed by the adipogenic differentiation of the cells within in the 3D collagen scaffold. Different culture setups were based on single hMSCs mixed in collagen as well as cell aggregates.

Collagen-based adipose tissue model:

Similar to the setup of the dermal part of the FTSM, first approaches for the generation of an adipose tissue model were based on the embedding of single hMSCs within a collagen hydrogel. Typically, the models were set up in Millicell inserts, with a final volume of 200 µl, a collagen concentration of approximately 6 mg/ml and a cell density of 3 x 10^6 hMSC/ml. The cell density was further increased for experimentations to a final cell concentration of 9 x 10^6 hMSCs/ml. Therefore, hMSCs were detached and the desired number of cells was resuspended in GNL, prior to be mixed with pCol in the ratio 1:2. For the equal distribution of cells, the mixing was performed using the syringe system (as explained for the FTSM generation) or by gently stirring the GNL-pCol mix using a pipette tip inside the culture insert. After incubation for 30 min, 1 ml of EM was added to the surrounding 12-well and additional 200 µl to the collagen surface. After 24 h, the adipogenic differentiation was initiated by changing the culture medium to ADM. The collagen-based adipose tissue models were cultured for up to 12 weeks with routinely media exchanges.

Scaffold-free culture Aggregate/spheroid

As an alternative to the 3D differentiation of equally distributed cells in collagen, a scaffold-free strategy was established. Therefore, hMSCs were detached and aggregated using a) 1.5 ml Eppendorf tubes or b) Elplasia well plates with microcavities. The applied protocol varied for each method:

a) 1 – 2.5 x 10^5 hMSCs were dispensed to and Eppendorf tube, followed by centrifugation at 300 g for 5 min. The resulting cell aggregate was transferred to a culture vessel using a 1000-µl-pipette, e.g. well plate for analysis or culture insert for further co-culture with *O. volvulus* larvae or adipose tissue modelling.

b) Elplasia plates were prepared according to instructions of the manufacturer. 2 – 4 x 10^4 hMSC/aggregate were seeded into the Elplasia plates with round cavities. A 24-well contains about 554 microcavities – total cell number of 1.1 – 2.2 x 10^6 hMSC were seeded per well in 2.5 ml ADM. After 7 – 10 days without media exchange the formed aggregates were harvested using a 1000-µl-pipette. The aggregates were transferred to culture inserts for the generation of the three-layered adipose tissue FTSM.

2.6.3 Generation of the three-layered skin model

Multilayered skin model consisting of the FTSM and an adipose tissue layer were set up using aggregated hMSCs. After their formation, the hMSC aggregates were placed onto the membrane of the Snapwell inserts, followed by further culture and differentiation. The aggregates attached to the membrane.

After three weeks of differentiation, the dermal model was generated on top of the adipose tissue layer. According to 2.6.1, 700 µl collagen hydrogel with hDF were mixed and plastically compressed. Similar to the FTSM protocol, the adipose tissue-dermis models were cultured in FM for 7 days before the setup of the epidermis and change to E10. After the Airlift, the models were cultured for 21 days with routinely media exchanges. The protocol for the stepwise generation of the multilayered skin model is illustrated in Figure 19.

2.7 Culture of *O. volvulus* larvae

L3 larvae used for the study are of pooled larvae batches that were isolated on one day from infected back flies, followed by cryopreservation. Cryopreserved vials of *O. volvulus* L3 larvae were sent from NYBC to Würzburg on dry ice. For co-culture experiments the larvae were prepared as follows.

2.7.1 Molting of L3 larvae

In the molting assays, the *O. volvulus* larvae were differentiated from the black fly-specific larval stage L3 to the first human-specific stage L4. Therefore, based on the expected recovery of larvae of a L3 batches, 2-4 vials of different batches were thawed for a co-culture experiment. After rapid thawing in the water bath, the L3 larvae were transferred from the cryovial to a 15-ml-centrifuge tube containing 10 ml of pre-warmed L3 wash medium. The larvae were allowed to sediment at room temperature, followed by the gentle removal of the supernatant. After adding again 10 ml of wash medium, the sedimentation was repeated 6 times. After sedimentation, the larvae were centrifuged twice at 1000 g and 10 °C for 10 min.

Determined on the expected number of larvae from the specific batch, the larvae were resuspended in wash medium to a concentration of 200 worms/ml. The larvae suspension was then transferred to a 96-well plate with 50 µl/ well, containing in average 10 worms. Subsequently, PBMCs were thawed in the water bath and resuspended in wash medium with 50 % FCS (2x), followed by the seeding of 1.5 x 10^5 PBMCs/well in 50 µl. Finally, 100 µl of wash medium supplemented with 25 % FCS (1x) is added to each well to a final volume of 200 µl with a final FCS concentration of 25 %. The L3-PBMC co-cultures were incubated for 7-14 days. The molting of larvae from L3 to L4 stages was documented and the molting efficiency determined. L4 larvae can be identified by a characteristic coiling pattern. The molting event can be confirmed by a shed cuticle for each L4 larva per well. The worms were collected in L4 medium while using a light microscope. The fresh molted L4 larvae were further used for the co-cultures with 2D HUVEC feeder layers and 3D tissue models. Figure 8 illustrates the different culture setups that were applied to L4s with a focus on the spatial arrangement of larvae and cells and/or tissue.

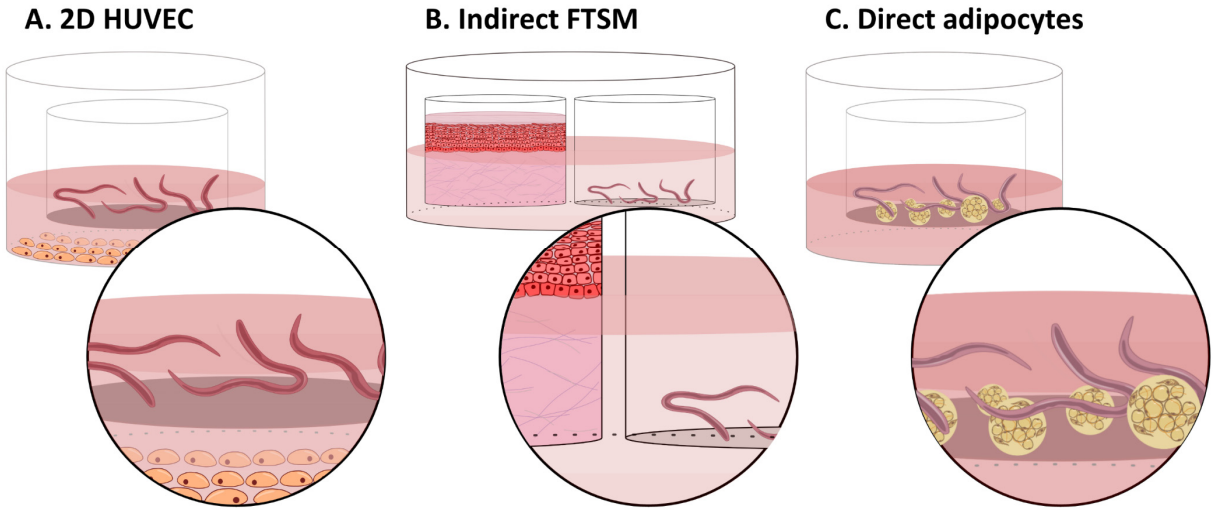

Figure 8: Co-culture setups for L4 larvae. A. Transwell with L4 larvae above a 2D HUVEC feeder layer. **B.** Indirect co-culture with FTSM. **C.** Direct co-culture with aggregated adipose tissue model.

2.7.2 Optimized 2D culture of L4 larvae

After molting from L3, the fresh L4 larvae were transferred to culture inserts and co-cultured above a HUVEC feeder layer in L4 medium, as shown in Figure 8A. Typically, HUVECs were seeded on Monday, followed by the transfer of L4 containing inserts

from the former co-culture plate on the wells containing freshly seeded HUVECs. For the documentation of larval survival and development, the following factors were documented.

2.7.3 Analysis of larvae motility and viability

The length and the motility of the larvae was documented weekly. The motility was observed using a light microscope and scored in four categories:

1) Coiling larvae

2) moving larvae

3) slow moving and already dark appearance

4) not moving/dead (dark appearance)

L4 larvae of category 1 and 2 were considered as viable, whereas categories 3 and 4 were considered as non-motile and dead. The [%-motility] was calculated as the portion of category 1 and 2 of the initial number of L4 larvae. The growth was analyzed by taking images of moving larvae in a position as straight as possible, followed by their length measurement using ImageJ.

2.7.4 Co-cultures of *O. volvulus* larvae and human tissue models

L4 larvae were co-cultured in different setups with human tissue models. A first approach was an indirect co-culture system. These experiments were performed at the NYBC.

Indirect co-culture of L4 larvae and FTSM

As shown in Figure 8B, for the indirect culture setup two Millicell culture inserts were placed in a 6-well, one containing 20 L4 larvae, the other containing a non-compressed FTSM (scaled down from Snapwell to the surface of Millicell). The larvae used for the indirect co-culture setups were 15 days old and precultured on HUVEC

feeder layers for one week. The co-culture media 3D-1 to 3D-3 were used for the culture of larvae and tissues. The best supporting medium was evaluated by analyzing the larvae growth and motility, as earlier described. The con-compressed FTSM was replaced every 4 weeks of culture. The optimized HUVEC co-culture served as the 2D control.

Co-cultures of L4 larvae with adipose tissue models

The adipose tissue aggregates enabled an indirect and direct co-culture setup. Therefore, hMSC aggregates were pre-differentiated for 3 weeks before the larvae co-culture. For the indirect culture, the adipose tissue aggregates were placed on the bottom of 12-wells, for the direct culture inside Millicell culture inserts that were placed in 12-wells (Figure 8C). 14-days old L4 larvae were placed to the aggregates for direct culture or into empty Millicell inserts, which were located above the aggregates. These co-culture setups were maintained in 3D-3 medium. Again, L4 larvae in the 2D culture system served as control. For 5 weeks, the larvae were analyzed for growth and motility, as earlier in 2.7.3.

2.8 Histology

Histological methods aim for a microscopical analysis of cells or on a larger scale also tissues. Therefore, the samples were processed to facilitate various methods of stainings for the analysis of cells from a molecular basis to the macroscopic formation of a tissue.

2.8.1 Chemical fixation of human cells and tissues

The processing of biological samples for histology typically contains a chemical fixation, which was achieved by Histofix (4 % PFA). After washing with PBS^-, 2D cells were covered with Histofix for about 10 min, followed by a replacement of Histofix with PBS^-. These samples can be stored until further use at 4 °C. For human tissues and tissue models, the fixation time was estimated by its thickness. Therefore, after

washing with PBS^- the tissue was submerged in Histofix for 1 h per mm of thickness. FTSM were fixated in Histofix for 2 h or alternatively for about 24 h in 4 °C.

2.8.2 Paraffin embedding and preparation of microsections

To allow micro sectioning of fixated tissue samples, the 3D tissue models were cut of the culture inserts and laid with biopsy pads in an embedding cassette. These cassettes were then transferred to an automated embedding machine. The embedding process relies on the exchange of water towards organic solvents and finally to paraffin. In the solid state, the samples are then able to be cut in micro slices.

Table 9: Program of automated paraffin embedding for the fixation of tissue samples.

Reagent	Duration [h]	Process
dH_2O	2	PFA removal
Ethanol 50 %	1	Dehydration
Ethanol 70 %	1	
Ethanol 80 %	1	
Ethanol 96 %	1	
2-Propanol I	1	
2-Propanol II	1	
2-Propanol-Xylol (1:2)	1	
Xylene I	1	Ethanol removal
Xylene II	1	
Paraffin I	1.5	Paraffin embedding
Paraffin II	1.5	

After the paraffin embedding, the tissue samples were molten. Typically, the samples were cut in the middle using a scalpel and placed with the cutting edge on the base of stainless-steel molds, which were filled with pre-warmed and liquid paraffin. The molds were then allowed to cool down and the paraffin solidifies. The solid paraffin blocks with the sample's cutting edge at the surface were processed at the microtome. For the analysis of the FTSM, multilayered skin and other tissue models, 4 µm slices were cut, whereas 10 – 20 µm slices were cut from adipose tissue models. The microsections were then mounted on microscope slides.

2.8.3 Deparaffinization and rehydration for histological stainings

The tissue slices on the microscope slides were deparaffinized to allow hematoxylin and eosin (HE) staining and immunofluorescence (IF) staining of antigens, as these staining methods are performed in aqueous conditions. Therefore, the microscope slides mounted with tissue slices were incubated at 60 °C for 1 h until the sample surrounding paraffin is melted. A descending ethanol series dissolved remaining paraffin and rehydrates the tissue samples.

Table 10: Rehydration of tissue microsections for further histological analysis.

Reagent	Duration [min]	Process
Xylene I	10	Deparaffinization
Xylene II	10	
Ethanol 96 % I	3x dip in/out	Rehydration
Ethanol 96 % II	3x dip in/out	
Ethanol 70 %	3x dip in/out	
Ethanol 50 %	3x dip in/out	
purified water	wash until no turbulence	Ethanol removal

2.8.4 Hematoxylin and eosin staining of tissue micro slices

The microscopic analysis of a HE staining delivers a sufficient overview of tissue morphology and cellular characteristics. The hematoxylin stains the cell nuclei purple-blue, whereas the eosin colorizes the cytoplasm and ECM in pink. Thus, this staining method is often used for pathology to gain a general overview of an organ or tissue and to recognize distinct changes, e.g. indicating a tumor formation. After rehydration by the descending ethanol series, the tissue slices underwent the following staining protocol.

Table 11: Protocol for HE staining of rehydrated tissue microsections.

Reagent	Duration [min]	Process
Hematoxylin	6	Nuclei staining
dH_2O	wash until no dye is released	Removal of remaining dye
Tap water	5	Increasing pH
Eosin	6	Cytoplasm staining

Reagent	Duration [min]	Process
dH_2O	wash until no dye is released	Removal of remaining dye
Ethanol 70 %	2x dip in/out	Dehydration by ascending alcohol series
Ethanol 96 %	2	
Propan-2-ol I	5	
Propan-2-ol II	5	
Xylene I	5	Ethanol removal
Xylene II	5	

After the completed HE staining, the samples were again dehydrated by the ascending ethanol series, finally incubated with xylene. For protection and sealing, the tissue slices were mounted with entellan, a non-aqueous mounting medium, followed by covering the microscope slides with a glass cover slip.

2.8.5 Immunohistological analysis of cellular antigens

For immunohistological staining of samples, the tissue slices were placed on polysine-coated microscope slides for an increased adhesion of the tissues. The samples were rehydrated using the ascending ethanol series, followed by encircling the tissue slice with a hydrophobic pen (PAP pen). This allows the application of small volumes directly on the tissue sample. For the staining procedure, the microscope slides were incubated in a dark chamber. Unspecific binding of antibodies was prevented by the application of 5 % serum of the secondary antibody species or 5 % BSA solution. After discarding the blocking solution, the slices were incubated over night with the primary antibody solution. The dilution factor was antibody-specific. After the incubation, the primary antibody solution was removed and the samples were washed three times for 5 min in wash buffer on the shaker. Subsequently the secondary antibody solution was applied with a dilution factor of 1:400. After 60 min of incubation in the dark, the samples were again washed three times in wash buffer. The tissue slices were directly covered with Fluoromount-G, an aqueous mounting medium containing 4′,6-Diamidin-2-phenylindol (DAPI), a blue fluorescent DNA dye. After sealing the slices with cover slips, the microscope slides were stored in the dark at 4 °C.

2.8.6 Oil Red O staining

For the staining of intercellular lipids, Oil Red O represents a commonly used dye. As a lysochrome it is a lipophilic dye, thereby staining lipids, triglycerides and fatty acids. The powder is prepared as a stock solution – 0.5 g in 100 ml of 99 % 2-propanol. For the working solution, six parts of the stock were mixed with four parts of dH2O and incubated for 24 h, followed by filtration. The Oil Red O dye was applied on fixated cells and tissues, and by lysis of the cells with 2-propanol, the dye could be detected by measuring the maximal light absorbance at 518 nm. Thus, Oil Red O was also used for the quantitative analysis of the lipid content of adipocytes.

Oil Red O staining of 2D differentiated adipocytes

For the pre-evaluation of cell culture media, supplements and culture factors, such as cell density, differentiation experiments were performed in 2D culture. Therefore, hMSCs, typically cultured in 12-wells were fixated using Histofix, subsequently followed by the staining protocol, shown in Table 12.

Table 12: Staining of intracellular lipids with Oil Red O in 2D cultured adipocytes.

Reagent	Volume [µl]	Time [min]	Process
PBS^-	1000	-	Rinsing
PFA (4 %)	-	10	Fixation
dH_2O	1000	-	Washing
2-Propanol (60 %)	800	5	Organic Solvent incubation
Oil Red O staining solution	400	10	Staining
2-Propanol (60 %)	800		Removal of dye
dH_2O	1000		Washing

At this stage, a microscopic observation could take place, by using a microscope. For the quantification of the accumulated lipid content, the cells were lysed by applying 800 µl of 99 % 2-propanol. After 5 min incubation on a shaker, duplicates of 200 µl were measured for the maximum adsorption at 510 nm using the Tecan plate reader.

Oil Red staining of 3D adipose tissue models

The lipid detection of 3D tissue models was examined in 24-well plates. Therefore, after washing and fixation, the following protocol was applied.

Table 13: Staining of intracellular lipids with Oil Red O in 3D adipose tissue models.

Reagent	Volume [µl]	Time [min]	Process
PBS^-	1000	-	Rinsing
PFA (4 %)	-	60	Fixation
dH_2O	1000	-	Washing
2-Propanol (60 %)	800	5	Organic Solvent incubation
Oil Red O staining solution	800	90 – 120	Staining
2-Propanol (60 %)	800	2	Removal of dye
dH_2O	1000	-	Washing

A quantification of the lipid content for 3D models was not done, as the lysis of cells within the collagen hydrogel was not consistent and has not been established.

2.8.7 Nile Red staining of adipocytes

Nile Red enables the specific detection of lipids as the lipophilic dye emits fluorescent light at a maximum of 553 nm in an organic solvent or lipophilic environment. For the staining of 2D cultured cells and 3D tissue models, the following staining solution was prepared. 1 µg/ml of Nile Red and 1 µg/ml DAPI in PBS^- were mixed with 0.2 % saponin. For 3D adipose tissue models, 1 ml of staining solution was added to the 24-well that contains the fixated tissue and incubated over night at 4 °C. Prior the microscopic analysis using a fluorescence microscope, the models were washed with PBS^- for three times.

Maturation analysis of differentiating adipocytes within the collagen hydrogel

During the differentiation of adipocytes, pre-adipocytes accumulate lipids that are stored in vacuoles. With the ongoing maturation, these lipid containing vacuoles fuse, resulting in a unilocular vacuole. This maturation progress was observed by using Nile Red/DAPI for the staining of adipocytes, followed by the analysis of vacuole number and size per cell. Therefore, 3 tile-scan pictures of 6 tiles were taken

of collagen-based adipose tissue models that were cultured until 6 to 12 weeks using the Leica fluorescence microscope. These pictures could serve for the count of nuclei (DAPI) and the number matured unilocular adipocytes (Nile Red), resulting in the adipocyte maturation rate. To depict the maturation progress, the number and the diameter of lipid containing vacuoles per cell were analysed using ImageJ for length measurements.

2.9 Statistics

Data from worm growth were recorded in a weekly routine to monitor the differences between larvae cultured in the 2D culture system and the experimental 3D culture conditions. Significant changes in the length of larvae were tested using Mann-Whitney U test for comparison of each group from the start to the end of culture in this system ($P < 0.0001$: ****) and using ANNOVA with Dunnet's analysis for comparison of the experimental 3D groups to the 2D cultured worms at D93 ($P \leq 0.001$: ***; $P < 0.0001$: ****). Other statistical analyses are stated in the figure captions. The analysis was performed with Graphpad Prism (Version 6.07).

3. Results

The development of a culture system for *O. volvulus* larvae based on human *in vitro* skin was initiated by the establishment of protocols for a 3D adipose tissue model. This first step was thought to enable the generation of a multilayered skin model composed of three layers – epidermis, dermis and subcutaneous adipose tissue. The well-established FTSM was aimed to be augmented by a fatty tissue layer. Therefore, hMSCs derived from bone marrow were applied as cell source, representing a cell type with great proliferative capacities and the ability of adipogenic differentiation. The cells derived from an in-house Biobank containing hMSCs of multiple donors that were evaluated for the characterization criteria of mesenchymal stromal cells.

3.1 Development of an adipose tissue model

First culture approaches of hMSCs were performed in 2D and aimed for the optimization of the differentiation to adipocytes. Here it needs to be mentioned, that experiments for the adipose tissue model development were performed with ADM and ADM+, as the beneficial effect of the additional supplementation was explored to a later time point.

Defining factors for the optimization of adipogenesis of hMSCs

The cell density of hMSCs during the differentiation is a well described factor that promotes the adipogenic lineage development in ADSCs [149]. Thus, the cell-density dependency was analyzed for the hBMSCs from the in-house Biobank. The cells were seeded with initial densities of 5×10^3, 2.5×10^4, 5×10^4, and 1×10^5/cm^2. After 24 h in EM, the adipogenic differentiation was initiated by ADM. The cells were analyzed weekly by an Oil Red O staining. Figure 9A shows the microscopic analysis of the intracellular lipid accumulations within differentiating hMSCs on day 7, 14 and 21. The staining reveals the typical 2D morphology of differentiating adipocytes comprised of multilocular lipid vacuoles. An increased seeding density resulted in an enhanced Oil Red O staining of cells from day 7 on. In contrast, hMSCs cultured in EM as the negative control (NC) showed no positive Oil Red O signal (Figure 9B). Whereas only single cells differentiated with a seeding density of 5×10^3 and

2.5 x 10^4/cm^2 after 21 days, hMSCs seeded with 5 x 10^4 and 1 x 10^5/cm^2 showed an extensive red staining of intracellular lipids. For each time point and seeding condition, the Oil Red O staining was quantitatively analyzed (Figure 9C). The photometric analysis by the measurement of absorption of light at 410 nm confirmed the result of the microscopic analysis. Compared to 5 x 10^3/cm^2 the Oil Red O signal was 6.4-fold increased for cells differentiated with a density of 2.5 x 10^4/cm^2, 9.3-fold increased for 5 x 10^4/cm^2 and 11.7-fold increased for 1 x 10^5/cm^2 after 21 days.

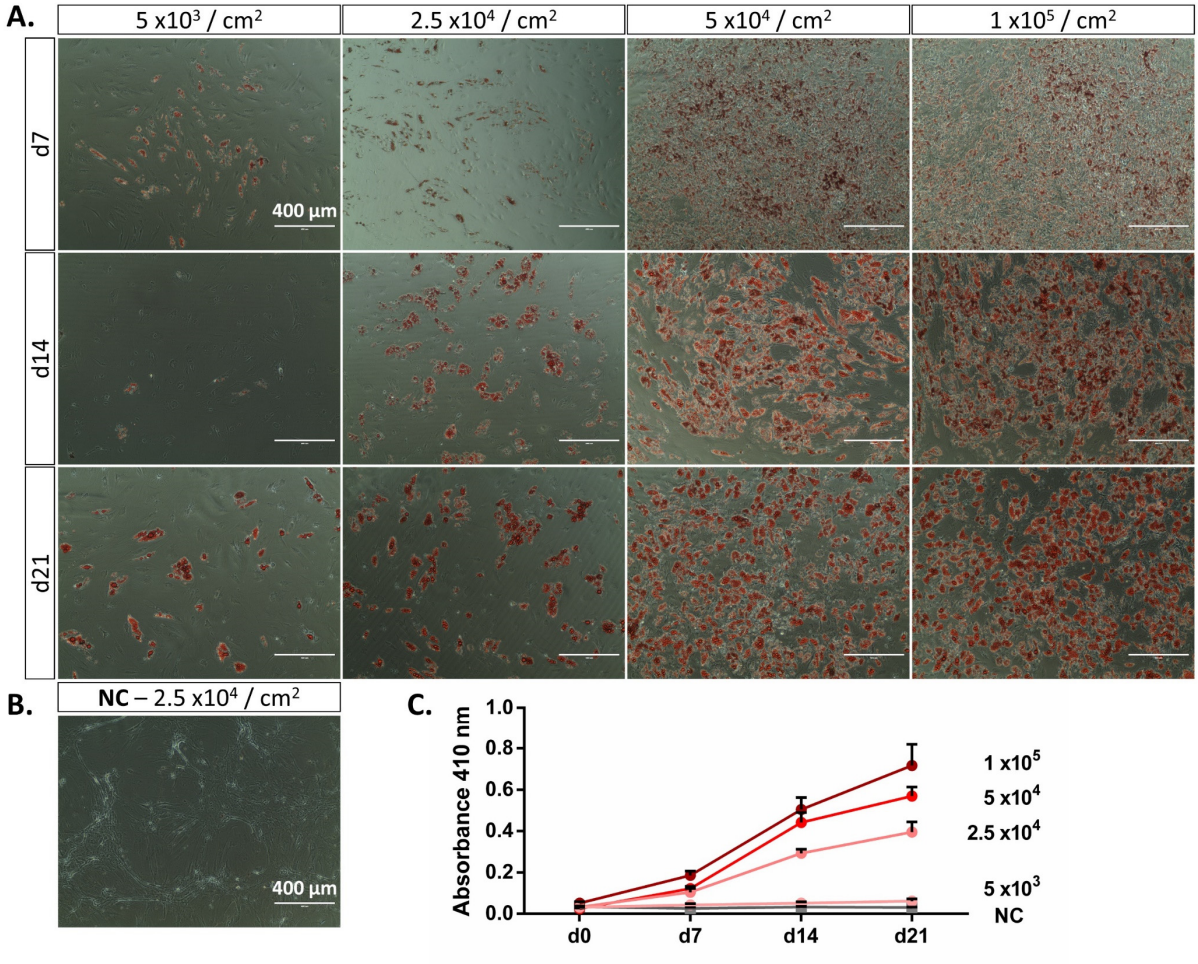

Figure 9: Cell density dependency of differentiating hMSCs in 2D culture. A. Time course experiment of adipogenic differentiation in dependency of seeding density. hMSCs seeded with cell densities of 5 x 10^3, 2.5 x 10^4, 5 x 10^4 and 1 x 10^5/cm^2 were stained for intercellular lipids with Oil Red O on day 7, 14 and 21. Scale bar = 400 µm. **B.** Negative control – hMSCs were maintained in EM for 21 days. No intracellular lipids were detected. Scale bar = 400 µm. **C.** Quantification of intracellular lipids. The semiquantitative analysis of Oil Red O-stained lipids depicts an increased lipid content with a rising cell density.

The dependency of cell density and differentiation efficiency led to the utilization of 5×10^4 hMSCs/cm^2 for further 2D experiments as this seeding density achieved a comparable high differentiation efficiency and allows larger experiments regarding the number of cells retrieved from a typical expansion culture of hMSCs. The differentiation of hMSCs was initiated by the change of culture medium to ADM containing the differentiation factors Dexamethason, 3-isobutyl-1-methylxanthine (IBMX), Indomethacin, and Insulin. To allow a higher rate of lipid accumulation during the lipogenesis, additional energy was supplemented as D-Glucose and a defined mixture of lipids in ADM+. Figure 10A-B shows the microscopic analysis of Oil Red O-stained adipocytes cultured in ADM and ADM+ and the NC. After 21 days of culture, differentiating adipocytes maintained in ADM+ contained more intracellular lipid vacuoles, as shown in the inset. The increased nutritional supply resulted in an enhanced storage of lipids. This observation was confirmed by the quantitative analysis of the Oil Red O signal by the photometric analysis of light absorption at 410 nm (Figure 10C). The graph depicts the lipid content of the cells cultured as NC and ADM+ normalized to the absorption of cells in ADM on day 21. The lipid content of adipocytes differentiated in ADM+ was significantly increased to 237 % compared to the ADM condition.

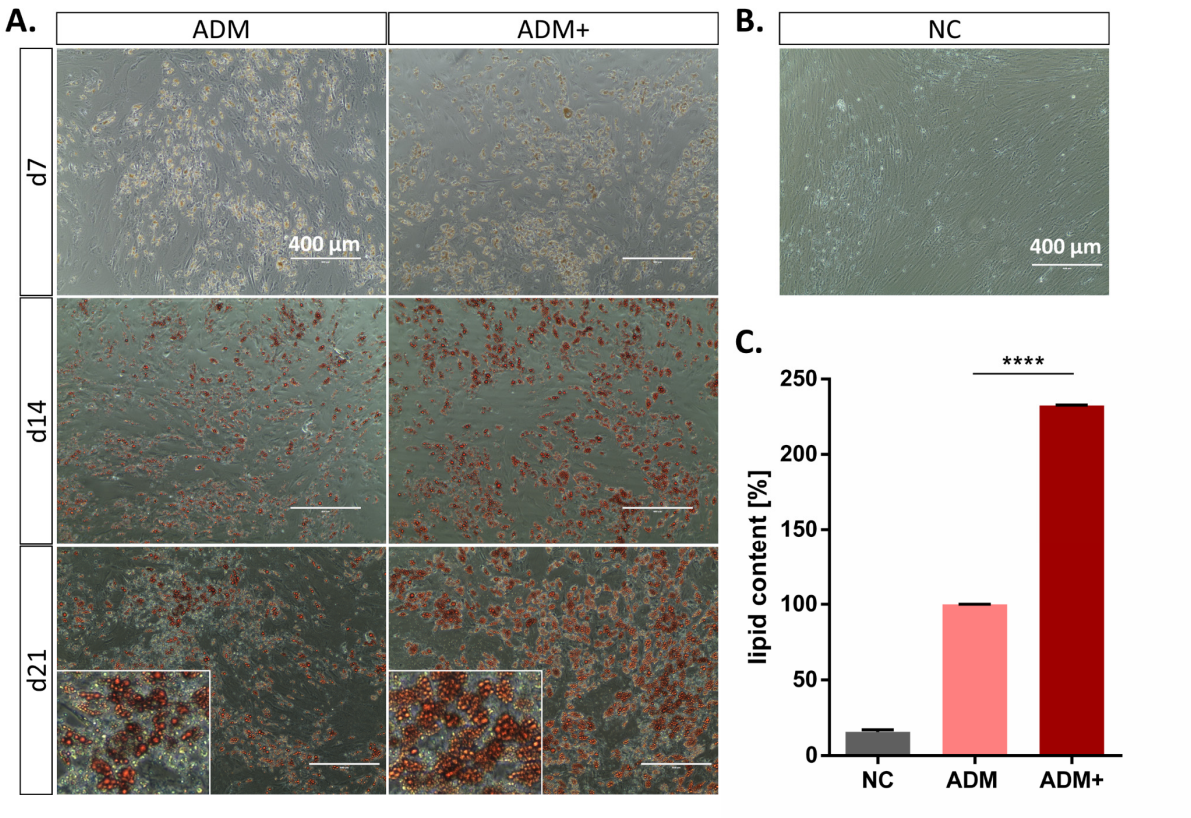

Figure 10: Enhanced accumulation of intracellular lipids by ADM+. A. Time course experiment of 2D adipogenic differentiation with ADM and ADM+ supplemented with additional D-Glucose and lipids. The seeding density is 5 x 10^4 cells/cm^2. Cells were stained with Oil Red O on day 7, 14 and 21. Scale bar = 400 µm. **B.** Oil Red O staining of negative control of adipogenic differentiation. After maintenance in EM for 21 days, no intracellular lipid vacuoles were detected after Oil Red O staining. Scale bar = 400 µm. **C.** Quantification of intracellular lipid accumulations of cells cultured in EM (NC), ADM and ADM+ on day 21. The measured absorption at 410 nm was normalized to the standard medium ADM. Unpaired t-test: ADM-ADM+ ****, p-value < 0,0001.

The results on the optimization of adipogenesis in 2D culture were translated towards the 3D culture of hMSCs in order to generate an adipose tissue model.

3D differentiation of hMSCs in collagen hydrogels

Similar to the dermal part of the FTSM, collagen hydrogels were applied to provide a 3D scaffold for the differentiation of hMSCs. As shown in 2D, the cell density-dependency was a crucial aspect for a sufficient adipogenic differentiation efficiency. This finding was translated to the seeding density of hMSCs on the collagen scaffolds. Thus, to find the optimal cell density hMSCs were seeded with densities of 0.5 x 10^6, 1 x 10^6, 1.5 x 10^6, 3 x 10^6, 6 x 10^6 and 9 x 10^6 cells/ml of collagen. The 3D constructs were cultured in ADM for 14 days followed by histological analysis.

Figure 11 shows microscopic images of HE-stained microsections. After 2 weeks, the differentiating adipocytes contain multiple lipid vacuoles, the morphological feature of early adipocytes (shown in insets).

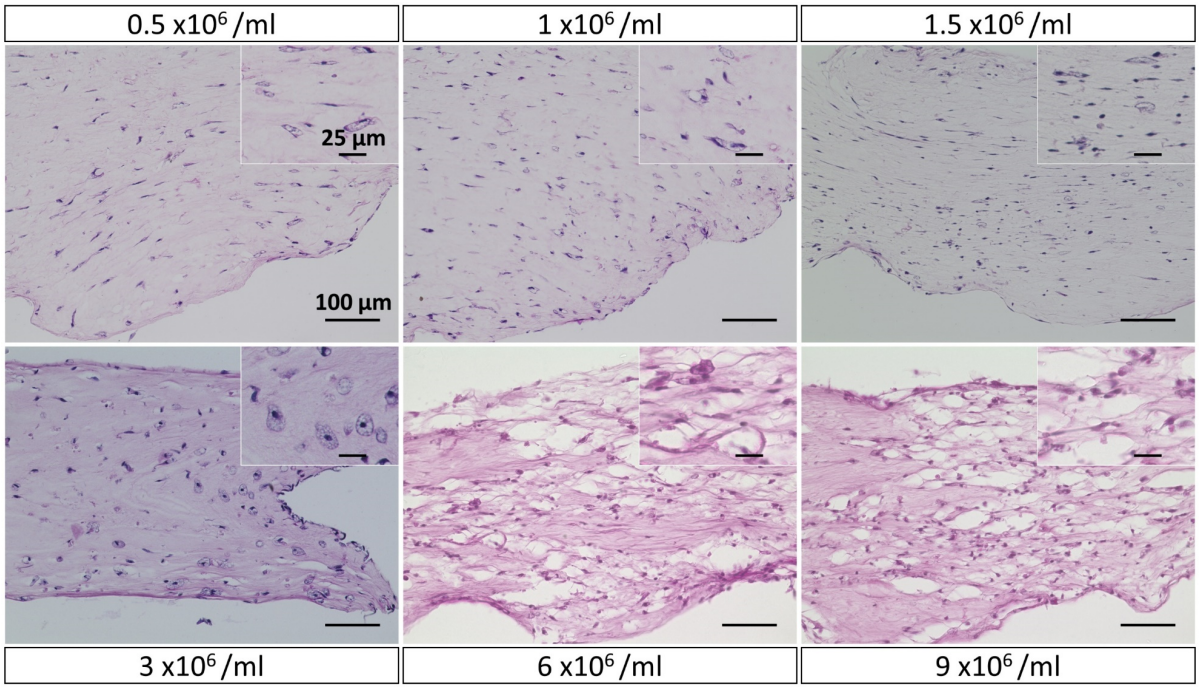

Figure 11: Adaption of cell density from 2D culture to the 3D collagen-based model. Microscopic images of HE-stained 3D collagen scaffolds seeded with increasing cell densities per volume (cells/ml of collagen hydrogel) after 2 weeks of differentiation in ADM. The inset shows a higher magnification showing the cell morphology of differentiating adipocytes within the collagen. Scale bar = 100µm, Inset Scale bar = 25 µm.

A density of 3 x 10^6 cells/ml of collagen shows an even distribution of differentiating adipocytes without cellular contact. The spatial distance of cells was higher compared to the higher cell concentrations of 6 x 10^6 and 9 x 10^6. However, the high cell numbers impede the practicability to perform experiments, as the required number of cells exceeded the yield of cells from typical expansion cultures of hMSCs. Thus, the following experiments were performed with 3 x 10^6 cells/ml. Figure 12A demonstrates the setup of the 3D collagen-based adipose tissue model within a cell culture insert and submerged in ADM+.

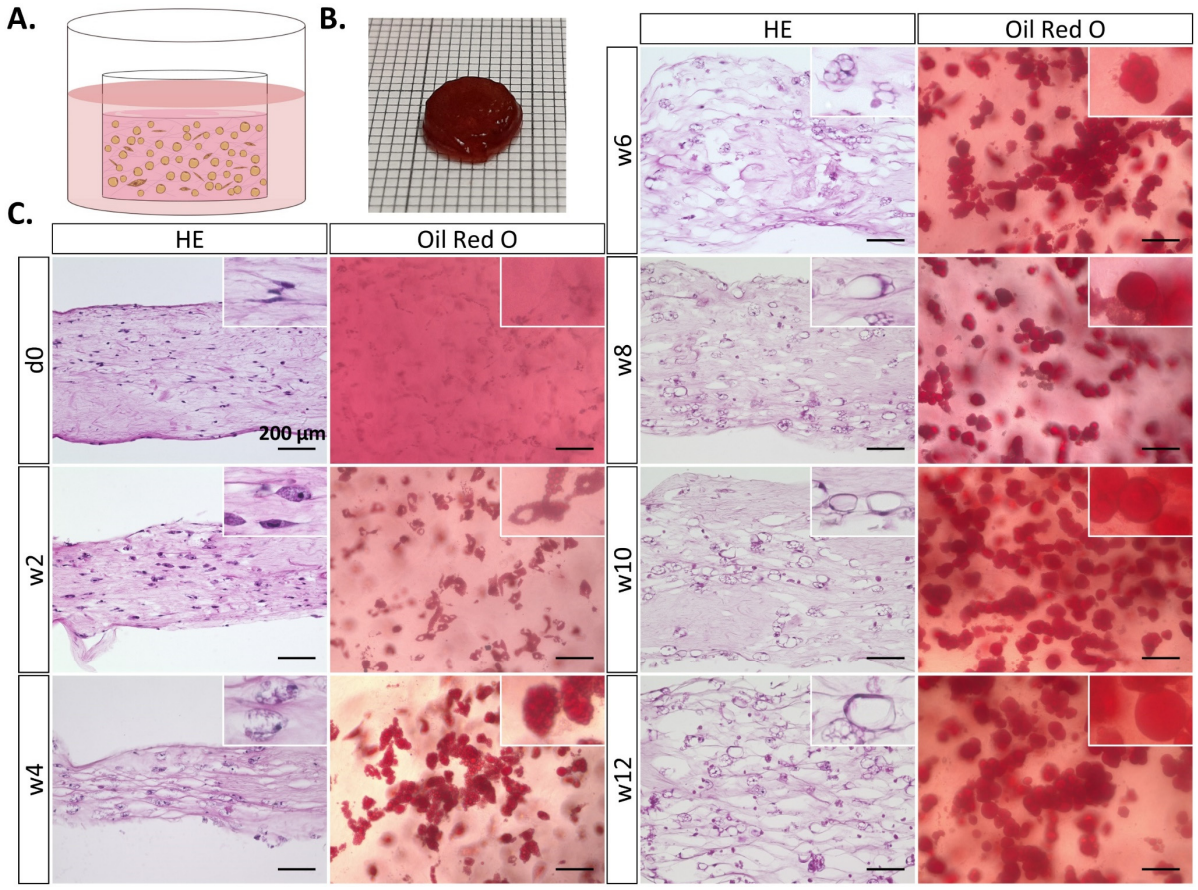

Figure 12: 3D adipose tissue model based on differentiation of hMSC embedded in a collagen hydrogel. **A.** Schematic illustration of the collagen-based adipose tissue model cultured submerged within a tissue culture insert. **B.** Macroscopic picture of a collagen-based adipose tissue model after 9 weeks of culture and Oil Red O staining. **C.** Time course experiment of adipogenically differentiating hMSCs in 3D collagen hydrogel on day 0, after 2, 4, 6, 8, 10 and 12 weeks of culture in ADM+. Microscopic analysis after HE staining demonstrates the cell distribution within the model also showing an enlargement of lipid containing vacuoles from week 4 (identifiable as holes - insets). The progressing accumulation of intracellular lipids was confirmed by Oil Red O staining of the adipose tissue models demonstrated by the increased number and size of stained lipid vacuoles within the differentiating adipocytes. A detailed image is shown in the insets. Scale bar = 200 µm.

hMSCs are mixed homogenously with the collagen during the setup procedure. After 24 h of pre-culture in EM, the differentiation was initiated with ADM+. A macroscopic image of an Oil Red O-stained 3D adipose tissue model after 9 weeks of culture is shown in Figure 12B. The mechanical integrity of the long-term cultured *in vitro* tissues was also confirmed by the histological analysis over a culture period of 12 weeks (Figure 12C). The HE staining depicts an increasing number and size of lipid vacuoles within the differentiating adipocytes. These vacuoles are typically recognizable as holes in the scaffold, because the lipid content is washed out during

the solvent treatment of the paraffin embedding process for the histological analysis. However, these lipids accumulations were detected by the Oil Red O staining that confirmed the adipogenic differentiation of hMSCs within the 3D collagen hydrogel. The microscopical analysis of both histological techniques demonstrated an elongated morphology on day 0. After 2 weeks of differentiation, the HE-stained cells have an enlarged cytoplasm surrounding the centrally located nuclei. Accordingly, the Oil Red O staining of the differentiating hMSCs detected intracellular lipids with a centered nucleus, here recognized as a gap. The size of the lipid vacuoles was increased after 4 weeks of culture, showing multilocular adipocytes. As demonstrated by both stains, HE and Oil Red O, the growth and fusion of intracellular lipid vacuoles progresses from week 6 to week 12 of culture. After 8 weeks, the histological images display adipocytes with a single lipid vacuole and a peripherally located nucleus. The number of these unilocular adipocytes rises until the end of culture. This process of vacuole fusion and growth due to lipid storage towards a unilocular adipocyte is a characteristic morphological feature. To enable the observation of adipocyte maturation within the 3D collagen-based adipose tissue model, scan image analysis of fluorescently labeled cells was performed. Therefore, the adipose tissue models were stained with Nile Red for the detection of lipids and DAPI for the labeling of DNA. The imaging via fluorescence microscopy facilitated the analysis of the ratio of nuclei (DAPI-signals) to unilocular adipocytes (single Nile Red-positive vacuoles). As demonstrated in Figure 13A, the number of unilocular adipocytes increased, indicated by the yellow arrows. White arrows mark

differentiating early adipocytes. Accordingly, the maturation rate of adipocytes was estimated from week 6 to week 12 of culture (Figure 13B).

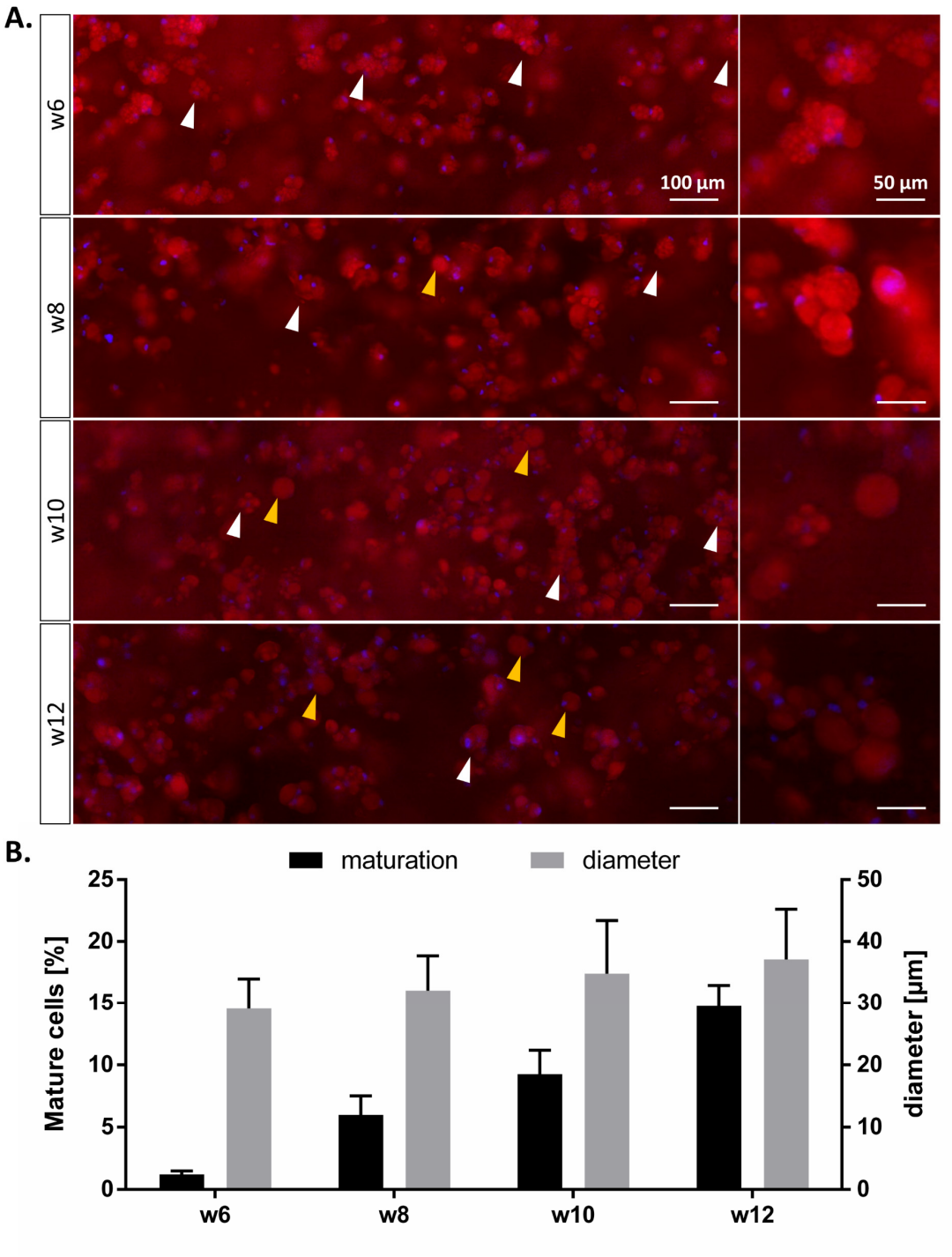

Figure 13: Maturation of adipocytes within the collagen-based adipose tissue model.

Figure 13: Maturation of adipocytes within the collagen-based adipose tissue model. A. Nile Red staining demonstrates the progression of adipocyte maturation from week 6 to week 12 of culture in ADM+. Differentiating early adipocytes containing multiple lipid vacuoles are marked by white arrows, unilocular matured adipocytes by yellow arrows. Scale bar = 100 µm. The right panel contains a higher magnification. Scale bar = 50 µm. **B.** Quantitative analysis of adipocyte maturation rates and cell size from week 6-12 of culture based on the Nile Red staining appearance.

The percentage of unilocular adipocytes increased from 1.23 % after 6 weeks to 6 % in week 8, 9.26 % in week 10 and finally reached 14.73 % after 12 weeks of culture. In the same time, the mature cells grew from 29.07 µm in mean diameter after 6 weeks to 34.080 µm in week 10. Eventually the adipocytes were found to have a final mean diameter of 37.09 µm.

Besides the morphological changes of differentiating adipocytes, molecular markers of adipogenesis were analyzed during the hMSC differentiation in the 3D adipose tissue model. Therefore, the adipose differentiation-related protein or Perilipin-2 (ADFP), and the pro-adipogenic transcription factor PPARγ were analyzed for their cellular localization via immunofluorescence labeling. Figure 14A shows microscopic images of antibody-mediated fluorescent staining of PPARγ from day 0 of culture to week 12 of differentiation. In the early culture phase, PPARγ in yellow was co-localized with the DAPI signal in cyan, indicating a nuclear localization highlighted by the yellow arrows. After 4 weeks of differentiation, the yellow PPARγ signal was more diffuse, and from week 6, a cytoplasmic localization was seen as indicated by the white arrows. The cytoplasmic signal was relatively weak but covered the areas of the adipocytes cross-sections, which can be assigned as cytoplasm. This was demonstrated by a merged two-part image of the fluorescent and brightfield channel showing an adipocyte in week 6 of differentiation. The immunofluorescent analysis of ADFP revealed a cytoplasmic localization of the protein from day 0 to the end of differentiation after 12 weeks (Figure 14B). Until week 4, the magenta ADFP signal surrounded the cyan DAPI signal. After 6 weeks, the ADFP was shown to co-localize with the structures of the lipid vacuoles indicated by the yellow arrows. According to the maturation analysis in Figure 13 the lipid-containing vacuoles were shown to increase in size. Here, the morphological feature of a peripheral nucleus is clearly recognizable from week 6 by the cyan DAPI signal and highlighted by the white arrows. Again, a two-part image of the fluorescent and brightfield channel demonstrates the localization of the fluorescent signals of ADFP and the nucleus of

an adipocyte within the surrounding collagen scaffold after 10 weeks. Confocal microscopy was applied to generate an overview of adipocytes within the collagen based adipose tissue model immunofluorescently labeled for the ECM protein collagen type III (Col III) and α-Smooth muscle actin (αSMA) (Figure 14C).

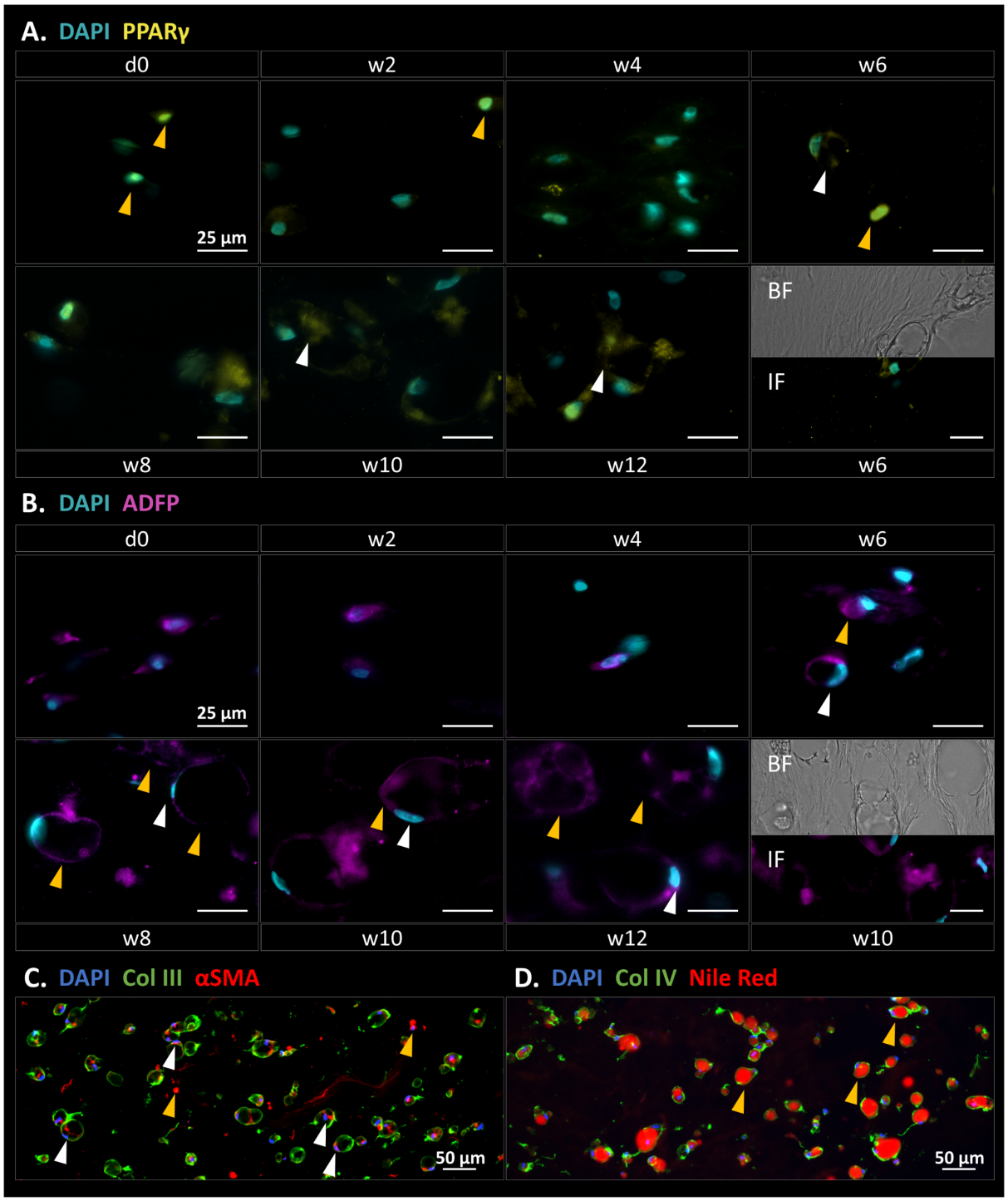

Figure 14: Marker analysis of differentiating adipocytes in collagen-based adipose tissue model.

Figure 14: Marker analysis of differentiating adipocytes in collagen-based adipose tissue model. A. Immunofluorescence staining of PPARγ (yellow) of differentiating adipocytes on day 0, after 2, 4, 6, 8, 10 and 12 weeks. The yellow arrows indicate the colocalization of PPARγ and nucleic DNA in early differentiating adipocytes (d0 – w6); white arrows indicate the cytoplasmic localization of PPARγ with ongoing culture. A combined brightfield image demonstrates the localization of the cell within the collagen environment after 6 weeks. Scale bar = 25 µm. **B.** Immunofluorescence staining of ADFP of differentiating adipocytes on day 0, after 2, 4, 6, 8, 10 and 12 weeks. ADFP (magenta) surrounds nuclei (cyan) of early differentiating adipocytes (d0 – week 4 – 6) and depicts lipid containing vacuole structures of maturing adipocytes (week 6 – 12, yellow arrow). The white arrows highlight the characteristic peripheral nuclei of a mature adipocyte from week 6 of culture on. A combined brightfield demonstrates the localization of the cell within the collagen after 10 weeks. Scale bar = 25 µm. **C.** Immunohistological analysis of Collagen III and αSMA within differentiating adipocytes. Scale bar = 50 µm. **D.** Immunohistological analysis of Collagen IV and staining of intracellular lipid vacuole with Nile Red. Scale bar = 50 µm.

The image shows the green Col III signal surrounding the maturing adipocytes that can be recognized by large single and double vacuole structures. A αSMA signal in red was shown to be localized in differentiating adipocytes in the vicinity of the nuclei (DAPI – blue), marked by white arrows and in non-differentiated hMSCs shown by yellow arrows. The localization of the ECM component collagen type IV (Col IV) was co-analyzed with the position of intracellular lipids by Nile Red staining. The confocal microscopy revealed that the green Col IV signal is found surrounding the adipocytes with a Nile-Red positive lipid vacuole and a peripheral nucleus, marked by yellow arrows.

An alternative strategy for the generation of adipose tissue models independent of a 3D scaffold was examined.

Scaffold-free creation of adipose tissue models

The 2D differentiation experiments revealed a cell density-dependent efficiency for the adipogenesis of hMSCs. To enable a high cell density without spatial distance of 3D cultured stromal cells, hMSCs were aggregated prior to the adipogenic differentiation. The differentiating hMSC aggregates increased macroscopically recognizable in size until day 22 of culture compared to the aggregates cultures as NC in EM as shown in Figure 15A. This growth was analyzed by the measurement of the area of cell aggregates cultured in cell culture wells (Figure 15B). The aggregates cultured in EM were 1.1 mm^2 in diameter on day 4 of culture, reached a minimum on

day 13 with a diameter of 0.76 mm² and a maximum of 1.21 mm² on day 22. In contrast, the differentiating hMSC aggregates had a diameter of 1.38 mm² on day 4 and reached a maximum of 2.67 mm² on day 11, a 1.9-fold increase in the area size. Until the end of culture, the average diameter of the aggregates decreased to 1.94 mm² on day 22. The histological analysis demonstrates the morphological appearance of hMSCs in the aggregated culture (Figure 15D) on day 22 of culture. Whereas the aggregates maintained in EM show densely packed cells, the aggregated cells cultured in ADM differentiated as the lipid vacuoles and peripheral nuclei demonstrate (detailed image in insets). This principle was adapted for the generation of adipose tissue models independent of a scaffold material for a 3D environment. Figure 15C illustrates the setup of a scaffold free adipose tissue model, composed of differentiating adipocytes within a culture insert and submerged by culture medium.

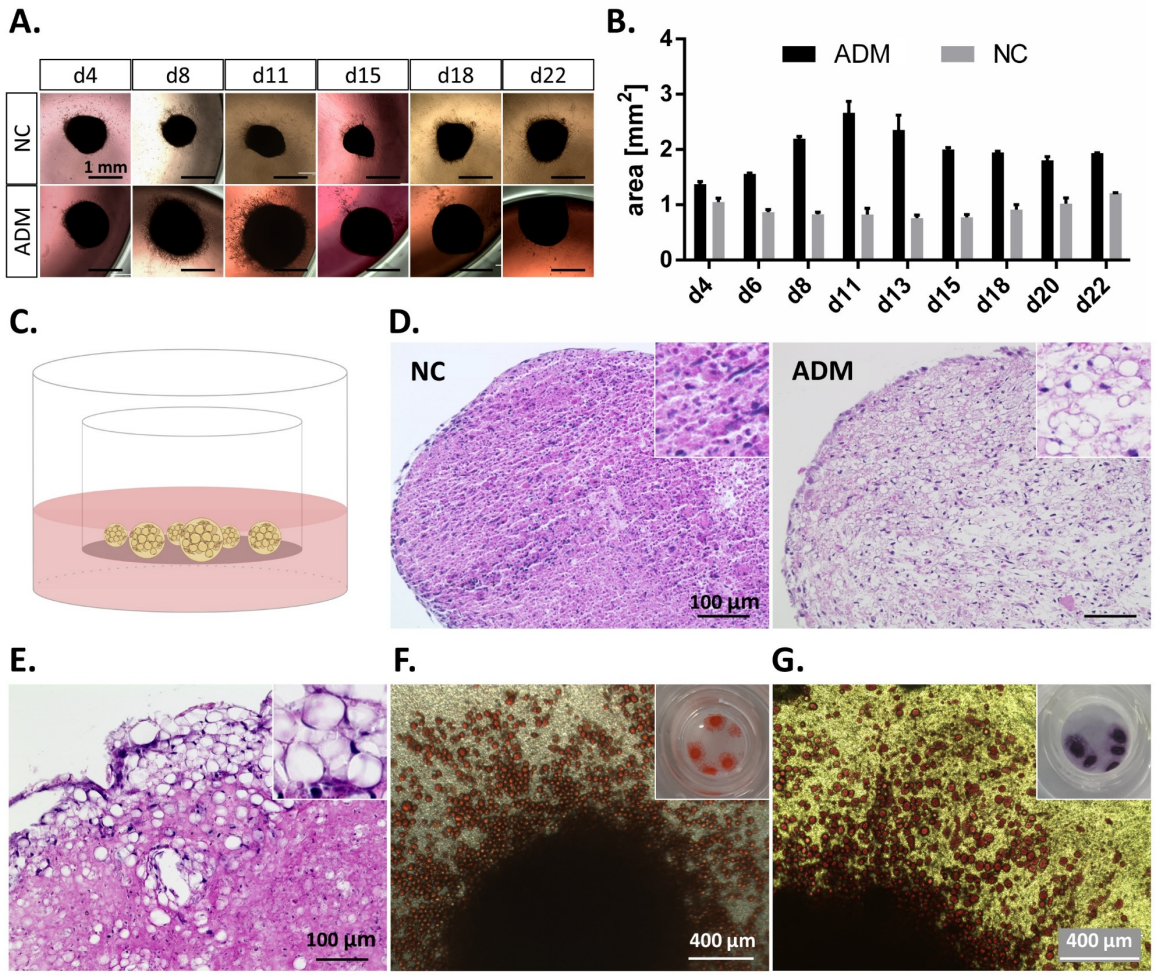

Figure 15: Scaffold-free generation of 3D adipose tissue models.

Figure 15: Scaffold-free generation of 3D adipose tissue models. A. Microscopic images of aggregated hMSCs demonstrate an increase in size during the differentiation in ADM from day 4 – 22 of culture. The aggregate diameter of the NC did not change strongly. Scale bar = 1 mm. **B.** The measurements of aggregate area (mm^2) are shown in the bar graph. The differentiating aggregates reach a maximum area of 2.67 mm^2 on day 11 of culture. The NCs show a relatively moderate size variation ranging from 0.76 – 1.21 mm^2. **C.** Schematic illustration of differentiating hMSC aggregates in a cell culture insert for the generation of 3D adipose tissue models. **D.** HE-stained microsections of aggregates cultured for 22 days. The insets show a higher magnification of cells with multilocular adipocytes indicated by "holes" after differentiation, whereas non-differentiated cells are condensed. Scale bar = 100 µm. **E.** The HE staining clearly depicts mature unilocular adipocytes (inset) within the outer layer of the aggregate followed by a core of condensed non-differentiated cells after 13 weeks of culture. Scale bar = 100 µm. **F.** The Oil Red O analysis confirms the adipogenic differentiation also showing unilocular adipocytes after 13 weeks. Cells appeared to proliferate on the culture insert membrane. Scale bar = 400 µm. The inset shows a macroscopic view of the Oil Red O-stained aggregates. **G.** The MTT analysis proved the viability of adipocytes after 13 weeks of culture (red/purple stain). Scale bar = 400 µm. The inset shows a macroscopic view of the MTT positive aggregates. The histological analysis was already published by Malkmus *et al.*, 2020 [71].

To prove the capability of the scaffold-free adipose tissue models for long-term cultures, the aggregates were maintained in ADM for 13 weeks. The tissues were then analyzed histologically. The HE staining reveals adipose tissue morphology of the outer cells of the aggregate, showing unilocular matured adipocytes (Figure 15E). The intracellular lipid accumulations were confirmed by an Oil Red O staining of fixated tissues within the culture insert, as demonstrated in Figure 15F. The microscopic image was taken by light microscopy showing the underside of the insert membrane. The visualized cells were migrated from the hMSC aggregate on the culture insert membrane. These cells were Oil Red O-positive and appeared as unilocular adipocytes. The macroscopic top view shows the Oil Red O staining of the complete aggregates within the culture insert (inset). Additionally, the viability of the long-term cultured adipose tissue models was evaluated via MTT. Again, the microscopic image was taken by light microscopy, proving the viability of differentiated adipocytes that were migrated on the culture insert membrane as shown in Figure 15G. The top view demonstrates the MTT-positive signal of the complete adipose tissue aggregates and a weak signal of non-differentiated hMSCs on the culture membrane surface.

The scaffold-free adipose tissue models were further analyzed for the expression and localization of adipogenesis markers. Thus, aggregated and differentiated

hMSCs were immunohistologically stained for the pro-adipogenic transcription factor PPARy, ADFP, GLUT4 and the ECM protein Collagen IV that is synthesized and secreted by adipocytes. Figure 16 shows the microscopic analysis of these marker proteins after 3 weeks of differentiation. Overall, the overview images demonstrate a localization of all analyzed antigens predominantly in the outer sphere of the cell aggregate, whereas the inner core has a higher density of DAPI signals. The detailed microscopic images revealed that the red PPARy signal is primarily located surrounding the cell nuclei (DAPI – blue) as indicated by white arrows. Similarly, ADFP was found to surround the nuclei (white arrows) as well as in the cytoplasm of the differentiating hMSCs, highlighted by the yellow arrows.

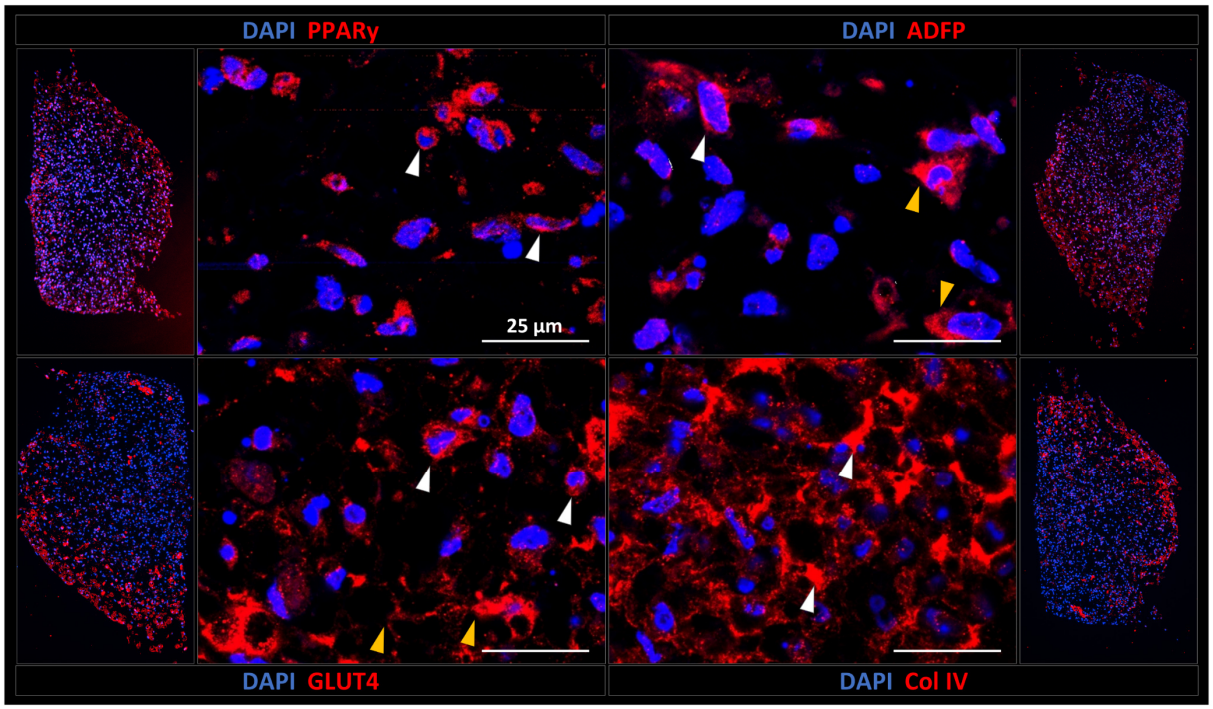

Figure 16: Immunohistological marker analysis of scaffold-free adipose tissue models. The adipogenically differentiated hMSC aggregates were analyzed for the expression of specific adipogenic differentiation markers PPARy, ADFP, GLUT4 and Collagen IV synthesized by adipocytes. The outer images show an overview of the cell aggregate, indicating the location of the analyzed protein markers within the adipose tissue model. The more detailed images depict the location on a cellular level. Scale bar = 25 µm.

The glucose transporter GLUT4 was shown to localize surrounding the nuclei and the lipid vacuole structures as indicated by the white and yellow arrows. The ECM protein Collagen IV signal was found in between the differentiating adipocytes as highlighted by the white arrows.

The aim of a protocol for the generation of basic adipose tissue models was achieved. This development was the basis of further experimentation – the generation of a multilayered skin model and larvae co-cultures.

3.2 Analysis of culture media compatibility of single tissue components

The aim of this study was the development of a multilayered skin tissue for the culture of *O. volvulus* larvae. Prior to the integration of the adipose tissue within the FTSM and eventually the application of the multilayered skin model for the larvae co-culture, the compatibility of tissue components for specific culture media and media components had to be examined.

First, the FTSM was analyzed for its capability to be cultured with alternative culture media. Figure 17A illustrates the basic principle of the FTSM that is cultured in a cell culture insert at the air-liquid-interface. Important components are the permeable polycarbonate membrane of the culture insert (1), the culture medium (2), the dermal model (3) and the epidermis (4). The surface of the latter one is shown from a top view in Figure 17B.

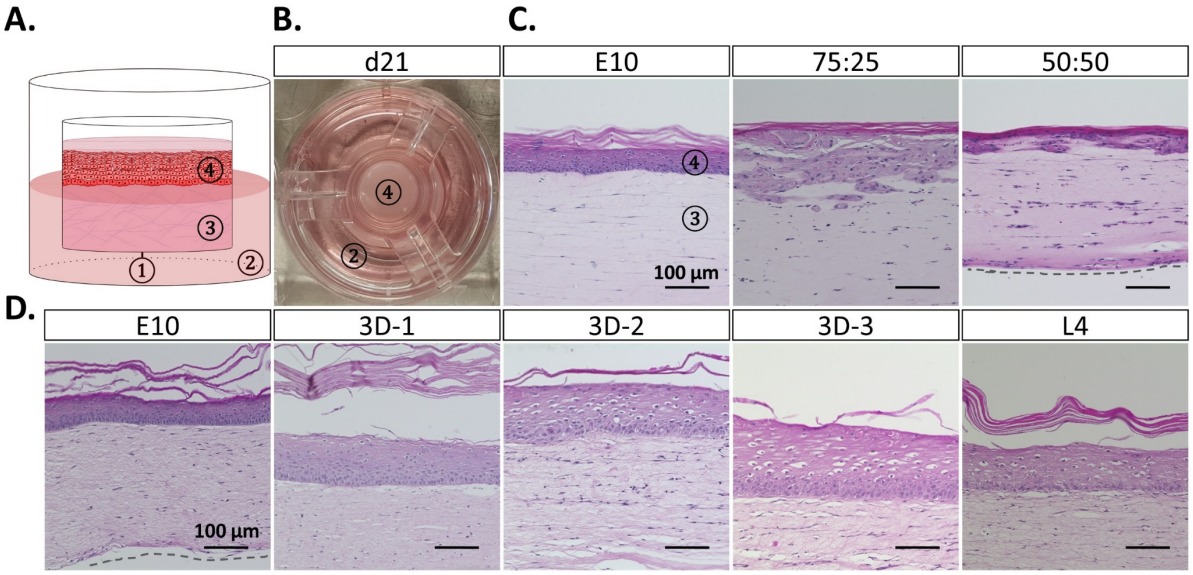

Figure 17: Evaluation of media compatibility of the FTSM with *O. volvulus* larvae media components and ADM.

Figure 17: Evaluation of media compatibility of the FTSM with *O. volvulus* larvae media components and ADM. A. Schematic illustration of the FTSM within cell culture insert and media at the air-liquid interface. Following components are indicated by numbers: (1) Permeable cell culture membrane, (2) cell culture media, (3) dermis and (4) epidermis. **B.** Top view on FTSM within cell culture insert cultured in a 6-well plate. **C.** Testing of the compatibility of the FTSM for ADM after 21 days of culture. The microscopic images of HE-stained microsections revealed a strong change in the epidermal morphology of FTSM cultured in E10:ADM mixes of 75:25 and 50:50 parts compared to the E10 control. Scale bar = 100 µm. **D.** HE staining of FTSM cultured in E10 as control and the experimental co-culture media 3D-1, -2, -3 and regular L4 medium. Scale bar = 100 µm. The histological analysis was already published by Malkmus *et al.*, 2020 [71].

Usually, the FTSM is cultured in E10 from the day of hEK seeding on the dermal tissue until the end of culture on day 21. To analyze the influence of adipocyte-specific medium on the formation of the FTSM, especially on the epidermis, the FTSM was cultured in a mixture of E10 and ADM with 75:25 and 50:50 parts (Figure 17C). The control model (E10) represents a stratified epidermal tissue with the distinct layers of differentiating keratinocytes. The epidermis (4) is clearly separated by the basal lamina from the dermal tissue (3), which contains the hDF oriented horizontally with the collagen fibers. The mixture of 75:25 E10:ADM caused the hEKs to migrate into the collagen without forming the epidermis specific tissue layers. Compared to the E10 control, the hDF within the dermal tissue are less oriented. The culture with similar parts of FTSM-specific E10 and ADM (50:50) cause an even more severe disturbance of the dermis, resulting a reduction of the collagen scaffold volume and thus a higher hDF concentration. The dashed line indicates the lower boundary of the dermal tissue model. The thickness of a hEK-layer on the dermis is strongly reduced and no epidermal tissue formation can be recognized. This culture media experiments demonstrates a vulnerability of the FTSM formation and the maturation of the epidermis to components of the adipogenic differentiation medium.

A similar experiment was performed using *O. volvulus* culture media components as shown in Figure 17D. Therefore, the experimental co-culture media 3D-1 to 3D-3 were applied for the culture of the FTSM after seeding of hEKs. The media were generated by a gradual supplementation of E10 with components of the larvae-specific L4 medium. The composition of the culture media is listed in Table 7. The FTSM cultured in the E10 control shows a normal epidermal morphology comprised of the specific strata. The different structural appearance of the collagen compared

to the E10-ADM experiment can be explained by a batch-to-batch variance of the isolated collagen from rat-tails. The histological analysis discovered that FTSMs cultured with the experimental co-culture media 3D-1 to 3D-3 media and L4 medium show mainly alterations associated with the formation of the epidermis. The keratinocytes of the *stratum basale* were affected by a change from highly prismatic basal cells (E10, 3D-1) to isoprismatic cells (3D-2, 3D-3, L4). Moreover, the latter culture media also caused a vacuolization of cells of the *stratum spinosum*. The reduced thickness of the *stratum corneum* of FTSM cultured in 3D-2 and -3 can be explained as histological artifact. However, the dermal part of the models cultured in the experimental co-culture media did not show differences.

These culture media experiments demonstrated an intolerance of the hEKs against ADM components, resulting in a disturbed formation of the epidermal tissue compared to the E10 control. The effect of the E10 medium on the adipogenesis of hMSCs was examined in 2D differentiation experiments. Experimental media combinations composed of ADM+ and E10 in ratios of 75:25, 50:50, 25:75 and 100 % E10 were supplemented with adipogenic differentiation factors. Figure 18A shows the results of the Oil Red O staining of the 2D differentiated hMSCs compared to the positive control (ADM+) and cells cultured in EM as negative control. A reduction of the Oil Red O positive cells with an increasing ratio of E10 is recognizable in the microscopic images after 21 days of differentiation. This trend could be confirmed by the semiquantitative analysis of the Oil Red O staining (Figure 18B). Normalized to the lipid content of the positive control, the differentiation in the media combination 75:25 led to 97.6 % of lipid accumulation, 50:50 reduced the lipid content to 74.7 % and 25:75 only reached 46.9 %. A strong reduction to 30.9 % was measured for hMSCs differentiated in 100 % E10.

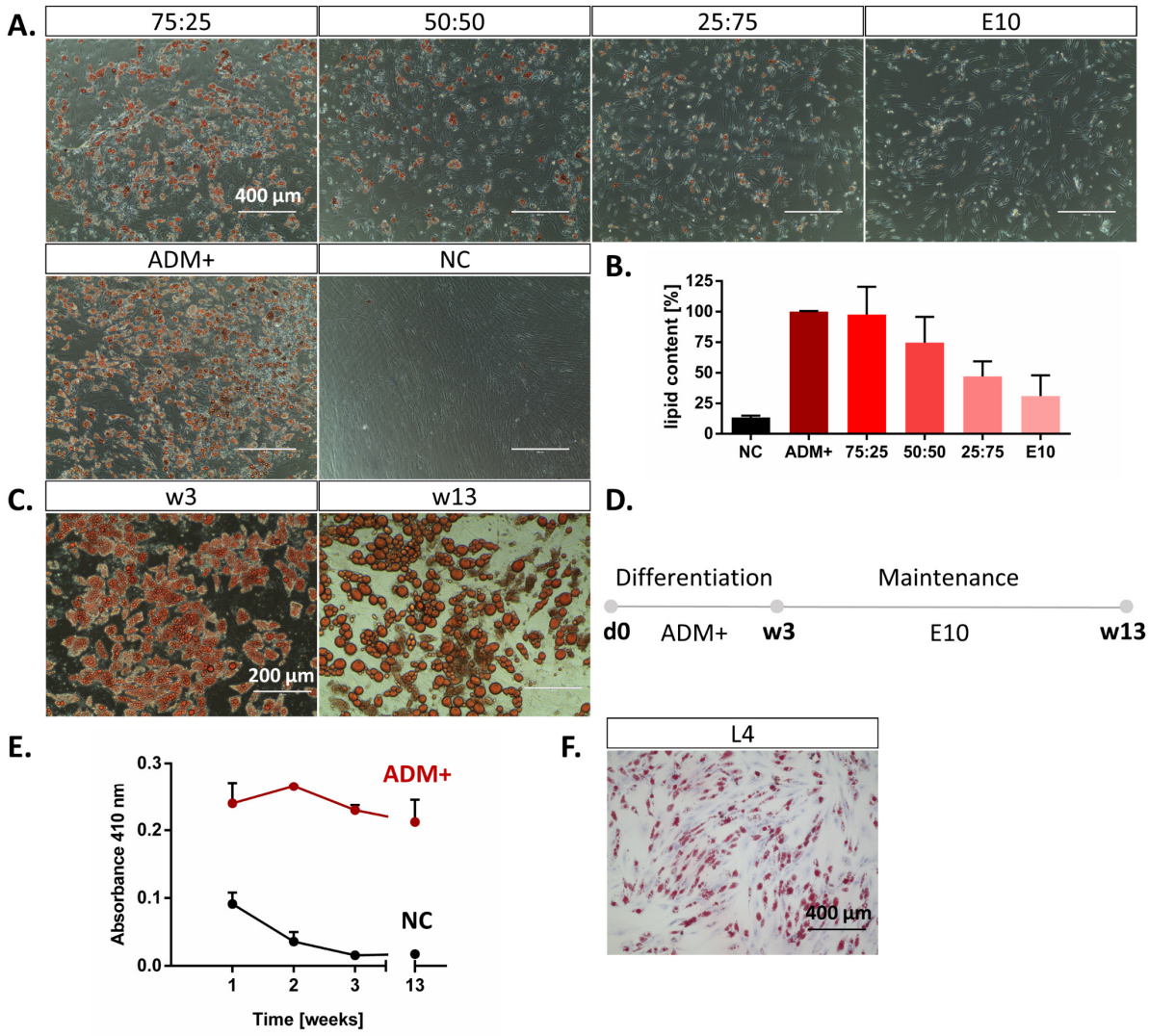

Figure 18: Compatibility of hMSCs in adipogenic differentiation for skin and larvae-specific culture media. A. Oil Red O staining of 2D cultured hMSCs in ADM:E10 mixtures of 75:25, 50:50, 25:75 and E10 supplemented with 1x concentrated differentiation factors. Scale bar = 400 µm. **B.** Results of intracellular lipid quantification were normalized to the ADM+ cultured cells demonstrate a decreasing Oil Red O signal. **C.** Oil Red O staining of hMSCs in adipogenic differentiation after 3 and 13 weeks. After an initial differentiation for 3 weeks the culture medium was changed from ADM+ to E10. After 13 weeks the adipocytes show enlarged intracellular lipid vacuoles. Scale bar = 200 µm. **D.** Time protocol for the differentiation of hMSCs and the maintenance in E10 medium. **E.** Quantitative analysis the intracellular lipid content by Oil Red O staining for hMSCs differentiated for 3 weeks and maintained in E10 until week 13 (ADM+) compared to the negative control (NC). **F.** Oil Red O analysis of hMSCs cultured in L4 medium supplemented with adipogenic differentiation factors after 2 weeks of culture revealed the formation of multilocular lipid vacuoles. Scale bar = 400 µm. The histological analysis was already published by Malkmus *et al.*, 2020 [71].

The intolerance of differentiating hMSCs to E10 medium and vice versa the intolerance of the FTSM to ADM evoked the need for a time-dependent protocol for

the differentiation of adipocytes and the ability of maintenance in E10 to eventually enable the integration of the adipose tissue model to the FTSM. It could be shown that a pre-differentiation for 3 weeks facilitated the preservation of the adipogenic differentiation fate throughout the following long-term culture in E10 for further 10 weeks (Figure 18D). This could be proven by the Oil Red O staining of differentiating hMSCs after 3 and 13 weeks of culture. The microscopic images in Figure 18C show a typical morphology for differentiating adipocytes in 2D containing multiple lipid vacuoles. After 10 weeks in E10 the lipid vacuoles fused to a few larger vacuoles per cell. The overall lipid content was analyzed by the Oil Red O quantification, as shown in Figure 18E. After 3 weeks of differentiation, the absorbance of the Oil Red O supernatant was 0.23 compared to the NC with 0.02. After 10 weeks of E10 culture, the lipid content was reduced to 91.6 % with an absorbance of 0.21. To analyze the tolerance of differentiating adipocytes to larvae-specific medium, hMSCs were differentiated in L4 supplemented with adipogenic differentiation factors. Figure 18F shows the Oil Red O positive cells after 2 weeks of culture. The accumulation of intracellular lipids proves the compatibility of hMSCs with larvae medium. These findings on the media compatibility, especially the pre-differentiation of adipocytes prior their maintenance in E10, were the base for the adipose tissue integration to the multilayered skin model.

3.3 Integration of the adipose tissue model into the FTSM

Finally, to integrate an adipose tissue into the FTSM, the hMSC aggregates were chosen to continue, due to practical aspects regarding an additive and stepwise generation process of the multilayered skin model as shown in Figure 19A. Another obstacle of the collagen-based adipose tissue model is the required plastic compression of the dermal tissue above. The hDF cause a remodeling of the collagen scaffold, resulting in shrinking of the dermis. The plastic compression generates a high-density collagen hydrogel allowing the remodeling by the hDF without the loss of volume. In the case of an additive strategy for the tissue generation, the collagen-based adipose tissue model would have been plastically compressed. The resulting increased collagen concentration within the adipocyte-containing scaffold would not match the stiffness of adipose tissue. hMSCs are known to respond to the

stiffness regarding the differentiation capacities, reducing the ability to differentiate into adipocytes. This effect could be reproduced in the master thesis of Laurin Glaser [157].

A first step for the integration to the FTSM was the analysis of the interaction of adipose tissue aggregates and the collagen hydrogel. Therefore, aggregated hMSC were embedded and differentiated in collagen as shown in Figure 19 B. The histological analysis revealed that the cells differentiated to adipocytes, represented by the multilocular lipid vacuoles. Cells were migrating from the aggregate into the surrounding collagen hydrogel, as indicated by the red dashed line marking the aggregate and arrows for the migration direction. The migration of differentiating cells was confirmed by confocal microscopy of Nile Red labeled adipocytes within the collagen (Figure 19C). A dense core of Nile Red-positive cells represents the aggregate as marked by the white line, whereas loose cells were radially migrating as indicated by the white arrows. The observation of aggregate integration led to the establishment of the additive three-step-protocol (Figure 19A). Aggregated hMSCs were pre-differentiated for 3 weeks in ADM+ to enable their maintenance and maturation in alternative culture media. The dermal model is added onto the differentiating adipose tissues, followed by the plastic compression. The viability of the adipocytes was confirmed by a quantitative MTT assay, showing MTT-positive aggregates on the bottom surface (Figure 19A). Eventually, after one week of culture in FM, the epidermis was generated by seeding hEKs. According to the protocol for the FTSM generation, the skin model was cultured for the maturation of the epidermis for further 21 days in E10. After 7 weeks of additive tissue generation, the resulting multilayered skin models were histologically analyzed. Figure 19D shows the HE staining of microsections of the multilayered skin model comprised of adipose tissue, dermis and epidermis. For the direct comparison, images of native human skin are presented (Figure 19F, H-I). Detailed representative images of the epidermis from the multilayered skin model and native human skin are compared in Figure 19E-F. Both tissues show the epidermis-specific formation of keratinocyte layers from prismatic basal cells in the *stratum basale*, flattened hEKs in the *stratum spinosum*, granular cells in the *stratum granulosum* and the terminally differentiated cornified cells of the *stratum corneum*. Whereas the dermis of the multilayered skin model is more oriented and only contains hDF, the native dermis contains multiple

sub-structures and an increased cell amount (Figure 19E-H). A representative image of the adipose tissue layer of the *in vitro* skin model displays different stages of hMSC differentiation – from differentiating multilocular hMSCs to matured unilocular adipocytes – within the integrated aggregates (Figure 19G).

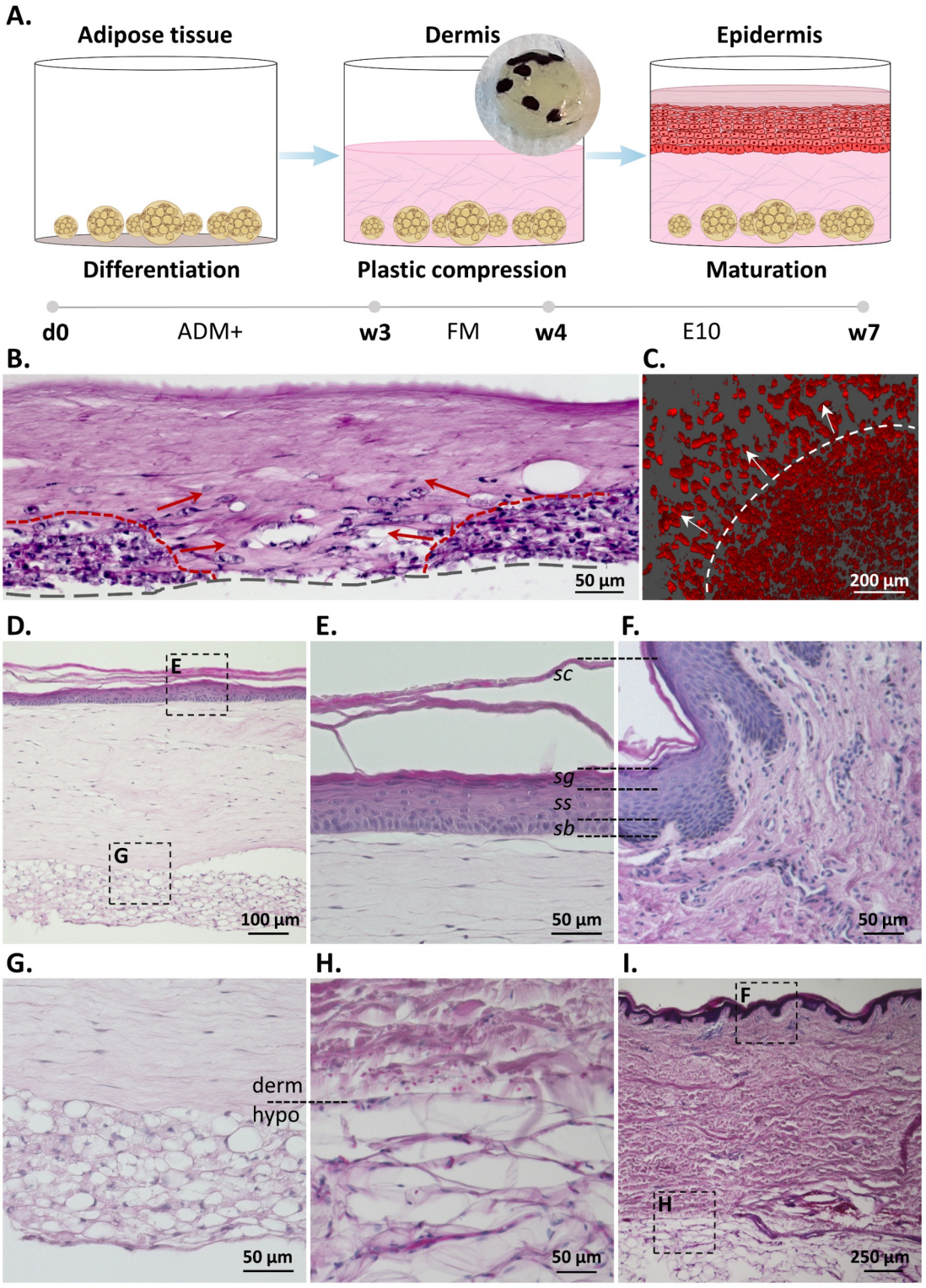

Figure 19: Integration of adipose tissue aggregates into the FTSM.

Figure 19: Integration of adipose tissue aggregates into the FTSM. A. Strategy for the integration of aggregated adipose tissue models into the FTSM. After the initial differentiation for 3 weeks, the dermis is added onto the adipose tissue followed by plastic compression and culture for 1 week in FM. The viability of differentiating cells after compression was proven by MTT (inset). After seeding hEK, the model was further cultured for 3 weeks in E10. **B.** Microscopic image of HE-stained collagen-embedded hMSC aggregates shows multilocular adipocytes (red dashed line) located on the culture insert membrane (grey dashed line). Cells appear to migrate outwards the hMSC aggregate, shown by red arrows. Scale bar = 50 µm. **C.** A confocal microscopy analysis of the Nile Red-stained construct confirms the observation of cell migration from the aggregate (white dashed line), demonstrated by the white arrows. Scale bar = 200 µm. **D.** HE staining of the multilayered skin model showing all three tissue layers. Scale bar = 100 µm. Representative detailed images are indicated by dashed boxes (E+G). **E.** Representative image of the reconstructed epidermis showing the distinct layers of keratinocyte differentiation. Scale bar = 50 µm. **F.** These layers are similarly found in the epidermis of native human skin. Scale bar = 50 µm. **G.** Integrated adipose tissue model at the interface of dermis (derm) and hypodermis (hypo). The adipocytes show different stages of differentiation from early adipocytes with multilocular lipid vacuoles and unilocular adipocytes with peripheral nuclei. Scale bar = 50 µm. **H.** Comparison to the tissue interface in native human skin. Scale bar = 50 µm. **I.** Histological image of native human skin containing the relevant tissues epidermis, dermis and subcutis. Dashed boxes indicate representative detailed images (F+H). Scale bar = 250 µm.

The dermis-hypoderm interface of native human skin is shown in Figure 19H, demonstrating a similar organization of adipocytes and matrix. However, in comparison hMSC-derived adipocytes did not reach the size of native adipocytes of the subcutaneous adipose tissue. The overall morphology of the multilayered skin model matches the anatomy of native human skin (Figure 19D, I). With the protocol for the generation of the multilayered skin model, the developmental tissue engineering part of this work was achieved.

3.4 Co-cultures of tissue models and *O. volvulus* larvae

The initial idea of the co-culture setup was to address the factors that were hypothesized as crucial for the translation of the *in vivo* niche: 1. ECM, 2. Skin-specific cells and 3. Larvae-tissue interaction. The second aspect was addressed in a first co-culture media evaluation. Similar to the analysis of the effect of culture media and components on the development of the FTSM and adipocytes (Figure 17, 18), *O. volvulus* L4 larvae were tested for their compatibility to cell and tissue-specific medium components. Therefore, the experimental co-culture media 3D-1 to 3D-3

were tested for their support of larval growth and viability compared to the larvae-specific L4 medium. The skin specific E10 medium was gradually supplemented with components of the L4 medium used for the 2D culture. The composition of the experimental media is described in Table 7. As illustrated in Figure 20, two culture platforms were used for the culture medium analysis – the 2D culture system based on a HUVEC feeder layer and the indirect co-culture of larvae and FTSM. The length measurement of L4 larvae cultured above the 2D HUVEC layer revealed a median length of 699.4 µm in E10, 754.4 µm in 3D-1, 772 µm in 3D-2, 785.2 µm in 3D-3 and 761 µm in the L4 control medium (Figure 20A). The number of larvae per condition ranged from 18-22.

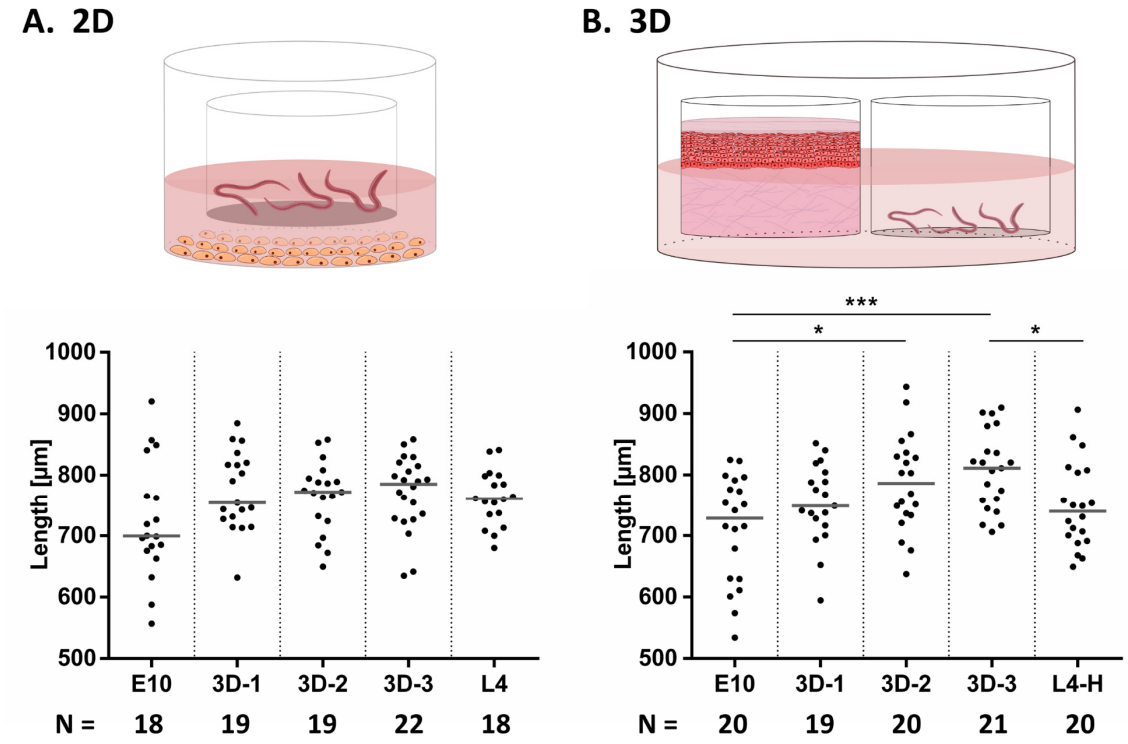

Figure 20: Testing of experimental co-culture media on *O. volvulus* larvae. A. Analysis of media influence on the growth of L4 larvae on day 7 in the 2D HUVEC culture system compared to the 2D control medium L4. The bar represents the median length. The growth between the different groups shows no significant difference, although representing a positive trend towards 3D-2 and 3D-3. Underneath the graph, the number of larvae per group is displayed. **B.** Media testing on the indirect FTSM co-culture system. Two culture inserts – containing FTSM and L4 larvae – were placed in a 6-well. After 7 days the trend of the results from 2D testing were confirmed in 3D. The bar represents the median length. Underneath the graph, the number of larvae displays group sizes. The larvae groups cultured in 3D-2 and 3D-3 were significantly bigger than larvae of groups E10 and control L4-H. Unpaired t-test: E10 – 3D-3 ***, p-value 0,0003; E10 – 3D-2 *, p-value 0,0118; 3D-3 – L4-H *, p-value 0,0102. These data were published by Malkmus *et al.*, 2020 [71].

As shown schematically in Figure 20B, the indirect co-culture was comprised of L4 larvae and a FTSM in separated culture inserts that were placed in a 6-well. Similar to the 2D culture, the human cells were hypothesized to secrete soluble factors that support the development of larvae *in vitro*. The analysis of larvae size gave a similar trend of growth response to the applied culture media 3D-1 to 3D-3. L4 cultured in E10 reached a length of 728.4 µm, 748.7 µm in 3D-1, 786 µm in 3D-2, 811.2 µm in 3D-3 and 739.7 µm in the control medium L4-H. The statistical analysis demonstrated a significantly increased size for larvae cultured in 3D-2 and -3 against larvae in E10 medium. Furthermore, larvae cultured in the control medium were significantly smaller than in 3D-3. Thus, the 3D media testing confirmed the trend of the 2D results. Hence, the most supportive culture media 3D-2 and 3D-3 were applied for further co-cultures of L4 larvae and complex tissue models.

The first crucial aspect stated for the translation of the *in vivo* niche was ECM. As already shown, the collagen-based adipose tissue model, the FTSM and the multilayered skin model consist of a collagen hydrogel as the main ECM component. Thus, strategies for the larvae integration into the collagen-based scaffolds were needed to also address factor 2 – tissue specific cells and factor 3 – direct contact. Certain requirements for the direct co-culture were a non-detrimental integration process, the ability to retrieve larvae from the tissue for downstream applications and ideally the observation of larvae for the monitoring of vital parameters. Different approaches were examined for their suitability for the integration of larvae as illustrated in Figure 21. The injection of L4 larvae by using a 10-µl pipette tip and the pouring of larvae after mixing them into the gelatinizing collagen (Figure 21A-B) resulted in the loss of larvae. The optical features of collagen hindered the observation within the scaffold by light microscopy (Figure 21C). Moreover, after the treatment of the larvae-containing hydrogels with collagenase the retrieval of L4 was very poor (Data not shown). To circumvent this issue, a culture compartment was created into the dermis by using a tissue punch (Figure 21D). In general, this enabled the observation of larvae by light microscopy, but the number of larvae decreased through the migration into the undefined wound in the dermis. A more sophisticated approach for the generation of a confined culture compartment in the dermis was the impression by a devised stamp. Figure 21E shows the basic principle of the collagen compression and thereby the generation of an imprint. The technical

illustration depicts the dimensions of the stamp. The microscopic image in Figure 21G demonstrated the possibility of monitoring the larvae during the culture. A co-culture of larvae within the confined culture compartment was performed and the growth kinetics were analyzed in Figure 21F.

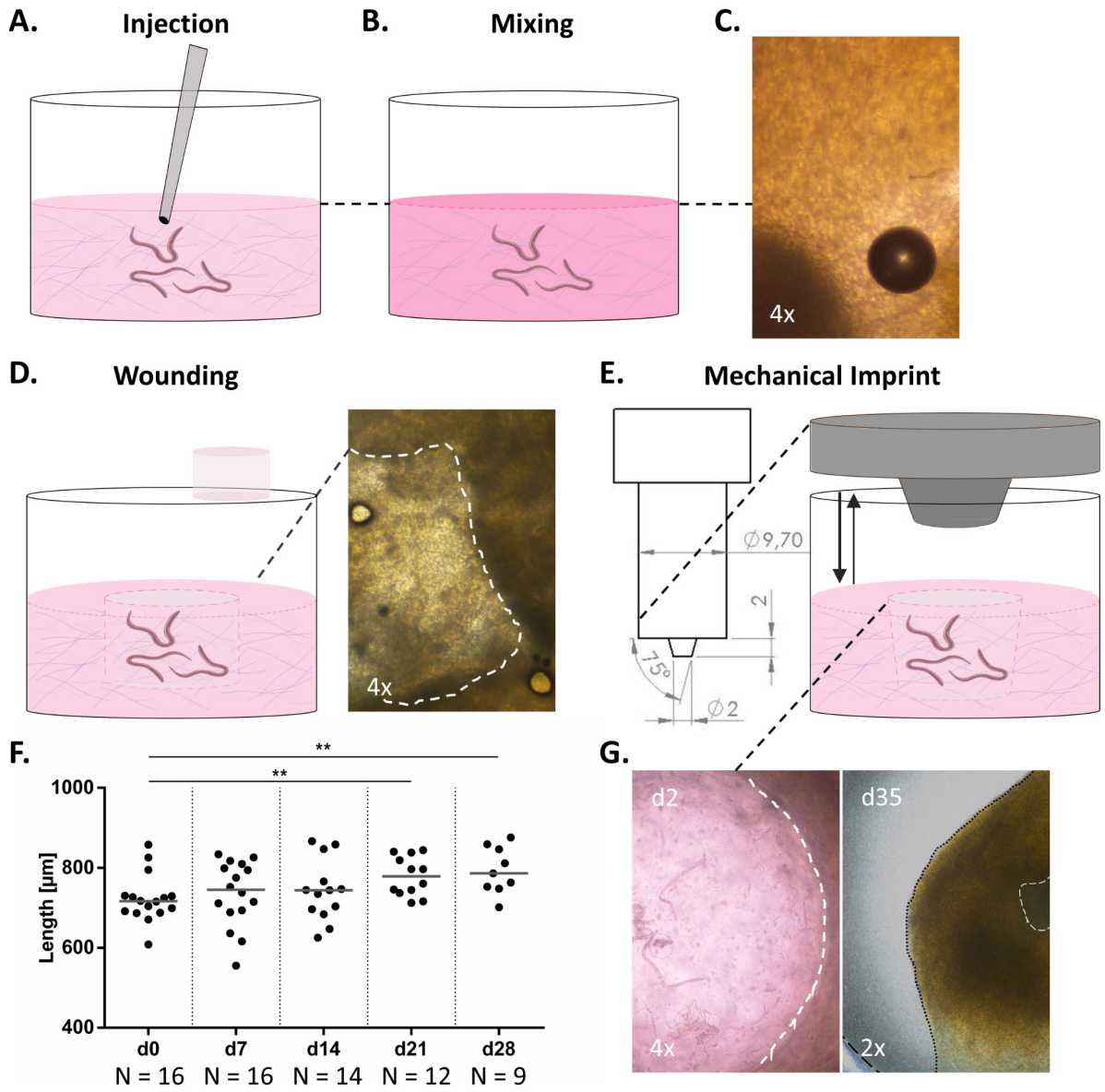

Figure 21: Approaches for the culture of *O. volvulus* larvae and collagen-based skin models in direct contact.

Figure 21: Approaches for the culture of *O. volvulus* larvae within dermal skin models in direct contact. **A.** Pipetting of larvae into the collagen hydrogel. **B.** Mixing of larvae into the collagen-GNL mix during the generation of the collagen hydrogel scaffold. **C.** Representative microscopic image of collagen hydrogel with larvae loaded by pipetting or mixing. Magnification: 4x. **D.** Generation of a wound by using a tissue punch for larvae deposition. Microscopic image of wound generated by tissue punch for larvae deposition. The white dashed line indicates the irregular edges. Magnification: 4x. **E.** Generation of a confined compartment within collagen by the application of a stamp (left, lengths in mm). The application of the stamp for compression generates the imprint. **F.** Growth kinetics of L4 larvae cultured within the confined compartment. The number of larvae that was found and measured within the imprint is noted for each time point. **G.** Microscopic image of L4 larvae in defined compartment on day 2 of culture (left). The white dashed line indicates the defined edges of the compartment. Magnification: 4x. Contraction of the scaffold and collapse of the culture compartment on d35 (right). The hydrogel loosened from the insert wall (dashed black line) and decreased in volume, shown by the spotted black line. The imprinted compartment containing the larvae shrank (dashed white line), impeding their observation. Magnification: 2x. These data were already published by Malkmus *et al.*, 2020 [71].

The measured length of L4 larvae increased from an initial median size of 716.5 µm on day 0 of co-culture to 744 µm on day 14, 778.5 µm on day 21 and reached a final length of 786.4 µm after 28 days of culture. Compared to the initial length, the larvae grew significantly until day 21 and 28 of co-culture. However, due to hDF-mediated remodeling and thus instability of the imprinted dermal tissue, the confined culture compartment collapsed as shown in Figure 21G. Furthermore, larvae were migrating into the unstable scaffold and thus could not be further monitored as indicated by the reduction of measured larvae per time point (Figure 21F).

Interestingly, a long-term culture of the described indirect co-culture of larvae and FTSM led to the observation of a strong migratory effect on FTSM-resident hDF. Figure 22A shows a picture of the larvae and tissue containing culture inserts and their proximity within the 6-well. The hDF migration towards the larvae-containing insert is demonstrated in Figure 22B, which resulted in the overgrowth of L4 worms on the culture membrane (Figure 22C). Scanning electron microscopy (SEM) confirmed this overgrowth and integration of larvae into a cluster of hDF and ECM. Figure 22D shows the SEM image of a captured worm. A detailed image demonstrates the interface of the larva and the newly formed tissue (inset). The growth kinetics of L4 larvae were monitored during the long-term culture until day 77 of co-culture representing day 92 of larvae after thawing, as shown in Figure 22E. As evaluated in previous experiments, the most supportive co-culture media 3D-2 and -3 were applied for the long-term culture of larvae and FTSM in the indirect setup. Compared

to the 2D control, on day 0 of co-culture the larvae were comparable in size, ranging from median length of 727.4 µm in 3D-2 to 746.2 µm in 3D-3 and 733.6 µm in 2D. After 21 days of culture, the growth data revealed a trend of enhanced growth for larvae cultured in 3D-3 with the FTSM compared to the 2D cultured worms. A significant increased length of larvae could be analyzed after 77 days of co-culture, reaching a size of 830.8 µm in 3D-2 and 816.3 µm in 3D-3, whereas larvae in 2D grew to 766.6 µm in median length. The final size of FTSM co-cultured larvae was significantly higher compared to 2D at the same time point and to the initial size on day 0, respectively. However, the number of data points representing the number of viable larvae on day 77 depict the reduced survival of *O. volvulus* L4 co-cultured in 3D-2 medium compared to 3D-3 and the 2D control larvae. As demonstrated by the graph in Figure 22F, the %-motility representing the larvae viability in all conditions was stable until day 21 of co-culture, followed by a strong reduction until day 77. The %-motility was comparable at 30.7 % for 3D-3 and 30 % for 2D, whereas the %-motility of L4 cultured in 3D-2 dropped to 15.8 %.

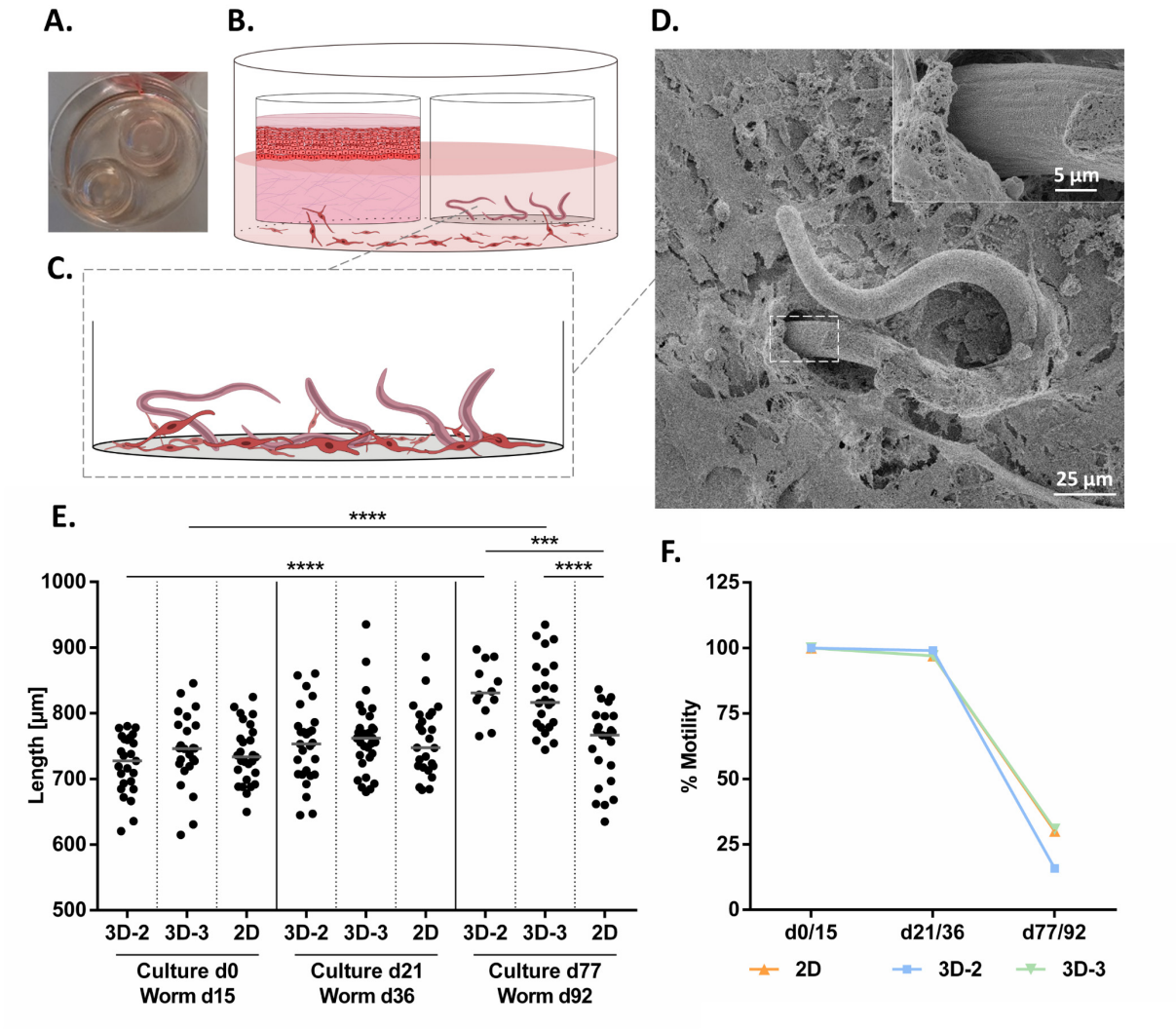

Figure 22: Indirect co-culture of *O. volvulus* L4 larvae and FTSM. A. Exemplary macroscopic image of indirect co-culture of larvae and FTSM in separate culture inserts in a 6-well. **B.** Illustration of co-culture components and observation of hDF migration towards larvae insert. **C.** The schematic image shows the overgrowth of worms within the culture well by hDF. **D.** SEM image of L4 larva integrated into a cluster of hDF and secreted ECM. Scale bar = 25 µm. The inset gives a more detailed image of the interface of worm-cell-matrix interaction. Scale bar = 5 µm. **E.** Analysis of growth kinetics observed for L4 larvae cultured indirectly with a FTSM in the culture media 3D-2 and 3D-3 compared to larvae in the 2D HUVEC co-culture. Unpaired t-test: 3D-2 d0-d77 ****, p-value: < 0.0001; 3D-3 d0-d77 ****, p-value: < 0.0001; d77 3D-2 – 2D ***, p-value: 0.0001; d77 3D-3 – 2D ****, p-value: < 0.0001. **F.** The graph shows the viability of larvae by the %-motility of L4 on day 0, 21 and 77 in the indirect co-culture system. These data were already published by Malkmus *et al.*, 2020 [71].

The experiment showed no detrimental effect by overgrowth with hDF, which represents a direct contact of larvae and cells or tissue model – crucial factor 3. The direct contact was further analyzed in the following experiment applying the scaffold-free adipose tissue model. Figure 23A illustrates the principle of the direct

co-culture of larvae and adipose tissue aggregates. L4 larvae and adipogenically differentiated hMSC aggregates were placed on the membrane of a single culture insert. The microscopic image shows the adipose tissue model (white dashed line), differentiating and non-differentiating hMSCs in the periphery and larvae in direct proximity. As an indirect control, *O. volvulus* L4 were cultured separated by the insert membrane with adipose tissue aggregates, as schematically shown by Figure 23B.

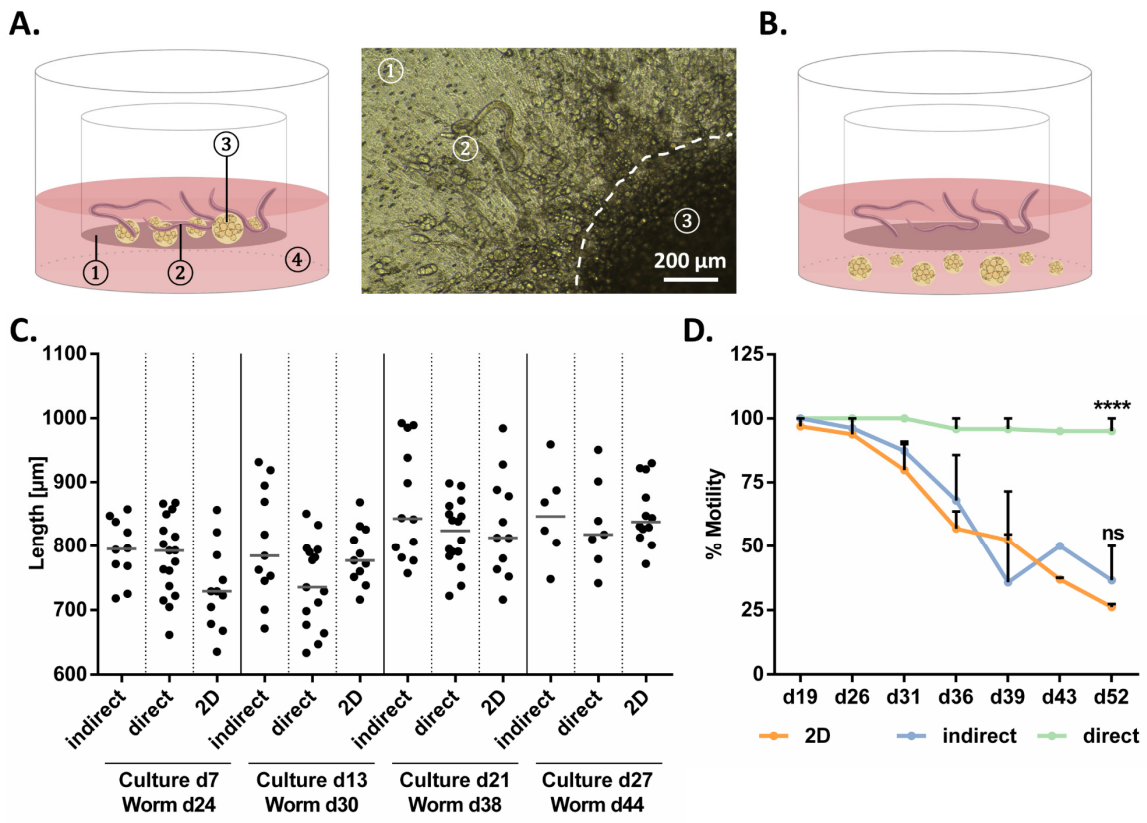

Figure 23: Co-culture setups of larvae and adipose tissue aggregates. A. Schematic illustration (left) of the direct co-culture of L4 larvae and adipose tissue models within a cell culture well enabling direct contact of worms and tissue models. The numbers indicate crucial culture components: (1) permeable culture membrane, (2) L4 larvae, (3) adipose tissue aggregate, (4) culture medium. A microscopic image of the direct culture shows larvae (2) on a membrane (1) covered with non-differentiated hMSCs and differentiating adipocytes next to an adipose tissue aggregate (3). Scale bar = 200 µm. **B.** Indirect culture setup separating larvae and adipose tissue models by permeable membrane. **C.** Growth kinetics of larvae culture in direct and indirect co-culture with adipose tissue models compared to the 2D HUVEC control. Larvae were only measured when found in a representative situation – strong coiling or a blocked view by cells and aggregates hampered the measurement of larvae in the direct condition. **D.** Motility analysis of L4 larvae cultured in the direct and indirect adipose tissue co-culture compared to the 2D culture control. These data were already published by Malkmus *et al.*, 2020 [71].

The growth kinetics of larvae cultured in both conditions were analyzed and compared to 2D cultured larvae as a control. In the direct co-culture, larvae were attached by the cells that migrated from the adipose tissue aggregates as shown by Figure 23A. This immobilization of larvae in a curved position hampered the analysis of larvae size, as the measurement is usually performed on larvae in a straight position. This led to an inconsistent progression of larvae growth and number in the direct co-culture shown in Figure 23C. The median size of larvae on d7 of co-culture was 795.1 µm in the indirect culture and 792.7 µm in direct contact, compared to 729.1 µm in the 2D control. After 13 days, the control larvae grew to 776.9 µm, whereas larvae in the adipose tissue co-cultures decreased in size, ranging from 735.3 µm in the indirect condition to 784.6 µm in the indirect setup. The further progression of larvae growth after 27 of culture reached 837.3 µm for 2D cultured larvae and 846.3 µm for larvae cultured separated from the adipose tissue. The final length of larvae in direct contact reached 828.4 µm. The number of data points of this condition was reduced due to inability of length measurement but motility observation was still possible. The %-motility of larvae in this co-culture experiment is demonstrated in Figure 23D. The motility scoring revealed a constant level of about 95 % for larvae from day 36 to 52 cultured in direct contact with adipose tissue models. In contrast, similar to the 2D control larvae, the %-motility strongly decreased from the start of co-culture to 36.5 % for indirect cultured worms and 26.1 % in the 2D control after 52 days.

4. Discussion

The aim of this study was the translation of the *in vivo* niche of *O. volvulus* into a culture system based on *in vitro* human skin. Therefore, the engineering of a multilayered skin composed of the three major skin tissues epidermis, dermis and a subcutis was achieved. A novel adipose tissue model has been developed and integrated into the FTSM. Together, this multilayered skin allowed the presentation of the crucial factor 1 – ECM, 2 – tissue-specific cells, and 3 – direct contact of larvae and tissue. However, the culture of *O. volvulus* larvae within the multilayered skin model could not have been studied, due to rather technical challenges. Nevertheless, interesting observations were made in co-cultures of larvae and skin tissue models of different complexity. Furthermore, two cultures modes – an indirect and direct culture – could distinguish important triggers for the *in vitro* maintenance and development of *O. volvulus* larvae.

4.1 Determination of culture media for the co-culture of larvae and *in vitro* tissues

The aimed co-culture of a human *in vitro* tissue together with an obligatory human parasite is a highly complex system, of which all single tissue components as well as the parasite require an individual pattern of nutrition, biological stimuli, chemical and physical impacts. Hence, for the generation of the tissue model composed of several cell types, here a culture medium fulfilling the needs of all components is required. Finally, to allow a larvae co-culture, an overall culture medium has to support both, human tissue models and *O. volvulus* L4 larvae. Therefore, an analysis of media combinations was performed to determine an overall culture medium.

Regarding the tissue model construction, the ability of the well-established FTSM to be cultured with ADM was tested. As shown in Figure 17C, the culture of FTSM in mixtures of E10 and ADM in ratios of 75:25 and 50:50 resulted in the migration of hEK into the dermis and a loss of dermal thickness, compared to the E10 control. This clearly depicts the disturbance of the epidermal and dermal formation by components of the ADM. Vice versa, the influence of the skin-specific E10 medium was analyzed on differentiating hMSCs in 2D (Figure 18A-B). With an increasing

proportion of E10 in the culture medium, the intracellular lipid accumulation was inhibited as demonstrated by Oil Red O staining and the lipid quantification. The reduced differentiation and lipid accumulation might be explained by the effect of epidermal growth factor (EGF) and hydrocortisone, supplements of the E10 medium. Both factors are discussed to have an anti-adipogenic function [158]. Whereas EGF was shown to support lipolysis and to reduce the intracellular lipid storage of pre-adipocytes in mice [159,160], hydrocortisone impedes the adipogenesis-supporting effect of insulin, thereby inhibiting adipogenic differentiation in *ex vivo* cultured pig adipose tissue [161]. Recent literature reports a dose-dependent inhibition of adipogenesis in hADSCs by EGF and hydrocortisone, thereby enabling the maintenance of lipid-containing adipocytes by low concentrations *in vitro* [162]. However, the follow-up experiment for the strategy of adipose tissue integration into the multilayered skin delivered an important observation. After a pre-differentiation phase of three weeks, the differentiating adipocytes preserved the adipocyte morphology for further ten weeks in E10 medium, shown by the unilocular appearance of the 2D differentiated cells and the Oil Red O quantification (Figure 18C-E). This result was surprising, as in the literature dedifferentiation of matured adipocytes obtained from liposuction is reported for skin-specific culture media, due to supplemented EGF and hydrocortisone [163]. This finding that pre-differentiated adipocytes can be maintained in E10 could be reproduced for the generation of the adipose tissue of a multilayered skin model using an alternative scaffold material [164].

Having identified the sequential use of cell culture media as a strategy for the additive tissue model generation (Figure 19A), the next component which had to be included for the co-culture system were the larvae. To allow the use of an optimal culture medium for all, tissue and larvae, experimental co-culture media were analyzed for their support on appropriate tissue formation, specifically cellular differentiation as well as the larval growth and survival. As explained in detail in Table 7, the culture media 3D-1 and 3D-2 were based on E10 gradually supplemented with larvae-specific supplements. The co-culture medium 3D-3 was based on a 1:1 mixture of E10 and L4-H medium additionally supplemented with L4 supplements. First, the influence of these media on the survival and growth of larvae was analyzed in the 2D culture system and 3D indirect FTSM co-culture (Figure 20). The larvae

sizes of both culture approaches show the same pattern. Larvae cultured in E10 showed the smallest size, increasing from 3D-1 to 3D-3 – reaching the highest median length in 2D and 3D. This observation proves the support of L4-specific supplements, such as glucose, sodium pyruvate, non-essential amino acids, and lipids to larval fitness [29,165]. These factors were missing in the E10 medium, which might explain the comparable low median length and the very small size of individual larvae below 600 µm in both, 2D and 3D.

Complementary, these experimental culture media were tested for their support of the tissue maintenance. From previous experiments, the ability of hMSCs to differentiate in L4 medium and larvae supplements could be demonstrated in the presence of differentiation factors (Figure 18F). More reason for concern was the culture of the FTSM in alternative media combinations. The experimental co-culture media altered the formation of the epidermis, e.g. by a vacuolization of the *stratum spinosum* and an increased epidermal thickness. The results for the media analysis on larvae, adipocytes, and FTSM suggested that 3D-2 and 3D-3 were applied for further co-culture experiments, even though these media did not support an optimal epidermal formation.

4.2 Increasing complexity of tissue co-cultures supported larval growth and viability

The aim of the study was to provide the crucial factors 1-3 with the multilayered skin to the co-cultured larvae. In this context, the co-culture within the tissue was proposed to enable the direct contact of larvae and tissue components. Thus, preliminary experiments were performed to identify the optimal integration strategy of larvae into collagen-based tissue models. Regrettably, the results depicted that the larvae integration into the collagen scaffold provoked distinct problems. The optical features of the dermal models did not allow an observation of the integrated larvae for the monitoring of vital parameters, such as growth, viability and eventually molting events. This issue would have worsened with the addition of the adipose tissue and the epidermis that are even more non-transparent for light microscopy. Additionally, the instability of the collagen hydrogel impeded the

formation of culture compartments within the dermal scaffold (Figure 21). These limitations avoided the initial aim of a direct co-culture of larvae within the multilayered skin. A possible strategy to overcome these rather technical challenges would be an increased collagen density by higher plastic compression factors. After the compression of the dermal component of the FTSM, the collagen hydrogel has a final calculated concentration of about 47 mg/ml compared to the initial 6.7 mg/ml – a 7-fold compression [137,139]. The compression achieved by the applied stamp only reached factor 2-3. A higher compression might also increase the long-term stability of an imprinted culture compartment. However, an advanced imaging strategy for the assessment of larvae survival, growth, position and movement within a tissue would enable an elaborated culture readout. Confocal Imaging of larvae would require a robust fluorescent labelling. In mice, fluorescently labelled L3 larvae of *L. sigmodontis* were imaged within the lymphatic vessels using the VivoTag 680 XL dye [166]. In preliminary experiments at the NYBC, this vital stain has been tested on *O. volvulus* L4 larvae (Figure 24). The dye was retained by the larvae and did not cause any detrimental effects. Using confocal microscopy, the stained larvae could be monitored within a plain collagen layer for one week. Regardless, the analysis of a long-term effect of the vital stain on the fitness of *O. volvulus* larvae would be mandatory. However, it represents a promising tool for larvae imaging.

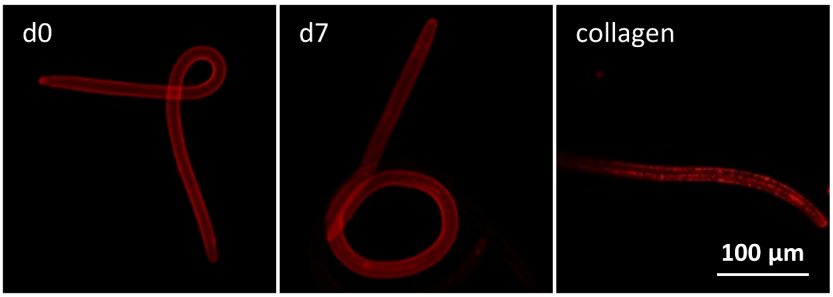

Figure 24: Preliminary experiments for fluorescent labelling of O. volvulus L4 larvae. Confocal microscopy of L4 larvae stained with VivoTag 680 XL at day 0 and after 7 days. The dye enabled microscopic analysis of larvae embedded in a thin collagen layer. Scale bar = 100 µm.

Despite the challenging direct culture setups, different alternative culture approaches have been used to study their support on larval growth and viability, all representing a different level of complexity. Figure 25 gives an overview of the applied co-cultures and depicts the relevant factors present each system.

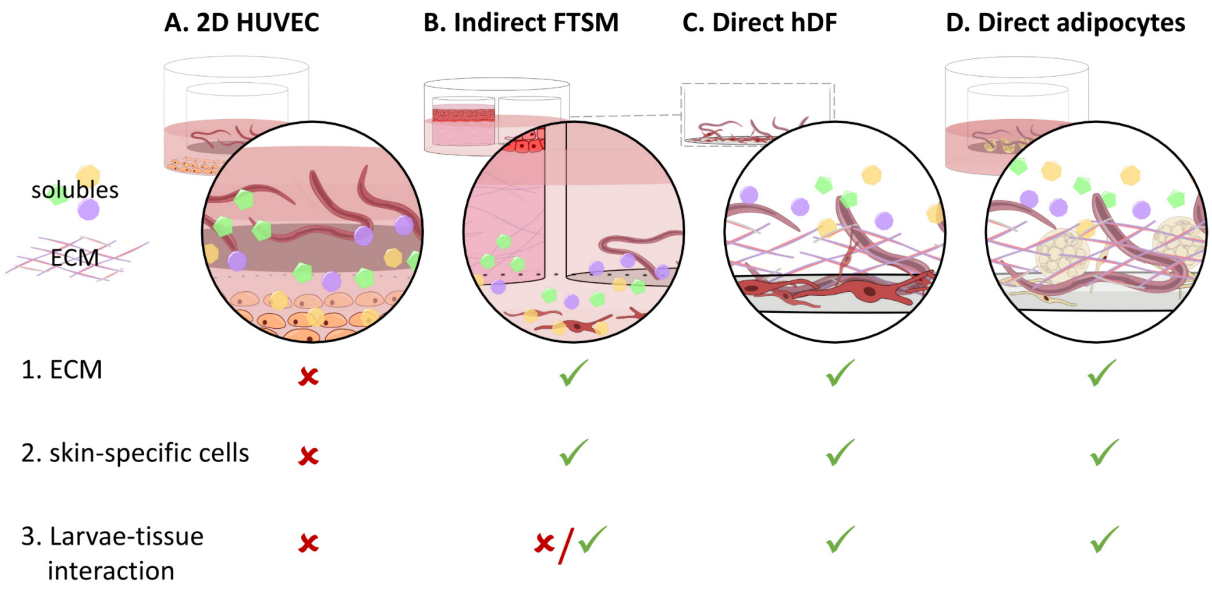

Figure 25: Overview of co-culture setups of *O. volvulus* larvae and *in vitro* tissue models. Representation of crucial *in vivo* factors that were addressed for the culture of *O. volvulus* larvae: 1. ECM, 2. skin-specific cells and 3. larvae-tissue interaction in the different culture approaches **A.** 2D HUVEC culture, **B.** Indirect culture with FTSM, **C.** Direct culture resulting from hDF migration within the indirect FTSM culture and **D.** Direct co-culture with adipose tissue aggregates. The detailed images also indicate the presence of solubles and ECM.

The direct physical contact to the postulated crucial tissue factors ECM and skin-specific cells is of importance for the resemblance of the *in vivo* niche. However, the contact between larvae and tissue also takes place on a molecular level by the interaction with solubles – a factor that is present in all culture systems. Soluble factors, such as growth factors, cytokines, enzymes, and other molecules secreted by both, larvae and cells, are responsible for the support of larval growth and development in the 2D culture system (Figure 2, 25A). The separation of HUVECs and *O. volvulus* larvae by the insert membrane with pore sizes of 3 µm only allows the exchange of solubilized molecules within the culture medium. An appropriate support of larvae development within the 2D culture was demonstrated by its application for several research approaches [29,167]. Moreover, the effect of solubles was also proven by the *in vivo* culture of larvae in diffusion chambers implanted to primates [26].

In contrast to the 2D culture, the indirect FTSM culture presented crucial factors 1 and 2 – skin specific cells seeded on the collagen scaffold (Figure 25B). The initial separation of larvae and the FTSM only allowed the bi-directional communication

by soluble factors. The significantly increased length of larvae co-cultured with the FTSM by 8.4 % in 3D-2 and 6.5 % in 3D-3 compared to the 2D control group demonstrates the enhanced support on larval growth (Figure 22E). This effect might be explained by the increased complexity of skin-specific cells in ECM represented by the FTSM and thus, a unique human secretory signature. However, the viability of larvae could not be improved by secreted factors of the 3D context (Figure 22F). In the progression of the indirect FTSM co-culture, hDF migrated towards the larvae-containing insert and penetrated the membrane. Finally, this hDF migration resulted in the overgrowth of the L4 larvae and thereby facilitated a direct contact. This was confirmed by the SEM imaging of a L4 larva, which was integrated into a newly formed tissue by hDF and secreted ECM without having a detrimental effect (Figure 22D). By chance, the indirect FTSM co-culture resulted in the presence of all three crucial factors (Figure 25C).

Similarly, the last culture approach based on adipose tissue aggregates also provided crucial factors 1-3, thereby resembling a parasite niche-specific environment, as onchocercomas are typically found in the subcutis [27]. The immunohistological analysis of the differentiating hMSC aggregates and collagen-based adipose tissue models depicted the expression of ECM proteins collagen type III and IV (Figure 14C-D, Figure 16). The use of aggregated adipose tissue models within a culture insert enabled the direct culture with the larvae and the possibility to monitor vital parameters (Figure 25D). Interestingly, the motility of L4 larvae was significantly increased by 58 % compared to the indirect culture and 69 % compared to the 2D control, whereas the growth of larvae was not positively affected. Additionally to the direct contact to adipose tissue components, the environment within the insert is augmented by the secretion of lipids to the culture medium [71], which might explain the location of L4 larvae in the proximity of the adipose tissue aggregates, as gradients of lipids might have been established. It is reported that the fitness of *O. volvulus* and many nematodes, such as *Brugia malayi* relies on free fatty acids, thus they express and secrete fatty acid binding proteins into the host tissue [168]. Fatty acids are required for multiple developmental and metabolic processes, such as embryogenesis, growth, differentiation, and the synthesis of glycoproteins [169]. Therefore, the L4 medium is supplemented with the lipid mixture. Especially cholesterol was described as crucial factor for the development of nematodes in

signaling and molting processes [170]. Furthermore, undifferentiated cells were found to migrate from the aggregates and cover the membrane surface, thereby forming a heterogeneous cell population of non-differentiated hMSCs, differentiating pre-adipocytes, and morphologically matured adipocytes. Similar to the direct hDF culture, L4 larvae were attached by non-differentiated cells without a harming impact. Notably, hMSCs are described to have a positive therapeutical impact by the secretion of trophic molecules [150,171]. The hMSC secretome is composed of growth factors, cytokines, micro vesicles and exosomes that are involved in processes of wound healing and thus, of interest for the development of novel therapeutics and drug delivery systems [172–174]. As hMSCs are found in a variety of human tissues, especially in the *in vivo* niche of developing *O. volvulus* larvae, adipose tissue and skin [145,150], the secretome of the cells might have enhanced the viability *in vitro*. However, despite the presence of soluble factors in the indirect culture with adipose tissue models, a 58 % reduction of motility compared to the direct condition was observed. This might be explained the coverage of the permeable membrane by hMSCs (Figure 23A). Eventually, a reduced diffusion through the membrane resulted in the enrichment of soluble factors in the adipose-tissue containing compartment. Furthermore, the culture medium submerging adipose tissue models and larvae is not renewed by media exchange as it happens for the conditioned medium in the culture well of the indirect culture. This additionally supports the theory of an increased enrichment and the establishment of a more favorable milieu within the direct culture insert. Thus, the indirect cultured larvae might not be provided with soluble factors to the same extent as the direct cultured L4.

Nevertheless, the role of soluble factors for a communication between the parasite and the host tissue could be highlighted. The augmentation of the culture medium with a human physiological signature that might be as complex as the co-cultured tissue model seems to have a beneficial impact on the fitness of *O. volvulus* larvae *in vitro*. The co-cultured tissue and cells release soluble factors dynamically, eventually in correspondence with received larval signals. The identification of factors involved in beneficial signaling for the production of a defined culture medium would be very cost- and time-intensive. Hence, the dynamic conditioning of the culture medium by the tissue model might be more favorable [71]. Besides the communication via

soluble factors mediated by niche-specific cells within a 3D context – crucial factor 1 and 2 – the data presented here suggest that the direct contact – factor 3 – seems to enhance the fitness of larvae *in vitro*. Moreover, the observation of the hDF migration towards the larvae resulting in a favorable direct culture gives a hint of an active bi-directional crosstalk between the parasite larvae and human tissue models.

4.3 Migration of cells as initial step of nodule formation

The overgrowth of larvae by hDF into a newly formed tissue was shown by SEM in Figure 22D. This *in vitro* integration might represent a first step of the nodule formation *in vivo*. Onchocercomas encapsulate the adult parasite within the human host. These nodules are composed of highly vascularized fibrous tissue containing multiple immune cells and notably, activated fibroblasts at the inner rim of the capsule [27,30,175]. This drives the hypothesis that the recruitment of hDF from the co-cultured FTSM might represent a first step of onchocercoma formation mediated by *O. volvulus* larvae. The hypothesis is supported by the observation of larvae integration into the newly formed dermal tissue after hDF migration, representing an important factor of the nodular niche. Usually, in humans a foreign body is detected by tissue-resident macrophages that initiate an inflammatory response, followed by the recruitment of fibroblasts, which are stimulated to secrete ECM. This macrophage-mediated immune reaction leads to the encapsulation of a foreign body in fibrous tissue [176], resulting in the isolation of the object in a collagenous fibrous capsule. The typical two-step capsule formation of a foreign body [177] seems to be circumvented in the observed integration of *O. volvulus* larvae, as migration and matrix production occurred without immune cell mediation. This cell recruitment and the support of larval fitness via soluble factors and direct contact underlines the crucial function of fibroblasts for the development of larvae *in vitro* and possibly *in vivo*. To further elucidate this context, it would be interesting to analyze the effect of extracted nodular ECM on the larvae development. Therefore, onchocercomas from nodulectomy could be decellularized and decomposed. This would allow an application of nodular matrix within the collagen or as a coating for the insert membrane to further icrease the biochemical complexity.

Although the aim of developing a culture system for the *in vitro* development of pre-adult *O. volvulus* worms could not be achieved, this study delivers a proof of concept for the general feasibility of applying *in vitro* tissue models for the support of *O. volvulus* larvae. The data acquired from the discussed co-culture approaches confirm our initial hypothesis, that all three crucial factors – the presence of niche-specific cells in a 3D context and especially direct contact – are essential for the support of fitness *in vitro*. The so increased complexity of the 3D tissue cultures enabled a more complex pattern of stimuli and signalling, compared to the 2D culture system. Interstingly, a tissue-dependent support could be observed. Whereas the FTSM or the hDF respectively supported the growth, the direct contact with the adipose tissue models sustained the larvae viability. A combination of the tissues in a culture setup that allows the monitoring of vital parameters over a long-term culture period might facilitate a synergetic effect and thereby the development of L4 larvae to pre-adult L5s and eventually adult parasites. The analysis of larvae development could be also evaluated on a molecular level. Many data of *O. volvulus* omics are available for different developmental stages and the Wolbachia endosymbiont [178–180]. The data acquisition might be performed via single worm transcriptomics, which could increase the in depth understanding of the development of larvae populations [181]. The results could be used to elaborate the culture conditions to support both, larvae and the endosymbiotic bacteria, by the supplementation of specifically required factors that might not be obtained from the *in vitro* environment despite their increased complexity. To emulate the complexity of the *in vivo* niche, this study aimed for the translation into an *in vitro* culture system, represented by the multilayered skin model.

4.4 Translation of the *in vivo* niche – Development of the adipose tissue model

For the translation of the three-layered skin composed of epidermis, dermis, and subcutis, a novel adipose tissue had to be developed and finally integrated into the FTSM. Therefore, hMSCs derived from human bone marrow of the in-house Biobank were analyzed for their suitability as cell source. Multiple reasons favored the use of hMSCs for the differentiation of adipocytes instead of using primary adipocytes, that

can be obtained from liposuction. First, hMSCs can be expanded to very high numbers, that were required to generate the adipose tissue models without the need of frequent adipocyte isolations. Also, the handling requirements of hMSCs are relatively moderate, compared to the susceptibility of primary adipocytes to mechanical damage. Furthermore, the ability of cryopreservation simplified the shipment of cells for experimentation to the NYBC. In combination with the experience of hMSC culture at the institute, the bone marrow-derived cells were chosen as cell source.

The first experiments with the hMSCs aimed to identify culture conditions for the optimization of the adipogenic differentiation and lipid accumulation. To allow the assessment of culture parameters, a protocol for the semi-quantitative Oil Red O analysis was adapted [182]. This allowed the quantification of the lipid content of a 2D hMSC culture. For the simplification of experiments, factors for promoting the adipogenesis were analyzed in 2D and the results were transferred to 3D. For the differentiation of hMSCs towards the adipogenic lineage protocols and differentiation factors are well established, using a mix of dexamethasone, insulin, indomethacin, and IBMX in different proportions [146,183]. In combination, these factors modulate the activity of PPARγ, a key regulator of adipogenesis [147]. To enhance the lipid accumulation, the standard differentiation medium (ADM) was supplemented with additional glucose and lipids to provide higher levels of energy and building blocks for lipogenesis (Figure 4). The effect of hypertrophy, the expansion of adipose tissue by the accumulation of triglycerides [76], was noticeable by an increased number of lipid vacuoles within the differentiating hMSCs (Figure 10). Moreover, the hypertrophic effect was measured via the semi-quantitative Oil Red O analysis, resulting in a 2.4-fold gain of intracellular lipids compared to the standard differentiation medium. Hence, the so called ADM+ was used for further differentiation experiments and the generation of 3D adipose tissue models [71,164].

Another adjustable culture parameter is the density of cells. A cell density-dependence of the adipogenic differentiation efficiency was reported for ADSCs [149]. A high cell density increases cell contacts between cells, which enhances intercellular communication via gap-junctions. These junctions connect the cytosol of adjacent cells and thereby supports the crosstalk, proliferation, and

differentiation – crucial processes for the tissue homeostasis [184,185]. This correlation of cell density and adipogenesis was confirmed with differentiating hBMSCs in 2D. The measurable intracellular lipid content of 1 x 10^5 hMSCs/cm^2 was 11.7-fold increased compared to 5 x 10^3 cells/cm^2. This finding was hypothesized to be transferable to the seeding of hMSCs into a collagen hydrogel for the generation of a 3D adipose tissue model.

The collagen type I isolated from rat tails serves as the scaffold for the dermal component of the FTSM. Hence, as a first approach the collagen hydrogel was applied to create a 3D environment for the underlying adipose tissue model. Furthermore, collagen type I also represents an ECM protein of adipose tissue [79,186]. Moreover, collagen microfibers were shown to stimulate the pre-adipocyte functionality [187]. To identify an optimal seeding density according to the cell density-dependence of hMSCs within the collagen hydrogel, multiple cell concentrations have been evaluated (Figure 11). Scaffolds seeded with a density of 3 x 10^6 hMSCs/ml represented an even distribution of cells. Moreover, it allowed the generation of a sufficient number of models for an experiment with the number of cells that are typically obtained from the 2D expansion culture of hMSCs. Hence, this cell density was chosen for further differentiation experiments. Similar to the 2D differentiated hMSCs, the differentiating adipocytes within the 3D environment showed first lipid vacuoles surrounding the cell nuclei, which start to fuse together until unilocular adipocytes occur from week 8 to 10 of differentiation (Figure 12). The fusion of intracellular lipid droplets to a single storage vacuole is a key characteristic feature of mature white adipocytes [82]. Notably, the acquirement of unilocular adipocytes from stem cells is controversially discussed. Commonly used immortalized cell lines of animal origin, such as 3T3-L1 or 3T3-F442, and the human Simpson-Golabi-Behmel syndrome cells can be differentiated adipogenically, but fail to reach a unilocular state [152,188]. Other human cell sources like ADSCs are reported to have a lower maturation rate compared to primary matured adipocytes [189]. To investigate the maturation of the bone marrow-derived hMSCs used in this study, a method for the quantification of unilocular adipocytes was established by the master student Laurin Glaser [157]. The microscopy of Nile Red-stained adipose tissue models revealed a 14.7 % proportion of unilocular adipocytes with a mean diameter of 37 µm (Figure 13). WAT *in vivo* contains about 50 % of matured cells with a

diameter ranging from 20-300 µm depending on the body location, sex and obesity status [80,81]. A study, which investigated the adipocyte size in relationship to obesity and insulin resistance (type 2 diabetes) of male humans, revealed a mean diameter of abdominal adipocytes of 63.4 µm in healthy individuals [190]. In a direct comparison, bone marrow adipocytes are smaller than subcutaneous adipocytes, ranging between 40 – 65 µm in diameter [191]. Thus, the adipocyte size in the collagen-based adipose tissue model is at the lower range compared to subcutaneous WAT and bone marrow adipose tissue. This confirms the observation, that diameters and especially the maturation time of adipocytes in 3D *in vitro* models show high ranges of up three months [187], which also represents the time required for the formation of unilocular cells in the presented collagen-based model.

Besides the morphological progression, the molecular marker profile of differentiation is relevant for the adipocyte maturation. The histological staining of the key regulator of adipogenesis PPARγ revealed a co-localization with the cell nuclei in the early differentiation. After the translation in the cytosol, the ligand-dependent PPARγ is transported into the nucleus due to its function as transcription factor. The pro-adipogenic PPARγ together with other transcriptions factors drive the adipogenesis and enhance the lipid accumulation and insulin sensitivity and thus is highly abundant in WAT [80,82,83]. However, PPARγ was shown to be dynamically shuttled between the cell nucleus and the cytoplasm in response to external signals [192]. This fact could explain the weak cytosolic signal from week 6 to 12 of differentiation, which is decreased by its distribution within the enlarging adipocytes (Figure 14A). ADFP, also termed adipose differentiation-related protein or perilipin 2, is found in premature adipocytes and during early differentiation located on the surface of lipid droplets [193]. However, during differentiation ADFP is exchanged by perilipin 1, which is exclusively found on mature adipocytes [194]. As ADFP was detected after 12 weeks of differentiation (Figure 14B), this finding might be a hint for a not complete maturation of the adipocytes. It would be interesting to further analyze the maturation status of the cells by the secretory profile, which has not been examined in this study.

The effect of cell density-dependence in the 3D adipose tissue model on the proportion of unilocular cells and the size was further investigated in the master thesis of Laurin Glaser [157]. In the early differentiation, high-cell density models

with concentrations of 9 x 10^6 hMSCs/ml of collagen hydrogel showed a non-significant increased rate of unilocular cells until week 10. The adipocyte size was slightly increased to 40.8 µm compared to 37 µm with 3 x 10^6 hMSCs/ml. Eventually, both cell concentration reached the same degree of morphological cell maturation. However, the high cell numbers led to the formation of high cell density-clusters by local non-homogenous distributions within the collagen hydrogel. These clusters appeared to have a close morphological resemblance to native WAT. This observation strengthens the hypothesis of the cell density-dependency on the adipogenesis of hMSCs in 3D. To facilitate a locally increased cell density, a parallel approach for the generation of scaffold-free 3D adipose tissue models was investigated.

To achieve a maximum cell density without spatial separation between differentiating adipocytes, hMSCs were aggregated prior the differentiation. Culture in ADM+ resulted in the increase of aggregate size, which is explained by the accumulation of intracellular lipids within the cells (Figure 15A-E). The decrease of size of the differentiating aggregates as well as the slight increase of non-differentiating aggregates might be explained by the outgrowth of hMSCs from the attached cells. This might have led to a decreased volume or a flattening of the aggregate, respectively. This outgrowth of hMSCs was proven by the Oil Red O and MTT-positive cells surrounding the aggregate after the long-term culture, as well as these cells were observed to attach *O. volvulus* L4 larvae in the direct co-culture (Figure 15F-G, Figure 23A). Notably, unilocular adipocytes were already found after 22 days of differentiation, proving the enhanced adipogenesis in dependence to cell density of hMSCs in 3D. Similar approaches using hADSCs confirm a physiological adipose tissue environment regarding ECM production and an enhanced adipogenesis [195,196]. The analysis of the marker profile revealed the expression of PPARγ and ADFP surrounding the nuclei. Similar to the collagen-based model, the differentiating adipocytes produced collagen type IV (Figure 14D, Fig. 16), a crucial ECM protein in WAT [79]. However, the aggregate size shown in the immunohistological analysis is above the critical size for diffusion, which is shown by the formation of a necrotic core. Hence, for further experiments the cell number was reduced from 2.5 x 10^5 to 1 x 10^5 hMSCs/aggregate.

Taken together, two systems were developed for the generation of the 3D adipose tissue model based on hMSCs. Both systems reflect advantages regarding their

applicability for different research questions. The collagen-based adipose tissue models enable the possibility to generate structures into the surrounding scaffold, such as a channel architecture for vascularization [197] or as aimed in this study, a confined culture compartment for a parasitic worm. Furthermore, the density of the scaffold, which influences the stiffness has an impact on the lineage commitment of hMSCs [198]. This mechanobiological influence was also addressed by Laurin Glaser, showing a densely packed adipose tissue model by combining the increased cell concentration of 9 x 10^6 hMSCs/ml and a reduced collagen concentration of 4 mg/ml [157]. However, modifications of the collagen scaffold would be required to allow a long-term stability as these models shrank due to collagen remodeling. Another drawback of this tissue model is the culture duration required for the differentiating adipocytes to mature. This major issue has been addressed by the aggregation of hMSCs as unilocular adipocytes were observed after 3 weeks. So far, both adipose tissue models are monocellular, they only contain hMSCs at different stages of adipogenic differentiation. For the vascularization of the tissue models, it would be interesting to analyze co-cultures of hMSCs with endothelial cells. It could be shown that co-cultures of hADSCs and HUVECs formed endothelial networks and capillary-like structures within a 3D scaffold [199,200]. Another source of adipocyte progenitors is represented by the stromal vascular fraction, which is additionally composed of endothelial cells, pericytes, and immune cells [81]. This cellular fraction seeded onto a biological scaffold or cultured as spheroids shows favorable tendencies for vascularization and represents a great potential for clinical applications [201,202].

An increased complexity in adipose tissue engineering will also contribute to the application in disease modelling. As discussed earlier, obesity represents a strongly increasing risk factor for public health causing obesity-related maladies, such as diabetes and ischaemic heart disease [1]. Moreover, as a niche tissue environment for *O. volvulus* and other human parasites [140], the development of complex adipose tissue models will be of importance in future medical research concerning diseases of civilization in western societies and NTDs in the global south. An example for a complex adipose tissue engineering is the multilayered skin model that represents the relevant tissues of human skin. For the development, the scaffold-free adipose tissue models allowed the integration into the FTSM.

4.5 Translation of the *in vivo* niche – Integration of adipose tissue to FTSM

Three key findings distinguished the scaffold-free adipose tissue for integration to the FTSM. First, the reduced maturation period shortens the overall time required for the generation of the multilayered skin model (Figure 15D). Second, the hMSC aggregates demonstrated the robustness for the plastic compression of the overlying dermal model (Figure 19A). Moreover, the adipose tissue aggregates proved a long-term cell lineage commitment, when cultured in E10 without de-differentiation of adipocytes (Figure 18C-E). This allowed an additive generation protocol starting with the pre-differentiation of hMSC aggregates for three weeks, followed by the protocol of the FTSM generation protocol. Still, this procedure requires 7 weeks of 3D cell culture. In contrast, the collagen-based adipose tissue model would have prolonged the generation process. Moreover, the increased scaffold density within in the collagen-based adipose tissue model after the dermal compression might have a mechanobiological impact on the differentiating adipocytes. The so increased stiffness resembles the osteogenic niche, thus hMSCs show a reduced adipogenic differentiation [157] and favor to differentiate towards the osteogenic lineage [198].

The multilayered skin model shows the characteristic features of the three major layers epidermis, dermis and subcutaneous adipose tissue, comparable to the human skin (Figure 19D-I). However, the distribution of the adipose tissue aggregates within the model is uneven. Depending on the application, a more regular adipose tissue layer would allow a more constant tissue model. Despite this disadvantage, the augmented FTSM represents a novel multilayered skin model with an adipose tissue composed of hMSCs. Other approaches for the development of a three-layered skin tissue applied primary mature adipocytes in collagen hydrogels [143,163], primary adipocytes and hADSCs in a fibrin hydrogel [203], and recently hADSCs bio printed in a suspended layer manufacturing approach [204]. The former skin tissue shows a highly matured adipose tissue, due to the use of primary adipocytes. A contraction of the epidermis due to the shrinkage of the dermal collagen is prevented by the addition of an external culture compartment for the dermis and subcutis underneath the culture membrane that contains the epidermal part [143]. Thus, the tissue layers are separated by the insert membrane. The hypodermal layer of the fibrin-based skin model using hADSCs and primary adipocytes contains large fat cells [203]. Unfortunately, the hEK of the epidermal part do not form the epidermis-specific

layers. The same is shown for the bio-printed skin tissue, which might be explained by the missing air-liquid-interface in the suspended layer printing setup [204]. In parallel to the skin model based on collagen, a three-layered skin tissue model based on electrospun carbon fibers was developed inhouse [164]. Here, the even distribution of adipocytes within a multilayered skin model could be achieved using electrospun carbon fiber scaffolds seeded with hMSCs that were allowed to proliferate into the fleece, which was clamped into a cell crown to avoid the contraction. After the differentiation, these adipose tissue fleeces were stacked with dermal fleeces and seeded with keratinocytes. Similar to the multilayered skin model, this 3D culture resulted in a mechanically stable tissue model composed of the three major skin layers. However, even showing unilocular adipocytes, the cell density does not reach a similar degree compared to native WAT or the local density of aggregated adipose tissue models.

Although, the translation of the *in vivo* niche of *O. volvulus* into an *in vitro* tissue model could be achieved, a direct co-culture with larvae – crucial factor 3 – was hindered due to aspects discussed in this study (Figure 21). However, the crucial factor 1 – ECM and factor 2 – skin-specific cells were present in the model. Nevertheless, the alternative culture systems that were applied for L4 co-culture revealed important aspects for the development of *O. volvulus* larvae *in vitro*. The initial hypothesis of a support of larvae by an increased complexity of the co-cultured tissue models could be verified.

5. Outlook

The here presented data deliver a proof of concept for the support of *O. volvulus* larvae development *in vitro* by 3D human tissue models. To further elucidate relevant cues for larvae development until adult stages, the application of tissue models might be refined.

For future co-culture experiments with *O. volvulus* larvae in the presence of the three crucial factors, several advancements might be applied to overcome the discussed challenges of a direct culture. For the creation of an imprint into the collagen scaffold, higher compression factors could be applied to facilitate an enhanced long-term stability. Another ECM-related advancement would be the utilization of decellularized and decomposed nodular tissue for the 3D scaffold material, thereby representing a parasite niche-specific component that might resemble a more *in vivo*-like environment. The observation of developing larvae within a tissue model represented an obstacle for the direct culture. The monitoring of vital parameters of larvae might be addressed by methodologies of advanced microscopy. Thus, the proposed labelling strategies using a vital dye would support this endeavor. Another labeling strategy is represented by transfection of larvae with a fluorescent marker as it could be shown for the filarial parasite *Brugia malayi* [205]. If a labeling strategy allows the monitoring of larvae within the multilayered skin, it would be also interesting to examine the co-culture of L4 on the fiber fleece-based multilayered skin [164].

The co-culture of larvae and adipose tissue aggregates represented a smart solution to circumvent the monitoring challenges. The biological complexity of this culture could be increased by using multi-cellular systems, such as spheroids of the stromal vascular fraction [202], which might lead to a synergetic effect – the support of growth and viability. In this regard, a spheroid-based co-culture would possibly represent an interesting approach that might increase the practicability and feasibility in non-expert labs for tissue engineering.

However, the less complex culture approach which was again confirmed to be supportive for larvae development, despite its limitations due to a low biological complexity, is represented by the 2D co-culture of a feeder layer. It would be

interesting to further study the influence on larvae fitness by hMSCs, which are known to secrete trophic molecules. Combinations of a feeder layer of hMSCs and skin and/or adipose tissue models would be an interesting co-culture experiment.

The analysis of a supportive influence on larvae development could be also evaluated on a molecular level. Many data of *O. volvulus* omics are available for different developmental stages and the Wolbachia endosymbiont. Omics data might be acquired via single worm transcriptomics [181]. The results could elaborate the culture conditions to support both, larvae and the endosymbiotic bacteria.

List of References

1. Vos T, Lim SS, Abbafati C, Abbas KM, Abbasi M, Abbasifard M, et al. Global burden of 369 diseases and injuries in 204 countries and territories, 1990–2019: a systematic analysis for the Global Burden of Disease Study 2019. Lancet [Internet]. 2020 Oct;396(10258):1204–22. Available from: https://linkinghub.elsevier.com/retrieve/pii/S0140673620309259

2. Kones R, Rumana U. Cardiometabolic diseases of civilization: history and maturation of an evolving global threat. An update and call to action. Ann Med [Internet]. 2017 Apr 3 [cited 2021 Sep 17];49(3):260–74. Available from: https://pubmed.ncbi.nlm.nih.gov/27936950/

3. M. Warren; S. Beck; D. Delgado. The State of Obesity: BETTER POLICIES FOR A HEALTHIER AMERICA 2019. Trust Am Heal [Internet]. 2019;92. Available from: http://stateofobesity.org/states/wv/

4. Schienkiewitz A, Mensink GBM, Kuhnert R, Journal CL. Overweight and obesity among adults in Germany. J Heal Monit. 2017;2(2):20–7.

5. Lin X, Xu Y, Pan X, Xu J, Ding Y, Sun X, et al. Global, regional, and national burden and trend of diabetes in 195 countries and territories: an analysis from 1990 to 2025. Sci Rep [Internet]. 2020 Dec 8 [cited 2021 Sep 16];10(1):14790. Available from: https://www.nature.com/articles/s41598-020-71908-9

6. Molyneux DH, Savioli L, Engels D. Neglected tropical diseases: progress towards addressing the chronic pandemic. Lancet [Internet]. 2017 Jan [cited 2021 Sep 17];389(10066):312–25. Available from: http://dx.doi.org/10.1016/S0140-6736

7. Álvarez-Hernández D-A, Rivero-Zambrano L, Martínez-Juárez L-A, García-Rodríguez-Arana R. Overcoming the global burden of neglected tropical diseases. Ther Adv Infect Dis [Internet]. 2020 Jan 19 [cited 2021 Sep 17];7:204993612096644. Available from: /pmc/articles/PMC7592315/

8. Hofstraat K, van Brakel WH. Social stigma towards neglected tropical diseases: a systematic review. Int Health [Internet]. 2016 Mar 3 [cited 2021 Sep 17];8(suppl 1):i53–70. Available from: https://academic.oup.com/inthealth/article/8/suppl_1/i53/2488349

9. Vlassoff C, Weiss M, Ovuga EBL, Eneanya C, Nwel PT, Babalola SS, et al. Gender and the stigma of onchocercal skin disease in Africa. Soc Sci Med [Internet]. 2000 May 16 [cited 2021 Sep 6];50(10):1353–68. Available from: https://pubmed.ncbi.nlm.nih.gov/10741573/

10. Lenk EJ, Redekop WK, Luyendijk M, Rijnsburger AJ, Severens JL. Productivity Loss Related to Neglected Tropical Diseases Eligible for Preventive Chemotherapy: A Systematic Literature Review. Gray DJ, editor. PLoS Negl Trop Dis [Internet]. 2016 Feb 18 [cited 2021 Sep 6];10(2):e0004397. Available from: https://pubmed.ncbi.nlm.nih.gov/26890487/

11. WHO Team Control of Neglected Tropical Diseases. Ending the neglect to attain the Sustainable Development Goals: a road map for neglected tropical diseases 2021–2030. Geneva: World Health Organization (https://www.who.int/neglected_diseases/Revised-DraftNTD-Roadmap-23Apr2020.pdf) [Internet]. 2020 [cited 2021 Sep 17]. Available from: https://www.who.int/publications/i/item/9789240010352

12. Herricks JR, Hotez PJ, Wanga V, Coffeng LE, Haagsma JA, Basáñez M-G, et al. The global burden of disease study 2013: What does it mean for the NTDs? Zhou X-N, editor. PLoS Negl Trop Dis [Internet]. 2017 Aug 3 [cited 2021 Sep 17];11(8):e0005424. Available from: https://journals.plos.org/plosntds/article?id=10.1371/journal.pntd.0005424

13. Hardwick RJ, Truscott JE, Oswald WE, Werkman M, Halliday KE, Pullan RL, et al. Individual adherence to mass drug administration in neglected tropical disease control: A probability model conditional on past behaviour. Downs JA, editor. PLoS Negl Trop Dis [Internet]. 2021 Jan 22 [cited 2021 Sep 17];15(1):e0009112. Available from: https://journals.plos.org/plosntds/article?id=10.1371/journal.pntd.0009112

14. Bethony JM, Cole RN, Guo X, Kamhawi S, Lightowlers MW, Loukas A, et al. Vaccines to combat the neglected tropical diseases. Immunol Rev [Internet]. 2011 Jan [cited 2022 Aug 24];239(1):237–70. Available from: https://pubmed.ncbi.nlm.nih.gov/21198676/

15. Hotez PJ. The global fight to develop antipoverty vaccines in the anti-vaccine era. Hum Vaccin Immunother [Internet]. 2018 Sep 2 [cited 2022 Aug 24];14(9):2128–31. Available from: https://pubmed.ncbi.nlm.nih.gov/29393710/

16. Lustigman S, Makepeace BL, Klei TR, Babayan SA, Hotez P, Abraham D, et al. Onchocerca volvulus: The Road from Basic Biology to a Vaccine. Trends Parasitol [Internet]. 2017 Sep 22;xx. Available from: http://linkinghub.elsevier.com/retrieve/pii/S1471492217302295

17. BionTech SE. BioNTech Provides Update on Plans to Develop Sustainable Solutions to Address Infectious Diseases on the African Continent [Internet]. [cited 2021 Sep 17]. Available from: https://investors.biontech.de/news-releases/news-release-details/biontech-provides-update-plans-develop-sustainable-solutions/

18. BioNTech SE. BioNTech beginnt Bau der ersten Produktionsstätte für mRNA-basierte Impfstoffe in Afrikatle [Internet]. [cited 2022 Aug 24]. Available from: https://biontechse.gcs-web.com/de/news-releases/news-release-details/biontech-beginnt-bau-der-ersten-produktionsstaette-fuer-mrna

19. Ung L, Jonas JB, Lietman TM, Chodosh J. COVID-19 and the Unfinished Agenda of VISION 2020. Am J Ophthalmol [Internet]. 2021 Apr 1 [cited 2021 Sep 17];224:30–5. Available from: https://linkinghub.elsevier.com/retrieve/pii/S0002939420306504

20. Booth M. Climate Change and the Neglected Tropical Diseases. In: Advances in

parasitology [Internet]. Adv Parasitol; 2018 [cited 2021 Sep 17]. p. 39–126. Available from: https://pubmed.ncbi.nlm.nih.gov/29753342/

21. Hamley JID, Blok DJ, Walker M, Milton P, Hopkins AD, Hamill LC, et al. What does the COVID-19 pandemic mean for the next decade of onchocerciasis control and elimination? Trans R Soc Trop Med Hyg [Internet]. 2021 Mar 6 [cited 2022 Aug 24];115(3):269–80. Available from: https://pubmed.ncbi.nlm.nih.gov/33515042/

22. African Programme for Onchocerciasis Control (APOC). Eighteenth Session of the Joint Action Forum. Bujumbura, Burundi. Final Communique. 2012.

23. WHO/Department of Control of Neglected Tropical Diseases. Progress report on the elimination of human onchocerciasis, 2017–2018. Wkly Epidemiol Rec [Internet]. 2018;16(93):201–20. Available from: http://www.who.int/wer%0Ahttp://www.who.int/wer2018,93,649-660No48%0Ahttp://www.who.int/wer

24. Murdoch ME. Mapping the burden of onchocercal skin disease*. Br J Dermatol [Internet]. 2021 Feb 21 [cited 2021 Sep 6];184(2):199–207. Available from: https://onlinelibrary.wiley.com/doi/10.1111/bjd.19143

25. Morris CP, Evans H, Larsen SE, Mitre E. A Comprehensive, Model-Based Review of Vaccine and Repeat Infection Trials for Filariasis. Clin Microbiol Rev [Internet]. 2013 Jul 1;26(3):381–421. Available from: http://cmr.asm.org/cgi/doi/10.1128/CMR.00002-13

26. Abraham D, Lange AM, Yutanawiboonchai W, Trpis M, Dickerson JW, Swenson B, et al. Survival and Development of Larval Onchocerca volvulus in Diffusion Chambers Implanted in Primate and Rodent Hosts. J Parasitol [Internet]. 1993 Aug;79(4):571. Available from: https://www.jstor.org/stable/3283385?origin=crossref

27. Schulz-Key H. The collagenase technique: How to isolate and examine adult Onchocerca volvulus for the evaluation of drug effects. Vol. 39, Tropical Medicine and Parasitology. 1988. p. 423–40.

28. Strote G, Bonow I, Krömer M, Rubio de Krömer T, Attah S, Opoku N. Chemotherapy for onchocerciasis: results of in vitro experiments with promising new compounds. Trop Med Int Health [Internet]. 1998 May;3(5):397–407. Available from: http://www.ncbi.nlm.nih.gov/pubmed/9623946

29. Voronin D, Tricoche N, Jawahar S, Shlossman M, Bulman CA, Fischer C, et al. Development of a preliminary in vitro drug screening assay based on a newly established culturing system for pre-adult fifth-stage Onchocerca volvulus worms. Basáñez M-G, editor. PLoS Negl Trop Dis [Internet]. 2019 Jan 17 [cited 2021 Sep 6];13(1):e0007108. Available from: https://dx.plos.org/10.1371/journal.pntd.0007108

30. Attout T, Hoerauf A, Dénécé G, Debrah AY, Marfo-Debrekyei Y, Boussinesq M, et al. Lymphatic vascularisation and involvement of Lyve-1+ macrophages in

the human Onchocerca nodule. PLoS One. 2009;4(12).

31. Kershaw WE, Duke BOL, Budden FH. Distribution of Microfilariae of O. Volvulus in the Skin. BMJ [Internet]. 1954 Sep 25 [cited 2021 Sep 6];2(4890):724–9. Available from: https://www.ncbi.nlm.nih.gov/pmc/articles/PMC2079088/

32. Taylor MJ, Hoerauf A, Bockarie M. Lymphatic filariasis and onchocerciasis. Lancet [Internet]. 2010 Oct 2 [cited 2022 Aug 24];376(9747):1175–85. Available from: https://pubmed.ncbi.nlm.nih.gov/20739055/

33. Haffner A, Guilavogui AZ, Tischendorf FW, Brattig NW. Onchocerca volvulus: microfilariae secrete elastinolytic and males nonelastinolytic matrix-degrading serine and metalloproteases. Exp Parasitol [Internet]. 1998 Sep [cited 2022 Aug 24];90(1):26–33. Available from: https://pubmed.ncbi.nlm.nih.gov/9709027/

34. Vuong PN, Bain O, Cabaret J, Petit G, Prod'hon J, Ranque P, et al. Forest and savanna onchocerciasis: comparative morphometric histopathology of skin lesions. Trop Med Parasitol [Internet]. 1988 Jun;39(2):105–10. Available from: http://www.ncbi.nlm.nih.gov/pubmed/3175464

35. Babalola O. Ocular onchocerciasis: current management and future prospects. Clin Ophthalmol [Internet]. 2011 Oct [cited 2021 Sep 6];5(1):1479. Available from: /pmc/articles/PMC3206119/

36. Higazi TB, Filiano A, Katholi CR, Dadzie Y, Remme JH, Unnasch TR. Wolbachia endosymbiont levels in severe and mild strains of Onchocerca volvulus. Mol Biochem Parasitol [Internet]. 2005 May [cited 2021 Sep 6];141(1):109–12. Available from: https://pubmed.ncbi.nlm.nih.gov/15811532/

37. Mckechnie NM, Braun G, Kläger S, Connor V, Kasp E, Wallace G, et al. Cross-reactive antigens in the pathogenesis of onchocerciasis. Ann Trop Med Parasitol [Internet]. 1993 Jan 15 [cited 2021 Sep 6];87(6):649–52. Available from: https://pubmed.ncbi.nlm.nih.gov/8122928/

38. Hall LR, Pearlman E. Pathogenesis of onchocercal keratitis (River blindness). Clin Microbiol Rev [Internet]. 1999 Jul [cited 2021 Sep 6];12(3):445–53. Available from: /pmc/articles/PMC100248/

39. Abiose A. Onchocercal eye disease Mectizan treatment and the impact of. Ann Trop Med Parasitol [Internet]. 1998 Apr 1 [cited 2021 Sep 6];92(3):11–22. Available from: https://pubmed.ncbi.nlm.nih.gov/9861263/

40. Amazigo UO. Detrimental effects of onchocerciasis on marriage age and breast-feeding. Trop Geogr Med [Internet]. 1994;46(5):322–5. Available from: http://www.ncbi.nlm.nih.gov/pubmed/7855922

41. Oladepo O, Brieger WR, Otusanya S, Kale OO, Offiong S, Titiloye M. Farm land size and onchocerciasis status of peasant farmers in south-western Nigeria. Trop Med Int Heal [Internet]. 2007 Aug 1 [cited 2021 Sep 6];2(4):334–40. Available from: https://pubmed.ncbi.nlm.nih.gov/9171841/

42. James SL, Abate D, Abate KH, Abay SM, Abbafati C, Abbasi N, et al. Global, regional, and national incidence, prevalence, and years lived with disability for 354 diseases and injuries for 195 countries and territories, 1990–2017: a systematic analysis for the Global Burden of Disease Study 2017. Lancet [Internet]. 2018 Nov 10 [cited 2021 Sep 6];392(10159):1789–858. Available from: http://www.thelancet.com/article/S0140673618322797/fulltext

43. Chesnais CB, Nana-Djeunga HC, Njamnshi AK, Lenou-Nanga CG, Boullé C, Bissek A-CZ-K, et al. The temporal relationship between onchocerciasis and epilepsy: a population-based cohort study. Lancet Infect Dis [Internet]. 2018 Nov 1 [cited 2021 Sep 6];18(11):1278–86. Available from: https://pubmed.ncbi.nlm.nih.gov/30268645/

44. NTD Modelling Consortium Onchocerciasis Group. The World Health Organization 2030 goals for onchocerciasis: Insights and perspectives from mathematical modelling: NTD Modelling Consortium Onchocerciasis Group. Gates open Res [Internet]. 2019 Sep 26;3:1545. Available from: https://gatesopenresearch.org/articles/3-1545/v1

45. Johnson TP, Tyagi R, Lee PR, Lee MH, Johnson KR, Kowalak J, et al. Nodding syndrome may be an autoimmune reaction to the parasitic worm Onchocerca volvulus. Sci Transl Med. 2017;9(377).

46. WHO/Department of Control of Neglected Tropical Diseases. Progress towards eliminating onchocerciasis in the WHO Region of the Americas: elimination of transmission in the north-east focus of the Bolivarian Republic of Venezuela. Relev Epidemiol Hebd. 2017;92(41):617–23.

47. Nicholls RS, Duque S, Olaya LA, López MC, Sánchez SB, Morales AL, et al. Elimination of onchocerciasis from Colombia: first proof of concept of river blindness elimination in the world. Parasit Vectors [Internet]. 2018 Dec 11;11(1):237. Available from: https://parasitesandvectors.biomedcentral.com/articles/10.1186/s13071-018-2821-9

48. Basáñez M-G, Pion SD, Boakes E, Filipe JA, Churcher TS, Boussinesq M. Effect of single-dose ivermectin on Onchocerca volvulus: a systematic review and meta-analysis. Lancet Infect Dis [Internet]. 2008 May [cited 2021 Sep 7];8(5):310–22. Available from: https://pubmed.ncbi.nlm.nih.gov/18471776/

49. Plaisier AP, Alley ES, Boatin BA, Van Oortmarssen GJ, Remme H, De Vlas SJ, et al. Irreversible effects of ivermectin on adult parasites in onchocerciasis patients in the Onchocerciasis Control Programme in West Africa. J Infect Dis [Internet]. 1995 Jul [cited 2021 Sep 7];172(1):204–10. Available from: https://pubmed.ncbi.nlm.nih.gov/7797912/

50. Walker M, Pion SDS, Fang H, Gardon J, Kamgno J, Basáñez M-G, et al. Macrofilaricidal Efficacy of Repeated Doses of Ivermectin for the Treatment of River Blindness. Clin Infect Dis [Internet]. 2017 Nov 29 [cited 2021 Sep 7];65(12):2026–34. Available from: https://pubmed.ncbi.nlm.nih.gov/29020189/

51. Coffeng LE, Stolk WA, Zouré HGM, Veerman JL, Agblewonu KB, Murdoch ME, et al. African Programme for Onchocerciasis Control 1995–2015: Updated Health Impact Estimates Based on New Disability Weights. Churcher TS, editor. PLoS Negl Trop Dis [Internet]. 2014 Jun 5 [cited 2021 Sep 7];8(6):e2759. Available from: https://journals.plos.org/plosntds/article?id=10.1371/journal.pntd.0002759

52. Vos T, Barber RM, Bell B, Bertozzi-Villa A, Biryukov S, Bolliger I, et al. Global, regional, and national incidence, prevalence, and years lived with disability for 301 acute and chronic diseases and injuries in 188 countries, 1990–2013: a systematic analysis for the Global Burden of Disease Study 2013. Lancet [Internet]. 2015 Aug;386(9995):743–800. Available from: https://linkinghub.elsevier.com/retrieve/pii/S0140673615606924

53. Keenan JD, Hotez PJ, Amza A, Stoller NE, Gaynor BD, Porco TC, et al. Elimination and Eradication of Neglected Tropical Diseases with Mass Drug Administrations: A Survey of Experts. Basáñez M-G, editor. PLoS Negl Trop Dis [Internet]. 2013 Dec 5;7(12):e2562. Available from: http://dx.plos.org/10.1371/journal.pntd.0002562

54. Wanji S, Nji TM, Hamill L, Dean L, Ozano K, Njouendou AJ, et al. Implementation of test-and-treat with doxycycline and temephos ground larviciding as alternative strategies for accelerating onchocerciasis elimination in an area of loiasis co-endemicity: the COUNTDOWN consortium multi-disciplinary study protocol. Parasit Vectors [Internet]. 2019 Dec 4;12(1):574. Available from: https://parasitesandvectors.biomedcentral.com/articles/10.1186/s13071-019-3826-8

55. Kelly-Hope LA, Cano J, Stanton MC, Bockarie MJ, Molyneux DH. Innovative tools for assessing risks for severe adverse events in areas of overlapping Loa loa and other filarial distributions: the application of micro-stratification mapping. Parasit Vectors [Internet]. 2014;7(1):307. Available from: http://parasitesandvectors.biomedcentral.com/articles/10.1186/1756-3305-7-307

56. Molyneux DH, Hopkins A, Bradley MH, Kelly-Hope LA. Multidimensional complexities of filariasis control in an era of large-scale mass drug administration programmes: A can of worms [Internet]. Vol. 7, Parasites and Vectors. 2014. p. 363. Available from: http://parasitesandvectors.biomedcentral.com/articles/10.1186/1756-3305-7-363

57. Gardon J, Gardon-Wendel N, Demanga-Ngangue, Kamgno J, Chippaux J-P, Boussinesq M. Serious reactions after mass treatment of onchocerciasis with ivermectin in an area endemic for Loa loa infection. Lancet [Internet]. 1997 Jul [cited 2022 Aug 24];350(9070):18–22. Available from: https://pubmed.ncbi.nlm.nih.gov/9217715/

58. Prichard RK. Ivermectin resistance and overview of the Consortium for Anthelmintic Resistance SNPs. Expert Opin Drug Discov [Internet]. 2007 Oct 5 [cited 2021 Sep 7];2(sup1):S41–52. Available from:

https://pubmed.ncbi.nlm.nih.gov/23489032/

59. Globisch D, Eubanks LM, Shirey RJ, Pfarr KM, Wanji S, Debrah AY, et al. Validation of onchocerciasis biomarker N -acetyltyramine- O -glucuronide (NATOG). Bioorg Med Chem Lett [Internet]. 2017 Aug;27(15):3436–40. Available from: http://dx.doi.org/10.1016/j.bmcl.2017.05.082

60. Hoerauf A. Mansonella perstans — The Importance of an Endosymbiont. N Engl J Med [Internet]. 2009 Oct 8 [cited 2021 Sep 7];361(15):1502–4. Available from: https://pubmed.ncbi.nlm.nih.gov/19812409/

61. Taylor MJ, Bandi C, Hoerauf A. Wolbachia.Bacterial Endosymbionts of Filarial Nematodes. In: Advances in Parasitology [Internet]. Academic Press; 2005 [cited 2021 Sep 7]. p. 245–84. Available from: https://linkinghub.elsevier.com/retrieve/pii/S0065308X05600048

62. Hoerauf A, Mand S, Adjei O, Fleischer B, Büttner DW. Depletion of wolbachia endobacteria in Onchocerca volvulus by doxycycline and microfilaridermia after ivermectin treatment. Lancet [Internet]. 2001 May 5 [cited 2021 Sep 7];357(9266):1415–6. Available from: https://pubmed.ncbi.nlm.nih.gov/11356444/

63. Hoerauf A, Specht S, Büttner M, Pfarr K, Mand S, Fimmers R, et al. Wolbachia endobacteria depletion by doxycycline as antifilarial therapy has macrofilaricidal activity in onchocerciasis: a randomized placebo-controlled study. Med Microbiol Immunol [Internet]. 2008 Sep 13 [cited 2021 Sep 7];197(3):295–311. Available from: https://pubmed.ncbi.nlm.nih.gov/17999080/

64. Specht S, Mand S, Marfo-Debrekyei Y, Debrah AY, Konadu P, Adjei O, et al. Efficacy of 2- and 4-week rifampicin treatment on the Wolbachia of Onchocerca volvulus. Parasitol Res [Internet]. 2008 Nov 5 [cited 2021 Sep 7];103(6):1303–9. Available from: https://pubmed.ncbi.nlm.nih.gov/18679718/

65. Klarmann-Schulz U, Specht S, Debrah AY, Batsa L, Ayisi-Boateng NK, Osei-Mensah J, et al. Comparison of Doxycycline, Minocycline, Doxycycline plus Albendazole and Albendazole Alone in Their Efficacy against Onchocerciasis in a Randomized, Open-Label, Pilot Trial. Basáñez M-G, editor. PLoS Negl Trop Dis [Internet]. 2017 Jan 5 [cited 2021 Sep 7];11(1):e0005156. Available from: https://pubmed.ncbi.nlm.nih.gov/28056021/

66. African Programme for Onchocerciasis Control (APOC). Report of the thirty-eighth session of the Technical Consultative Committee (TCC) [Internet]. Ouagadougou; 2014. Available from: https://apps.who.int/iris/handle/10665/275862

67. Njouendou AJ, Ritter M, Ndongmo WPC, Kien CA, Narcisse GTV, Fombad FF, et al. Successful long-term maintenance of Mansonella perstans in an in vitro culture system. Parasit Vectors [Internet]. 2017 Dec 10;10(1):563. Available from: https://parasitesandvectors.biomedcentral.com/articles/10.1186/s13071-017-

2515-8

68. Fombad FF, Njouendou AJ, Ndongmo PC, Ritter M, Chunda VC, Metuge HM, et al. Effect of flubendazole on developing stages of Loa loa in vitro and in vivo: A new approach for screening filaricidal agents. Parasites and Vectors. 2019;12(1):1–9.

69. Zofou D, Fombad FF, Gandjui NVT, Njouendou AJ, Kengne-Ouafo AJ, Chounna Ndongmo PW, et al. Evaluation of in vitro culture systems for the maintenance of microfilariae and infective larvae of Loa loa. Parasit Vectors [Internet]. 2018 Dec 2;11(1):275. Available from: https://parasitesandvectors.biomedcentral.com/articles/10.1186/s13071-018-2852-2

70. Lu IM, Kassis T, Rogers AM, Schudel A, Weil J, Evans CC, et al. Optimization of culture and analysis methods for enhancing long-term Brugia malayi survival, molting and motility in vitro. Parasitol Open [Internet]. 2018 Jan 11;4:e3. Available from: https://www.cambridge.org/core/product/identifier/S205570941700019X/type/journal_article

71. Malkmus C, Jawahar S, Tricoche N, Lustigman S, Hansmann J. Preliminary evaluations of 3-dimensional human skin models for their ability to facilitate in vitro the long-term development of the debilitating obligatory human parasite Onchocerca volvulus. Fairfax K, editor. PLoS Negl Trop Dis [Internet]. 2020 Nov 5 [cited 2020 Nov 18];14(11):e0008503. Available from: https://dx.plos.org/10.1371/journal.pntd.0008503

72. Patton JB, Bennuru S, Eberhard ML, Hess JA, Torigian A, Lustigman S, et al. Development of Onchocerca volvulus in humanized NSG mice and detection of parasite biomarkers in urine and serum. Specht S, editor. PLoS Negl Trop Dis [Internet]. 2018 Dec 12;12(12):e0006977. Available from: http://dx.doi.org/10.1371/journal.pntd.0006977

73. Gilaberte Y, Prieto-Torres L, Pastushenko I, Juarranz Á. Anatomy and Function of the Skin. In: Nanoscience in Dermatology [Internet]. Elsevier; 2016 [cited 2021 Sep 8]. p. 1–14. Available from: https://linkinghub.elsevier.com/retrieve/pii/B978012802926800001X

74. Coelho M, Oliveira T, Fernandes R. Biochemistry of adipose tissue: an endocrine organ. Arch Med Sci [Internet]. 2013 Apr 20;9(2):191–200. Available from: http://www.termedia.pl/doi/10.5114/aoms.2013.33181

75. Cypess AM, Lehman S, Williams G, Tal I, Rodman D, Goldfine AB, et al. Identification and Importance of Brown Adipose Tissue in Adult Humans. N Engl J Med [Internet]. 2009 Apr 9 [cited 2021 Sep 10];360(15):1509–17. Available from: https://pubmed.ncbi.nlm.nih.gov/19357406/

76. Chait A, den Hartigh LJ. Adipose Tissue Distribution, Inflammation and Its Metabolic Consequences, Including Diabetes and Cardiovascular Disease. Front Cardiovasc Med [Internet]. 2020 Feb 25 [cited 2021 Sep 10];7. Available from: https://pubmed.ncbi.nlm.nih.gov/32158768/

77. Björntorp P. "Portal" adipose tissue as a generator of risk factors for cardiovascular disease and diabetes. Arterioscler An Off J Am Hear Assoc Inc [Internet]. 1990 Jul;10(4):493–6. Available from: https://www.ahajournals.org/doi/10.1161/01.ATV.10.4.493

78. Reddy P, Lent-Schochet D, Ramakrishnan N, McLaughlin M, Jialal I. Metabolic syndrome is an inflammatory disorder: A conspiracy between adipose tissue and phagocytes. Clin Chim Acta [Internet]. 2019 Sep 1 [cited 2021 Sep 10];496:35–44. Available from: https://pubmed.ncbi.nlm.nih.gov/31229566/

79. Ruiz-Ojeda, Méndez-Gutiérrez, Aguilera, Plaza-Díaz. Extracellular Matrix Remodeling of Adipose Tissue in Obesity and Metabolic Diseases. Int J Mol Sci [Internet]. 2019 Oct 2 [cited 2021 Sep 11];20(19):4888. Available from: /pmc/articles/PMC6801592/

80. Stenkula KG, Erlanson-Albertsson C. Adipose cell size: importance in health and disease. Am J Physiol Integr Comp Physiol [Internet]. 2018 Aug 1 [cited 2021 Sep 11];315(2):R284–95. Available from: https://journals.physiology.org/doi/abs/10.1152/ajpregu.00257.2017

81. Frühbeck G. Overview of Adipose Tissue and Its Role in Obesity and Metabolic Disorders. In: Methods in Molecular Biology [Internet]. Humana Press; 2008 [cited 2020 May 12]. p. 1–22. Available from: http://link.springer.com/10.1007/978-1-59745-245-8_1

82. Sarjeant K, Stephens JM. Adipogenesis. Cold Spring Harb Perspect Biol [Internet]. 2012 Sep 1 [cited 2021 Sep 11];4(9):a008417–a008417. Available from: /pmc/articles/PMC3428766/

83. Rosen E, Eguchi J, Xu Z. Transcriptional targets in adipocyte biology. Expert Opin Ther Targets [Internet]. 2009 Aug 17 [cited 2021 Sep 11];13(8):975–86. Available from: https://pubmed.ncbi.nlm.nih.gov/19534570/

84. Kwok KHM, Lam KSL, Xu A. Heterogeneity of white adipose tissue: molecular basis and clinical implications. Exp Mol Med [Internet]. 2016 Mar 11 [cited 2021 Sep 10];48(3):e215–e215. Available from: https://pubmed.ncbi.nlm.nih.gov/26964831/

85. Qatanani M, Lazar MA. Mechanisms of obesity-associated insulin resistance: many choices on the menu. Genes Dev [Internet]. 2007 Jun 15 [cited 2021 Sep 10];21(12):1443–55. Available from: https://pubmed.ncbi.nlm.nih.gov/17575046/

86. Song Z, Xiaoli A, Yang F. Regulation and Metabolic Significance of De Novo Lipogenesis in Adipose Tissues. Nutrients [Internet]. 2018 Sep 29 [cited 2021 Sep 12];10(10):1383. Available from: /pmc/articles/PMC6213738/

87. Merkel M, Eckel RH, Goldberg IJ. Lipoprotein lipase. J Lipid Res [Internet]. 2002 Dec 1 [cited 2021 Sep 12];43(12):1997–2006. Available from: https://pubmed.ncbi.nlm.nih.gov/12454259/

88. Wu Q, Ortegon AM, Tsang B, Doege H, Feingold KR, Stahl A. FATP1 Is an

Insulin-Sensitive Fatty Acid Transporter Involved in Diet-Induced Obesity. Mol Cell Biol [Internet]. 2006 May [cited 2021 Sep 12];26(9):3455–67. Available from: https://pubmed.ncbi.nlm.nih.gov/16611988/

89. Endemann G, Stanton LW, Madden KS, Bryant CM, White RT, Protter AA. CD36 is a receptor for oxidized low density lipoprotein. J Biol Chem [Internet]. 1993 Jun;268(16):11811–6. Available from: https://linkinghub.elsevier.com/retrieve/pii/S0021925819502721

90. Bolsoni-Lopes A, Alonso-Vale MIC. Lipolysis and lipases in white adipose tissue – An update. Arch Endocrinol Metab [Internet]. 2015 Aug [cited 2021 Sep 12];59(4):335–42. Available from: https://pubmed.ncbi.nlm.nih.gov/26331321/

91. Zhang Y, Proenca R, Maffei M, Barone M, Leopold L, Friedman JM. Positional cloning of the mouse obese gene and its human homologue. Nature [Internet]. 1994 Dec 1 [cited 2021 Sep 12];372(6505):425–32. Available from: https://www.nature.com/articles/372425a0

92. Friedman JM, Halaas JL. Leptin and the regulation of body weight in mammals. Nature [Internet]. 1998 Oct 22 [cited 2021 Sep 12];395(6704):763–70. Available from: https://pubmed.ncbi.nlm.nih.gov/9796811/

93. Stern JH, Rutkowski JM, Scherer PE. Adiponectin, Leptin, and Fatty Acids in the Maintenance of Metabolic Homeostasis through Adipose Tissue Crosstalk. Cell Metab [Internet]. 2016 May 10 [cited 2021 Sep 12];23(5):770–84. Available from: https://linkinghub.elsevier.com/retrieve/pii/S1550413116301620

94. Scherer PE, Williams S, Fogliano M, Baldini G, Lodish HF. A Novel Serum Protein Similar to C1q, Produced Exclusively in Adipocytes. J Biol Chem [Internet]. 1995 Nov 10 [cited 2021 Sep 14];270(45):26746–9. Available from: https://linkinghub.elsevier.com/retrieve/pii/S0021925818880590

95. Kusminski CM, Holland WL, Sun K, Park J, Spurgin SB, Lin Y, et al. MitoNEET-driven alterations in adipocyte mitochondrial activity reveal a crucial adaptive process that preserves insulin sensitivity in obesity. Nat Med [Internet]. 2012 Oct 9 [cited 2021 Sep 14];18(10):1539–49. Available from: https://www.nature.com/articles/nm.2899

96. Hardy OT, Perugini RA, Nicoloro SM, Gallagher-Dorval K, Puri V, Straubhaar J, et al. Body mass index-independent inflammation in omental adipose tissue associated with insulin resistance in morbid obesity. Surg Obes Relat Dis [Internet]. 2011 Jan 1 [cited 2021 Sep 14];7(1):60–7. Available from: https://linkinghub.elsevier.com/retrieve/pii/S1550728910005204

97. Bäsler K, Bergmann S, Heisig M, Naegel A, Zorn-Kruppa M, Brandner JM. The role of tight junctions in skin barrier function and dermal absorption. J Control Release [Internet]. 2016 Nov 28 [cited 2021 Sep 10];242:105–18. Available from: https://pubmed.ncbi.nlm.nih.gov/27521894/

98. Kirschner N, Houdek P, Fromm M, Moll I, Brandner JM. Tight junctions form a barrier in human epidermis. Eur J Cell Biol [Internet]. 2010 Nov [cited 2021 Sep

10];89(11):839–42. Available from: https://pubmed.ncbi.nlm.nih.gov/20732726/

99. Nemes Z, Steinert PM. Bricks and mortar of the epidermal barrier. Exp Mol Med [Internet]. 1999 Mar 1 [cited 2021 Sep 8];31(1):5–19. Available from: https://pubmed.ncbi.nlm.nih.gov/10231017/

100. Breitkreutz D, Koxholt I, Thiemann K, Nischt R. Skin Basement Membrane: The Foundation of Epidermal Integrity—BM Functions and Diverse Roles of Bridging Molecules Nidogen and Perlecan. Biomed Res Int [Internet]. 2013 [cited 2021 Sep 10];2013:1–16. Available from: /pmc/articles/PMC3618921/

101. West HC, Bennett CL. Redefining the Role of Langerhans Cells As Immune Regulators within the Skin. Front Immunol [Internet]. 2018 Jan 5 [cited 2021 Sep 8];8(JAN):1941. Available from: http://journal.frontiersin.org/article/10.3389/fimmu.2017.01941/full

102. Breitkreutz D, Mirancea N, Nischt R. Basement membranes in skin: unique matrix structures with diverse functions? Histochem Cell Biol [Internet]. 2009 Jul 31 [cited 2021 Sep 10];132(1):1–10. Available from: https://pubmed.ncbi.nlm.nih.gov/19333614/

103. Sugawara K, Tsuruta D, Ishii M, Jones JCR, Kobayashi H. Laminin-332 and -511 in skin. Exp Dermatol [Internet]. 2008 Jun [cited 2021 Sep 10];17(6):473–80. Available from: https://onlinelibrary.wiley.com/doi/10.1111/j.1600-0625.2008.00721.x

104. Brown TM, Krishnamurthy K. Histology, Dermis [Internet]. StatPearls. StatPearls Publishing; 2021 [cited 2021 Sep 10]. Available from: https://www.ncbi.nlm.nih.gov/books/NBK535346/

105. Ramos T, Moroni L. Tissue Engineering and Regenerative Medicine 2019: The Role of Biofabrication—A Year in Review. Tissue Eng Part C Methods [Internet]. 2020 Feb 1 [cited 2020 Nov 23];26(2):91–106. Available from: https://www.liebertpub.com/doi/10.1089/ten.tec.2019.0344

106. Knoll A, Scherer T, Poggendorf I, Lutkemeyer D, Lehmann J. Flexible Automation of Cell Culture and Tissue Engineering Tasks. Biotechnol Prog [Internet]. 2004 Dec 3 [cited 2021 Sep 8];20(6):1825–35. Available from: https://pubmed.ncbi.nlm.nih.gov/15575718/

107. Schmid FF, Schwarz T, Klos M, Schuberthan W, Walles H, Hansmann J, et al. Applicability of a Dual-Arm Robotic System for Automated Downstream Analysis of Epidermal Models. Appl Vitr Toxicol [Internet]. 2016 Jun 15 [cited 2020 Oct 20];2(2):118–25. Available from: http://www.liebertpub.com/doi/10.1089/aivt.2015.0027

108. Mekhileri N V, Lim KS, Brown GCJ, Mutreja I, Schon BS, Hooper GJ, et al. Automated 3D bioassembly of micro-tissues for biofabrication of hybrid tissue engineered constructs. Biofabrication [Internet]. 2018 Jan 12 [cited 2021 Sep 8];10(2):024103. Available from: https://iopscience.iop.org/article/10.1088/1758-5090/aa9ef1

109. Lavik E, Langer R. Tissue engineering: current state and perspectives. Appl Microbiol Biotechnol [Internet]. 2004 Jul 20 [cited 2021 Sep 8];65(1):1–8. Available from: https://pubmed.ncbi.nlm.nih.gov/15221227/

110. Van Norman GA. Limitations of Animal Studies for Predicting Toxicity in Clinical Trials. JACC Basic to Transl Sci [Internet]. 2019 Nov 1 [cited 2020 Oct 26];4(7):845–54. Available from: https://linkinghub.elsevier.com/retrieve/pii/S2452302X1930316X

111. Doke SK, Dhawale SC. Alternatives to animal testing: A review. Saudi Pharm J SPJ Off Publ Saudi Pharm Soc [Internet]. 2015 Jul 1 [cited 2021 Feb 8];23(3):223–9. Available from: http://www.ncbi.nlm.nih.gov/pubmed/26106269

112. Hay M, Thomas DW, Craighead JL, Economides C, Rosenthal J. Clinical development success rates for investigational drugs. Nat Biotechnol [Internet]. 2014 Jan 9;32(1):40–51. Available from: http://www.ncbi.nlm.nih.gov/pubmed/24406927

113. Diavatopoulos DA, Cummings CA, Schouls LM, Brinig MM, Relman DA, Mooi FR. Bordetella pertussis, the Causative Agent of Whooping Cough, Evolved from a Distinct, Human-Associated Lineage of B. bronchiseptica. Hultgren S, editor. PLoS Pathog [Internet]. 2005 Dec 30 [cited 2020 Nov 23];1(4):e45. Available from: https://dx.plos.org/10.1371/journal.ppat.0010045

114. Russell W, Burch R. The Principles of Humane Experimental Technique. Med J Aust [Internet]. 1960 Mar;1(13):500–500. Available from: https://onlinelibrary.wiley.com/doi/abs/10.5694/j.1326-5377.1960.tb73127.x

115. Fatehullah A, Tan SH, Barker N. Organoids as an in vitro model of human development and disease. Nat Cell Biol [Internet]. 2016 Mar 25 [cited 2021 Sep 8];18(3):246–54. Available from: https://pubmed.ncbi.nlm.nih.gov/26911908/

116. Barrila J, Crabbé A, Yang J, Franco K, Nydam SD, Forsyth RJ, et al. Modeling Host-Pathogen Interactions in the Context of the Microenvironment: Three-Dimensional Cell Culture Comes of Age. Maurelli AT, editor. Infect Immun [Internet]. 2018 Nov 1 [cited 2021 Sep 8];86(11). Available from: https://pubmed.ncbi.nlm.nih.gov/30181350/

117. Duque-Correa MA, Maizels RM, Grencis RK, Berriman M. Organoids – New Models for Host–Helminth Interactions. Trends Parasitol [Internet]. 2020 Feb;36(2):170–81. Available from: http://www.ncbi.nlm.nih.gov/pubmed/31791691

118. Yu JR, Navarro J, Coburn JC, Mahadik B, Molnar J, Holmes JH, et al. Current and Future Perspectives on Skin Tissue Engineering: Key Features of Biomedical Research, Translational Assessment, and Clinical Application. Adv Healthc Mater [Internet]. 2019 Mar 1 [cited 2021 Sep 14];8(5):1801471. Available from: https://onlinelibrary.wiley.com/doi/full/10.1002/adhm.201801471

119. Draize JH, Woodard G, Calvery HO. Methods for the study of irritations and

toxicity of substances applied topically to the skin and mucous membranes. J Pharmacol Exp Ther. 1944;82(3):377–90.

120. Andrade TA, Aguiar AF, Guedes FA, Leite MN, Caetano GF, Coelho EB, et al. Ex vivo Model of Human Skin (hOSEC) as Alternative to Animal use for Cosmetic Tests. Procedia Eng [Internet]. 2015 Jan 1 [cited 2021 Sep 14];110:67–73. Available from: https://linkinghub.elsevier.com/retrieve/pii/S1877705815012527

121. Hwang J, Jeong H, Lee N, Hur S, Lee N, Han JJ, et al. Ex Vivo Live Full-Thickness Porcine Skin Model as a Versatile In Vitro Testing Method for Skin Barrier Research. Int J Mol Sci [Internet]. 2021 Jan 11 [cited 2021 Sep 14];22(2):657. Available from: https://pubmed.ncbi.nlm.nih.gov/33440780/

122. Alépée N, Tornier C, Robert C, Amsellem C, Roux M-H, Doucet O, et al. A catch-up validation study on reconstructed human epidermis (SkinEthic™ RHE) for full replacement of the Draize skin irritation test. Toxicol Vitr [Internet]. 2010 Feb [cited 2021 Sep 14];24(1):257–66. Available from: https://pubmed.ncbi.nlm.nih.gov/19733228/

123. Poumay Y, Dupont AF, Marcoux AS, Leclercq-Smekens M, He´rinhe´rin AM, Coquette AA. A simple reconstructed human epidermis: preparation of the culture model and utilization in in vitro studies.

124. Schmid FF, Groeber-Becker F, Schwab S, Thude S, Walles H, Hansmann J. A standardized method based on pigmented epidermal models evaluates sensitivity against UV-irradiation. ALTEX [Internet]. 2018 Jul 9 [cited 2020 Oct 30];35(3):390–6. Available from: https://www.altex.org/index.php/altex/article/view/248

125. Kiesewetter L, Littau L, Walles H, Boccaccini AR, Groeber-Becker F. Reepithelialization in focus: Non-invasive monitoring of epidermal wound healing in vitro. Biosens Bioelectron [Internet]. 2019 Oct 1 [cited 2020 May 13];142:111555. Available from: https://linkinghub.elsevier.com/retrieve/pii/S0956566319306347

126. Desmet E, Ramadhas A, Lambert J, Van Gele M. In vitro psoriasis models with focus on reconstructed skin models as promising tools in psoriasis research. Exp Biol Med [Internet]. 2017 Jun 1 [cited 2020 Oct 26];242(11):1158–69. Available from: /pmc/articles/PMC5478008/?report=abstract

127. Vörsmann H, Groeber F, Walles H, Busch S, Beissert S, Walczak H, et al. Development of a human three-dimensional organotypic skin-melanoma spheroid model for in vitro drug testing. Cell Death Dis [Internet]. 2013 Jul 11 [cited 2020 Oct 28];4(7):719. Available from: www.nature.com/cddis

128. Jannasch M, Groeber F, Brattig NW, Unger C, Walles H, Hansmann J. Development and application of three-dimensional skin equivalents for the investigation of percutaneous worm invasion. Exp Parasitol [Internet]. 2015 Mar 1 [cited 2020 May 13];150:22–30. Available from: https://linkinghub.elsevier.com/retrieve/pii/S0014489415000065

129. Witte RP, Kao WJ. Keratinocyte-fibroblast paracrine interaction: the effects of substrate and culture condition. Biomaterials [Internet]. 2005 Jun;26(17):3673–82. Available from: http://www.ncbi.nlm.nih.gov/pubmed/15621258

130. Wiegand C, Hewitt NJ, Merk HF, Reisinger K. Dermal Xenobiotic Metabolism: A Comparison between Native Human Skin, Four in vitro Skin Test Systems and a Liver System. Skin Pharmacol Physiol [Internet]. 2014 [cited 2021 Sep 15];27(5):263–75. Available from: https://www.karger.com/Article/FullText/358272

131. Randall MJ, Jüngel A, Rimann M, Wuertz-Kozak K. Advances in the Biofabrication of 3D Skin in vitro: Healthy and Pathological Models. Front Bioeng Biotechnol [Internet]. 2018 Oct 31 [cited 2020 Oct 21];6(OCT):154. Available from: www.frontiersin.org

132. Rossi A, Appelt-Menzel A, Kurdyn S, Walles H, Groeber F. Generation of a Three-dimensional Full Thickness Skin Equivalent and Automated Wounding. J Vis Exp [Internet]. 2015 Feb 26 [cited 2021 Sep 15];(96). Available from: https://pubmed.ncbi.nlm.nih.gov/25741763/

133. Moulin V, Castilloux G, Jean A, Garrel DR, Auger FA, Germain L. In vitro models to study wound healing fibroblasts. Burns [Internet]. 1996 Aug [cited 2021 Sep 15];22(5):359–62. Available from: https://pubmed.ncbi.nlm.nih.gov/8840034/

134. Ackermann K, Lombardi Borgia S, Korting HC, Mewes KR, Schäfer-Korting M. The Phenion® Full-Thickness Skin Model for Percutaneous Absorption Testing. Skin Pharmacol Physiol [Internet]. 2010 Feb [cited 2021 Sep 15];23(2):105–12. Available from: https://pubmed.ncbi.nlm.nih.gov/20016252/

135. Speer DP, Chvapil M, Eskelson CD, Ulreich J. Biological effects of residual glutaraldehyde in glutaraldehyde-tanned collagen biomaterials. J Biomed Mater Res [Internet]. 1980 Nov [cited 2021 Sep 15];14(6):753–64. Available from: https://pubmed.ncbi.nlm.nih.gov/6820019/

136. Lotz C, Schmid FF, Oechsle E, Monaghan MG, Walles H, Groeber-Becker F. Cross-linked Collagen Hydrogel Matrix Resisting Contraction To Facilitate Full-Thickness Skin Equivalents. ACS Appl Mater Interfaces [Internet]. 2017 Jun 21 [cited 2021 Sep 15];9(24):20417–25. Available from: www.acsami.org

137. Reuter C, Walles H, Groeber F. Preparation of a Three-Dimensional Full Thickness Skin Equivalent. In: Methods in Molecular Biology [Internet]. 2017. p. 191–8. Available from: http://link.springer.com/10.1007/978-1-4939-7021-6_14

138. Vidal SEL, Tamamoto KA, Nguyen H, Abbott RD, Cairns DM, Kaplan DL. 3D biomaterial matrix to support long term, full thickness, immuno-competent human skin equivalents with nervous system components. Biomaterials [Internet]. 2019 Apr 1 [cited 2021 Sep 15];198:194–203. Available from: https://pubmed.ncbi.nlm.nih.gov/29709325/

139. Reuter C, Imdahl F, Hauf L, Vafadarnejad E, Fey P, Finger T, et al. Vector-borne Trypanosoma brucei parasites develop in artificial human skin and persist as skin tissue forms (Preprint). bioRxiv [Internet]. 2021 May 13 [cited 2021 Sep 15];2021.05.13.443986. Available from: https://www.biorxiv.org/content/10.1101/2021.05.13.443986v1

140. Tanowitz HB, Scherer PE, Mota MM, Figueiredo LM. Adipose Tissue: A Safe Haven for Parasites? Trends Parasitol [Internet]. 2017 Apr 1 [cited 2021 Sep 15];33(4):276–84. Available from: /pmc/articles/PMC5376508/

141. Berman JJ. Animals. In: Taxonomic Guide to Infectious Diseases [Internet]. Elsevier; 2019 [cited 2021 Sep 15]. p. 169–227. Available from: https://linkinghub.elsevier.com/retrieve/pii/B9780128175767000055

142. Lu J-D, Xue J. Poisoning. In: Critical Care Nephrology [Internet]. Elsevier; 2019 [cited 2021 Sep 15]. p. 600-629.e7. Available from: https://linkinghub.elsevier.com/retrieve/pii/B9780323449427001011

143. Schmidt FF, Nowakowski S, Kluger PJ. Improvement of a Three-Layered in vitro Skin Model for Topical Application of Irritating Substances. Front Bioeng Biotechnol [Internet]. 2020 May 8;8(May):1–11. Available from: https://www.frontiersin.org/article/10.3389/fbioe.2020.00388/full

144. Poulos SP, Dodson M V, Hausman GJ. Cell line models for differentiation: preadipocytes and adipocytes. Exp Biol Med [Internet]. 2010 Oct 1 [cited 2021 Sep 15];235(10):1185–93. Available from: https://journals.sagepub.com/doi/10.1258/ebm.2010.010063

145. Werner K, Jakubietz MG, Jakubietz RG, Schmidt K, Muhr C, Bauer-Kreisel P, et al. Toward reconstruction of the subcutaneous fat layer with the use of adipose-derived stromal cell-seeded collagen matrices. Cytotherapy [Internet]. 2014;16(12):1700–8. Available from: http://dx.doi.org/10.1016/j.jcyt.2014.06.007

146. Lazar A, Dinescu S, Costache M. Adipose tissue engineering and adipogenesis – a review. Rev Biol Biomed Sci [Internet]. 2018 Jul 9;1(1):17–26. Available from: https://rev-biomed.unibuc.ro/2018/07/09/adipose-tissue-engineering-and-adipogenesis-a-review/

147. Gomillion CT, Burg KJL. Stem cells and adipose tissue engineering. Biomaterials [Internet]. 2006 Dec 1 [cited 2021 Sep 15];27(36):6052–63. Available from: https://linkinghub.elsevier.com/retrieve/pii/S0142961206006570

148. Beahm EK, Walton RL, Patrick CW. Progress in adipose tissue construct development. Clin Plast Surg [Internet]. 2003 Oct [cited 2021 Sep 15];30(4):547–58. Available from: https://pubmed.ncbi.nlm.nih.gov/14621302/

149. Wiesner M, Berberich O, Hoefner C, Blunk T, Bauer-Kreisel P. Gap junctional intercellular communication in adipose-derived stromal/stem cells is cell density-dependent and positively impacts adipogenic differentiation. J Cell

Physiol [Internet]. 2018 Apr 27;233(4):3315–29. Available from: http://doi.wiley.com/10.1002/jcp.26178

150. Mushahary D, Spittler A, Kasper C, Weber V, Charwat V. Isolation, cultivation, and characterization of human mesenchymal stem cells. Cytometry A [Internet]. 2017 Oct 26;(Cd):1–13. Available from: http://doi.wiley.com/10.1002/cyto.a.23242

151. Dominici M, Le Blanc K, Mueller I, Slaper-Cortenbach I, Marini F., Krause DS, et al. Minimal criteria for defining multipotent mesenchymal stromal cells. The International Society for Cellular Therapy position statement. Cytotherapy [Internet]. 2006 Aug [cited 2021 Sep 16];8(4):315–7. Available from: https://pubmed.ncbi.nlm.nih.gov/16923606/

152. Rogal J, Binder C, Kromidas E, Roosz J, Probst C, Schneider S, et al. WAT-on-a-chip integrating human mature white adipocytes for mechanistic research and pharmaceutical applications. Sci Rep [Internet]. 2020;10(1):1–12. Available from: http://dx.doi.org/10.1038/s41598-020-63710-4

153. Tanzi MC, Farè S. Adipose tissue engineering: state of the art, recent advances and innovative approaches. Expert Rev Med Devices [Internet]. 2009 Sep 9 [cited 2021 Sep 11];6(5):533–51. Available from: https://pubmed.ncbi.nlm.nih.gov/19751125/

154. Peer LA. The neglected "Free fat graft," Its behavior and clinical use. Am J Surg [Internet]. 1956 Jul [cited 2021 Sep 16];92(1):40–7. Available from: https://pubmed.ncbi.nlm.nih.gov/13327157/

155. Puissant B, Barreau C, Bourin P, Clavel C, Corre J, Bousquet C, et al. Immunomodulatory effect of human adipose tissue-derived adult stem cells: comparison with bone marrow mesenchymal stem cells. Br J Haematol [Internet]. 2005 Apr [cited 2021 Sep 16];129(1):118–29. Available from: https://pubmed.ncbi.nlm.nih.gov/15801964/

156. Kim I, Bang SI, Lee SK, Park SY, Kim M, Ha H. Clinical Implication of Allogenic Implantation of Adipogenic Differentiated Adipose-Derived Stem Cells. Stem Cells Transl Med [Internet]. 2014 Nov 1 [cited 2021 Sep 16];3(11):1312–21. Available from: https://europepmc.org/articles/PMC4214848

157. Glaser L. Identification of cues for enhanced 3D adipogenic differentiation of human mesenchymal stromal cells. University Hospital Würzburg; 2020.

158. Huber B, Czaja AM, Kluger PJ. Influence of epidermal growth factor (EGF) and hydrocortisone on the co-culture of mature adipocytes and endothelial cells for vascularized adipose tissue engineering. Cell Biol Int [Internet]. 2016 May 1 [cited 2022 Feb 8];40(5):569–78. Available from: https://onlinelibrary.wiley.com/doi/10.1002/cbin.10595

159. Serrero G, Mills D. Physiological role of epidermal growth factor on adipose tissue development in vivo. Proc Natl Acad Sci U S A [Internet]. 1991 May 1 [cited 2022 Feb 8];88(9):3912–6. Available from: /pmc/articles/PMC51563/?report=abstract

160. Hauner H, Röhrig K, Petruschke T. Effects of epidermal growth factor (EGF), platelet-derived growth factor (PDGF) and fibroblast growth factor (FGF) on human adipocyte development and function. Eur J Clin Invest [Internet]. 1995 Feb [cited 2022 Feb 8];25(2):90–6. Available from: https://onlinelibrary.wiley.com/doi/10.1111/j.1365-2362.1995.tb01532.x

161. Walton PE, Etherton TD, Evock CM. Antagonism of insulin action in cultured pig adipose tissue by pituitary and recombinant porcine growth hormone: potentiation by hydrocortisone. Endocrinology [Internet]. 1986 Jun [cited 2022 Feb 8];118(6):2577–81. Available from: https://pubmed.ncbi.nlm.nih.gov/3516665/

162. Volz A-C, Huber B, Schwandt AM, Kluger PJ. EGF and hydrocortisone as critical factors for the co-culture of adipogenic differentiated ASCs and endothelial cells. Differentiation [Internet]. 2017 May 1 [cited 2022 Feb 8];95:21–30. Available from: https://pubmed.ncbi.nlm.nih.gov/28135608/

163. Huber B, Link A, Linke K, Gehrke SA, Winnefeld M, Kluger PJ. Integration of Mature Adipocytes to Build-Up a Functional Three-Layered Full-Skin Equivalent. Tissue Eng Part C Methods [Internet]. 2016;22(8):756–64. Available from: http://online.liebertpub.com/doi/10.1089/ten.tec.2016.0141

164. Weigel T, Malkmus C, Weigel V, Wußmann M, Berger C, Brennecke J, et al. Fully Synthetic 3D Fibrous Scaffolds for Stromal Tissues—Replacement of Animal-Derived Scaffold Materials Demonstrated by Multilayered Skin. Adv Mater [Internet]. 2022 Jan 21 [cited 2022 Feb 8];2106780. Available from: https://onlinelibrary.wiley.com/doi/full/10.1002/adma.202106780

165. Kurzchalia T V., Ward S. Why do worms need cholesterol? Nat Cell Biol [Internet]. 2003 Aug;5(8):684–8. Available from: http://www.ncbi.nlm.nih.gov/pubmed/12894170

166. Kilarski WW, Martin C, Pisano M, Bain O, Babayan SA, Swartz MA. Inherent biomechanical traits enable infective filariae to disseminate through collecting lymphatic vessels. Nat Commun [Internet]. 2019 Dec 1;10(1):2895. Available from: http://dx.doi.org/10.1038/s41467-019-10675-2

167. Cotton JA, Bennuru S, Grote A, Harsha B, Tracey A, Beech R, et al. The genome of Onchocerca volvulus, agent of river blindness. Nat Microbiol [Internet]. 2016 Nov 21;2(November):16216. Available from: http://www.ncbi.nlm.nih.gov/pubmed/27869790

168. Garofalo A, Kennedy MW, Bradley JE. The FAR proteins of parasitic nematodes: their possible involvement in the pathogenesis of infection and the use of Caenorhabditis elegans as a model system to evaluate their function. Med Microbiol Immunol [Internet]. 2003 Feb [cited 2020 Aug 27];192(1):47–52. Available from: https://pubmed.ncbi.nlm.nih.gov/12592563/

169. Zhan B, Arumugam S, Kennedy MW, Tricoche N, Lian L-Y, Asojo OA, et al. Ligand binding properties of two Brugia malayi fatty acid and retinol (FAR) binding proteins and their vaccine efficacies against challenge infection in gerbils. Lammie PJ, editor. PLoS Negl Trop Dis [Internet]. 2018 Oct 8 [cited

2020 Aug 27];12(10):e0006772. Available from: https://pubmed.ncbi.nlm.nih.gov/30296268/

170. Matyash V, Entchev E V., Mende F, Wilsch-Bräuninger M, Thiele C, Schmidt AW, et al. Sterol-derived hormone(s) controls entry into diapause in Caenorhabditis elegans by consecutive activation of DAF-12 and DAF-16. PLoS Biol [Internet]. 2004 Oct [cited 2020 Sep 17];2(10):e280. Available from: /pmc/articles/PMC517820/?report=abstract

171. Gnecchi M, He H, Liang OD, Melo LG, Morello F, Mu H, et al. Paracrine action accounts for marked protection of ischemic heart by Akt-modified mesenchymal stem cells. Nat Med [Internet]. 2005 Apr;11(4):367–8. Available from: http://www.nature.com/articles/nm0405-367

172. Teixeira FG, Salgado AJ. Mesenchymal stem cells secretome: current trends and future challenges. Neural Regen Res [Internet]. 2020 Jan;15(1):75–7. Available from: http://www.nrronline.org/text.asp?2020/15/1/75/264455

173. Mocchi M, Bari E, Marrubini G, Bonda AF, Perteghella S, Tartara F, et al. Freeze-Dried Mesenchymal Stem Cell-Secretome Pharmaceuticalization: Optimization of Formulation and Manufacturing Process Robustness. Pharmaceutics [Internet]. 2021 Jul 23;13(8):1129. Available from: https://www.mdpi.com/1999-4923/13/8/1129

174. Herrmann M, Diederichs S, Melnik S, Riegger J, Trivanović D, Li S, et al. Extracellular Vesicles in Musculoskeletal Pathologies and Regeneration. Front Bioeng Biotechnol [Internet]. 2021 Jan 20;8. Available from: https://www.frontiersin.org/articles/10.3389/fbioe.2020.624096/full

175. Gatrill AJ, Mackenzie CD, McMahon JE, Williams JF, Guderian RH. A histocytochemical study of the macrophages present in tissue responses to adult Onchocerca volvulus. Histochem J [Internet]. 1987 Sep [cited 2020 Sep 17];19(9):509–19. Available from: https://pubmed.ncbi.nlm.nih.gov/3440761/

176. Grainger DW. All charged up about implanted biomaterials. Nat Biotechnol [Internet]. 2013 Jun 10;31(6):507–9. Available from: http://www.nature.com/articles/nbt.2600

177. Jannasch M. In vitro chemotaxis and tissue remodeling assays quantitatively characterize foreign body reaction. ALTEX [Internet]. 2017;34(2):253–66. Available from: https://www.altex.org/index.php/altex/article/view/54

178. Grote A, Lustigman S, Ghedin E. Lessons from the genomes and transcriptomes of filarial nematodes. Mol Biochem Parasitol [Internet]. 2017 Jul;215:23–9. Available from: https://linkinghub.elsevier.com/retrieve/pii/S0166685117300129

179. Armstrong SD, Xia D, Bah GS, Krishna R, Ngangyung HF, LaCourse EJ, et al. Stage-specific Proteomes from Onchocerca ochengi, Sister Species of the Human River Blindness Parasite, Uncover Adaptations to a Nodular Lifestyle. Mol Cell Proteomics [Internet]. 2016;15(8):2554–75. Available from: http://www.mcponline.org/lookup/doi/10.1074/mcp.M115.055640

180. Bennuru S, Cotton JA, Ribeiro JMC, Grote A, Harsha B, Holroyd N, et al. Stage-Specific Transcriptome and Proteome Analyses of the Filarial Parasite Onchocerca volvulus and Its Wolbachia Endosymbiont. MBio [Internet]. 2016;7(6):1–11. Available from: http://www.ncbi.nlm.nih.gov/pubmed/27881553

181. Sun S, Rödelsperger C, Sommer RJ. Single worm transcriptomics identifies a developmental core network of oscillating genes with deep conservation across nematodes. Genome Res [Internet]. 2021 Sep;31(9):1590–601. Available from: http://genome.cshlp.org/lookup/doi/10.1101/gr.275303.121

182. Aldridge A, Kouroupis D, Churchman S, English A, Ingham E, Jones E. Assay validation for the assessment of adipogenesis of multipotential stromal cells--a direct comparison of four different methods. Cytotherapy [Internet]. 2013 Jan;15(1):89–101. Available from: http://dx.doi.org/10.1016/j.jcyt.2012.07.001

183. Pittenger MF, Mackay AM, Beck SC, Jaiswal RK, Douglas R, Mosca JD, et al. Multilineage Potential of Adult Human Mesenchymal Stem Cells. Science (80-) [Internet]. 1999 Apr 2;284(5411):143–7. Available from: https://www.science.org/doi/10.1126/science.284.5411.143

184. Evans WH, Boitano S. Connexin mimetic peptides: specific inhibitors of gap-junctional intercellular communication. Biochem Soc Trans [Internet]. 2001 Aug 1;29(4):606–12. Available from: https://portlandpress.com/biochemsoctrans/article/29/4/606/62951/Connexin-mimetic-peptides-specific-inhibitors-of

185. Jørgensen NR, Teilmann SC, Henriksen Z, Civitelli R, Sørensen OH, Steinberg TH. Activation of L-type Calcium Channels Is Required for Gap Junction-mediated Intercellular Calcium Signaling in Osteoblastic Cells. J Biol Chem [Internet]. 2003 Feb;278(6):4082–6. Available from: https://linkinghub.elsevier.com/retrieve/pii/S0021925819308233

186. Spencer M, Unal R, Zhu B, Rasouli N, McGehee RE, Peterson CA, et al. Adipose Tissue Extracellular Matrix and Vascular Abnormalities in Obesity and Insulin Resistance. J Clin Endocrinol Metab [Internet]. 2011 Dec;96(12):E1990–8. Available from: https://academic.oup.com/jcem/article-lookup/doi/10.1210/jc.2011-1567

187. Louis F, Kitano S, Mano JF, Matsusaki M. 3D collagen microfibers stimulate the functionality of preadipocytes and maintain the phenotype of mature adipocytes for long term cultures. Acta Biomater [Internet]. 2019 Jan;84:194–207. Available from: https://linkinghub.elsevier.com/retrieve/pii/S1742706118307116

188. Li X, Easley CJ. Microfluidic systems for studying dynamic function of adipocytes and adipose tissue. Anal Bioanal Chem [Internet]. 2018 Jan 6;410(3):791–800. Available from: http://link.springer.com/10.1007/s00216-017-0741-8

189. Volz A-C, Omengo B, Gehrke S, Kluger PJ. Comparing the use of differentiated adipose-derived stem cells and mature adipocytes to model adipose tissue in

vitro. Differentiation [Internet]. 2019 Nov;110:19–28. Available from: https://linkinghub.elsevier.com/retrieve/pii/S0301468119300544

190. Verboven K, Wouters K, Gaens K, Hansen D, Bijnen M, Wetzels S, et al. Abdominal subcutaneous and visceral adipocyte size, lipolysis and inflammation relate to insulin resistance in male obese humans. Sci Rep [Internet]. 2018 Dec 16;8(1):4677. Available from: http://www.nature.com/articles/s41598-018-22962-x

191. Hardouin P, Rharass T, Lucas S. Bone Marrow Adipose Tissue: To Be or Not To Be a Typical Adipose Tissue? Front Endocrinol (Lausanne) [Internet]. 2016 Jun 30;7. Available from: http://journal.frontiersin.org/Article/10.3389/fendo.2016.00085/abstract

192. Umemoto T, Fujiki Y. Ligand-dependent nucleo-cytoplasmic shuttling of peroxisome proliferator-activated receptors, PPARα and PPARγ. Genes to Cells [Internet]. 2012 Jul;17(7):576–96. Available from: https://onlinelibrary.wiley.com/doi/10.1111/j.1365-2443.2012.01607.x

193. Itabe H, Yamaguchi T, Nimura S, Sasabe N. Perilipins: a diversity of intracellular lipid droplet proteins. Lipids Health Dis [Internet]. 2017 Dec 28;16(1):83. Available from: https://lipidworld.biomedcentral.com/articles/10.1186/s12944-017-0473-y

194. Brasaemle DL, Barber T, Wolins NE, Serrero G, Blanchette-Mackie EJ, Londos C. Adipose differentiation-related protein is an ubiquitously expressed lipid storage droplet-associated protein. J Lipid Res [Internet]. 1997 Nov;38(11):2249–63. Available from: https://linkinghub.elsevier.com/retrieve/pii/S0022227520349397

195. Klingelhutz AJ, Gourronc FA, Chaly A, Wadkins DA, Burand AJ, Markan KR, et al. Scaffold-free generation of uniform adipose spheroids for metabolism research and drug discovery. Sci Rep [Internet]. 2018 Dec 11;8(1):523. Available from: http://dx.doi.org/10.1038/s41598-017-19024-z

196. Hoefner C, Muhr C, Horder H, Wiesner M, Wittmann K, Lukaszyk D, et al. Human Adipose-Derived Mesenchymal Stromal/Stem Cell Spheroids Possess High Adipogenic Capacity and Acquire an Adipose Tissue-like Extracellular Matrix Pattern. Tissue Eng Part A [Internet]. 2020 Aug 1;26(15–16):915–26. Available from: https://www.liebertpub.com/doi/10.1089/ten.tea.2019.0206

197. Krziminski C, Kammann S, Hansmann J, Edenhofer F, Dandekar G, Walles H, et al. Development of a bioreactor system for pre-endothelialized cardiac patch generation with enhanced viscoelastic properties by combined collagen I compression and stromal cell culture. J Tissue Eng Regen Med [Internet]. 2020 Dec 18 [cited 2021 Oct 4];14(12):1749–62. Available from: https://pubmed.ncbi.nlm.nih.gov/32893470/

198. Benayahu D, Wiesenfeld Y, Sapir-Koren R. How is mechanobiology involved in mesenchymal stem cell differentiation toward the osteoblastic or adipogenic fate? J Cell Physiol [Internet]. 2019 Aug 11;234(8):12133–41. Available from: https://onlinelibrary.wiley.com/doi/10.1002/jcp.28099

199. Cai X, Xie J, Yao Y, Cun X, Lin S, Tian T, et al. Angiogenesis in a 3D model containing adipose tissue stem cells and endothelial cells is mediated by canonical Wnt signaling. Bone Res [Internet]. 2017;5(March):1–13. Available from: http://dx.doi.org/10.1038/boneres.2017.48

200. Parshyna I, Lehmann S, Grahl K, Pahlke C, Frenzel A, Weidlich H, et al. Impact of omega-3 fatty acids on expression of angiogenic cytokines and angiogenesis by adipose-derived stem cells. Atheroscler Suppl [Internet]. 2017 Nov;30:303–10. Available from: http://linkinghub.elsevier.com/retrieve/pii/S156756881730082X

201. Wittmann K, Dietl S, Ludwig N, Berberich O, Hoefner C, Storck K, et al. Engineering Vascularized Adipose Tissue Using the Stromal-Vascular Fraction and Fibrin Hydrogels. Tissue Eng Part A [Internet]. 2015;21(7–8):1343–53. Available from: http://online.liebertpub.com/doi/10.1089/ten.tea.2014.0299

202. Muller S, Ader I, Creff J, Leménager H, Achard P, Casteilla L, et al. Human adipose stromal-vascular fraction self-organizes to form vascularized adipose tissue in 3D cultures. Sci Rep [Internet]. 2019 Dec 10;9(1):7250. Available from: http://www.nature.com/articles/s41598-019-43624-6

203. Kober J, Gugerell A, Schmid M, Kamolz L-P, Keck M. Generation of a Fibrin Based Three-Layered Skin Substitute. Biomed Res Int [Internet]. 2015;2015:1–8. Available from: http://www.hindawi.com/journals/bmri/2015/170427/

204. Moakes RJA, Senior JJ, Robinson TE, Chipara M, Atansov A, Naylor A, et al. A suspended layer additive manufacturing approach to the bioprinting of tri-layered skin equivalents. APL Bioeng [Internet]. 2021 Dec 1;5(4):046103. Available from: https://aip.scitation.org/doi/10.1063/5.0061361

205. Liu C, Mhashilkar AS, Chabanon J, Xu S, Lustigman S, Adams JH, et al. Development of a toolkit for piggyBac-mediated integrative transfection of the human filarial parasite Brugia malayi. Geary TG, editor. PLoS Negl Trop Dis [Internet]. 2018 May 21;12(5):e0006509. Available from: https://dx.plos.org/10.1371/journal.pntd.0006509

Publications and Conference Contributions

Publications

Malkmus C, Jawahar S, Tricoche N, Lustigman S, Hansmann J. **Preliminary evaluations of 3-dimensional human skin models for their ability to facilitate *in vitro* the long-term development of the debilitating obligatory human parasite Onchocerca volvulus.** *PLoS Neglected Tropical Diseases*, November 2020

Weigel T, Malkmus C, Weigel V, Wußmann M, Berger C, Brennecke J, Groeber-Becker F, Hansmann J. **Fully Synthetic 3D Fibrous Scaffolds for Stromal Tissues—Replacement of Animal-Derived Scaffold Materials Demonstrated by Multilayered Skin.** *Advanced Materials*, January 2022

Conference Contributions

2021 **3D Cell Culture (3DCC)**, DECHEMA, Freiburg (online), Poster:

Optimizing 3D human skin models to facilitate long-term development of *O. volvulus*, a debilitating obligatory human parasite

Malkmus C, Jawahar S, Tricoche N, Lustigman S, Hansmann J.

2020 **Eureka! 2020**, Graduate School of Life Sciences, Würzburg (online), Poster:

Optimizing 3D human skin models to facilitate long-term development of *O. volvulus*, a debilitating obligatory human parasite

Malkmus C, Jawahar S, Tricoche N, Lustigman S, Hansmann J.

2019 **3D Infect**, Graduiertenkolleg 2157 der Universität Würzburg, Würzburg Poster:

Establishment of a 3D tissue culture system for *Onchocerca volvulus* based on human skin

Malkmus C, Jawahar S, Tricoche N, Lustigman S, Hansmann J.

2018 **Eureka! 2018**, Graduate School of Life Sciences, Würzburg (online), Poster:

Establishment of a 3D tissue culture system for *Onchocerca volvulus* based on human skin

Malkmus C, Jawahar S, Tricoche N, Lustigman S, Hansmann J.

Acknowledgements

First, I want to thank the former head of institute Prof. Dr. Heike Walles and Dr. Marco Metzger for giving me the opportunity to work and write my thesis in the Department of Tissue Engineering and Regenerative Medicine of the University Hospital Würzburg.

My special thanks go to Prof. Dr. Jan Hansmann for his great supervision of my thesis. His interdisciplinary background, professional competence and valuable ideas contributed very much to this work. Thank you for the ongoing support, feedback, motivation and pleasant trips to New York.

I would also like to thank the other members of my thesis committee for their time, patience and discussions. Thank you, Prof. Dr. Christian Janzen for the constant support since my master thesis until the supervision of this doctor thesis and the interest in my work. I was pleased to see that there was a lot of common interest in the topic of *Onchocerca* within the committee. Thank you, Dr. Sara Lustigman for introducing me into the world of parasites with so much passion and joy. I really learnt a lot during my stays at the New York Blood Center. I also want to thank Prof. Dr. Uwe Gbureck for the fulfillment of the chairperson.

I really enjoyed working at the Institute and would like to thank all the members and students I was able to work with. Especially I would like to thank the assistance of the department Özlem Elbert and Anna Stefl for their constant support in any concern and for the good spirit they spread. I was lucky to work in two research groups during my time at the TERM. First, Dr. Florian Groeber-Becker and Dr. Christian Lotz gave me the chance to do my master thesis in the skin group. This valuable time prepared me to further continue with my PhD in the group of Prof. Dr. Jan Hansmann. Thanks to the two working groups I was able to gain more interdisciplinary insights and learned to apply different scientific perspectives.

The working days would not have been so pleasant if I had not been able to spend so many pleasant hours in the office with lots of coffee and colleagues. Especially the small office with Dr. Anna Leikeim, Dr. Christian Lotz, Dr. Ramkumar Ramani Mohan, Dr. Anna Schliermann, Dr. Robin Fischer, Sanjana Mathew, Jihyoung Choi, Lukas Königer and Marc Möllman was a very good place for good conversations and

lots of fun. In the office, we also appreciated very much the presence of co-coffee-drinkers Tom Däullary, Nina Marichikj, Maximiliane Wußmann, Dr. Christina Fey, Dr. Lisa Kiesewetter and everybody else who joined.

In many phases of my thesis, I have very intensively worked with colleagues on particular projects and experiments. Here I would like to thank Sabine Gätzner for her patience and time that she spent with me on analyzing larvae. I thank Amelie Reigl and Dr. Dieter Groneberg for their great imaging-competence and the supply of Confocal Microscopy images. I also thank Lukas Königer for the nice co-work and important insights in the lab automation. Furthermore, I would like to thank my Master student Laurin Glaser sharing the passion for adipose tissue.

I was lucky to have the New York Blood Center as cooperation partner in my project, not only because I was able to visit New York City for an internship and project meetings. It was a pleasure to work with the team of the Molecular Parasitology Nancy Tricoche, Shabnam Jawahar, Michael Schlossman, and Dr. Sara Lustigman.

Besides work, I was always lucky to have many friends around. The Würzburger Stammtisch was responsible for having pleasant evenings talking about other topics than work, even though some colleagues found their way into this circle of friends, namely Thomas Däullary and Lukas Königer. I would also like to thank Dr. Fabian Imdahl for his constant friendship since we met during the fire alarm in the botanical garden.

Last but not least, I thank my family for everything I am. I could not have achieved all this without your unconditional support. I also thank my partner Ronja for making life and everything else more enjoyable.

Affidavit

I hereby confirm that my thesis entitled "Establishment of a 3D *in vitro* skin culture system for the obligatory human parasite *Onchocerca volvulus*" is the result of my own work. I did not receive any help or support from commercial consultants. All sources and / or materials applied are listed and specified in the thesis.

Furthermore, I confirm that this thesis has not yet been submitted as part of another examination process neither in identical nor in similar form.

…… ……

Place, Date Signature

Eidesstattliche Erklärung

Hiermit erkläre ich an Eides statt, die Dissertation „Establishment of a 3D *in vitro* skin culture system for the obligatory human parasite *Onchocerca volvulus*" eigenständig, d.h. ins-besondere selbständig und ohne Hilfe eines kommerziellen Promotionsberaters, angefertigt und keine anderen als die von mir angegebenen Quellen und Hilfsmittel verwendet zu haben.

Ich erkläre außerdem, dass die Dissertation weder in gleicher noch in ähnlicher Form bereits in einem anderen Prüfungsverfahren vorgelegen hat.

…… ……

Ort, Datum Unterschrift